UCSF
UC San Francisco Electronic Theses and Dissertations

Title

Cellular and molecular mechanisms of neurite targeting in the zebrafish visual system

Permalink

https://escholarship.org/uc/item/5nd203sf

Author

Nevin, Linda M

Publication Date

2008-04-08

Peer reviewed|Thesis/dissertation

eScholarship.org
Powered by the California Digital Library
University of California

Cellular and Molecular Mechanisms of Neurite Targeting in the Zebrafish Visual System

by

Linda Nevin

DISSERTATION

Submitted in partial satisfaction of the requirements for the degree of

DOCTOR OF PHILOSOPHY

in

Neuroscience

in the

GRADUATE DIVISION

of the

UNIVERSITY OF CALIFORNIA, SAN FRANCISCO

copyright © Linda Nevin

2008

Acknowledgements

This thesis would not have been possible without the contributions of many people at UCSF. Foremost, I would like to thank my *Doktorvater,* Herwig Baier, for his guidance and friendship. I am particularly indebted to the early graduate students of the Baier laboratory—Jeremy Kay, Matt Smear, Mike Orger, and Ann Wehman—for their generosity and kindness to a novice colleague. Tong Xiao's personal and scientific advice have been of great help, and I am fortunate to have such a talented collaborator as I finish experiments. My collaboration with Wendy Staub has also been crucial; her discipline as a researcher and her plain common sense are irreplaceable assets. I am grateful to Herwig for encouraging Wendy to work with me. This thesis is dedicated to Herwig and the members of the Baier lab, past and present.

I would like to acknowledge my UCSF committee, Herwig Baier, Grae Davis, Michael Stryker, and Fen-Biao Gao. Each has contributed meaningfully to my project. Special thanks go to Michael Stryker for keeping the continuity of our UCSF community alive by transiting from Parnassus to Mission Bay for our meetings. I am also grateful to outside committee member Kang Shen for agreeing to join.

The co-authors of Chapter 2 made the following contributions. Jeremy Kay completed the primary screen for VBA mutants, began the characterization of IPL sublaminae, positionally mapped the *mra* mutation, and generated *mra* chimeras. Michael Taylor developed the ERG protocols and supervised the recordings. Herwig Baier directed and supervised the research that forms the basis for Chapters 2, 3, and 4.

Endless gratitude goes to my parents, Larry and Merrian Nevin, and to my husband, Eric Keisman Jr.

Cellular and Molecular Mechanisms of Neurite Targeting in the Zebrafish Visual System

Linda Nevin

Abstract

Histologically discrete, parallel layers occur frequently in the nervous system. In many cases, each lamina is a target for innervation by a subset of neurons. We are interested in how neurites select their target laminae. Young zebrafish larvae develop two laminated neuropils in the visual system: the inner plexiform layer (IPL) of the retina and the synaptic region of the optic tectum. Using cell type-specific markers, we have characterized the IPL and tectal neuropil in detail, identifying the complement of neurites that compose each lamina. Using these maps, we investigated of the role of activity in IPL sublamination, and completed a forward genetic screen to identify molecules regulating lamination in the retina and tectum. In mammals, retinal activity is important for the sublamination of ganglion cell (GC) dendrites. Using pharmacological tools and the *brudas/NSF* mutant, we show that the zebrafish IPL develops in an activity-independent manner, at least until 7 dpf. Hard-wiring mechanisms may be conserved across these species, but other, activity-dependent mechanisms are not. Our screen uncovered five informative mutants. We exploited the *moonraker (mra)* and *notorious (noto)* mutants to explore the importance of cell-cell interactions in IPL development. Transplantation studies with *mra* demonstrate that a subset of amacrine cells (ACs) rely

on cell non-autonomous cues to sublaminate. The *mra* locus encodes DEAD-box protein 19, an RNA helicase not previously implicated in neurite targeting. In *noto,* GC, AC, and bipolar cell neurites appear to branch outside their target sublaminae. These IPL defects are autonomous to GCs; GC dendrites are able to instruct the sublamination of partner neurites. In the tectal neuropil, *noto* GC axons and some tectal dendrites are highly disorganized. While wildtype axons project to a single tectal lamina, *noto* GCs can form arbors in two or three. We explored the developmental relationship between GC axons tectal dendrites by characterizing the tectum of *lakritz (lak)* mutants, which lack GCs. Our observations uncovered only slight defects in *lak* mutant tectal dendritogenesis. The grossly visible aspects of lamination in the tectum are largely GC-independent.

TABLE OF CONTENTS

ACKNOWLEDGEMENTS..........iii

ABSTRACT..........iv

CHAPTER 1..........1
General Introduction

CHAPTER 2..........17
Activity-independent assembly of retinal synaptic layers by cell-cell interactions

CHAPTER 3..........92
Retinal ganglion cell axons arborize in inappropriate laminae in the *notorious* mutant

CHAPTER 4..........108
Characterization of tectal cell morphologies in wildtype and *lakritz* mutant larvae

CONCLUSIONS..........120

LIST OF ILLUSTRATIONS

Chapter 2

Table 1……………71

Table 2……………72

Figure 1……………73

Figure 2……………74

Figure 3……………75

Figure 4……………76

Figure 5……………77

Figure 6……………78

Figure 7……………79

Figure 8……………80

Figure 9……………80

Figure 10……………81

Figure 11……………82

Figure 12……………83

Figure 13……………84

Figure 14……………85

Figure 15……………86

Figure 16……………87

Figure 17……………88

Supp Fig 1……………89

Supp Fig 2……………89

Supp Fig 3……………89

Supp Fig 4……………90

Supp Fig 5……………90

Supp Fig 6……………91

Chapter 3

Figure 18……………104

Figure 19……………105

Figure 20……………106

Figure 21……………107

Chapter 4

Figure 22……………119

Chapter 1: General Introduction

Why neurite lamination?

I became interested in the nervous system because of its relevance to my experience of living. The questions most fundamental to our understanding of the human condition are rooted in neuroscience. How do we control our actions? What is the nature of consciousness? How did consciousness evolve as a solution to the problem of survival in the face of competition? This thesis addresses none of these questions directly. Rather, it is part of a bottom-up approach, in which we identify common properties of the nervous system and try to learn why they are true and what function they serve. I chose to study one of the unique signatures of the nervous system—the highly asymmetric, morphologically complicated shape of its cells. Even if stripped of the assumptions we are wont to make as human brains studying brains, we could still observe that the shapes of neurites are costly to develop but necessary for function. If we want to know how the nervous system came to function as it does, we must understand what factors regulate the morphology of neurons. As the brain evolved, these factors pushed axons to extend to ever more distant targets and dendrites to build large complex arbors, contrary to the pull of equilibrium.

The study of single cell morphology is time-consuming, which conflicts with the forward genetic approach we wanted to use. Fortunately for neuroscientists, neurons fall into classes with similar morphologies, and their projections *en masse* are often organized into layers, also called strata or laminae. Neurons of different classes can extend neurites to a single layer, where these neurites can interact and form synapses. In other cases, a single neuron might arborize dendritic branches into two layers, and form distinct connections in each. The purpose of neuronal lamination is unknown, but is often assumed to be a mechanism whereby neurites locate their synaptic partners. Alternatively, the separation of arbors on a dendritic branch might be important for the segregation of charge. Laminated tissue may comprise stacks of layers containing both cell bodies and synapses, or, cell bodies and synapses may be segregated into distinct layers. The frequency of laminated tissues in the vertebrate nervous system is striking; spinal cord, cerebral cortex, retina, hippocampus, and cerebellum are each organized into parallel layers. As is true for the asymmetric morphology of neurons, the prevalence of layers suggests that lamination is central to nervous system function. Because of its tractability and presumed importance, lamination of neural tissues was the focus of my thesis work.

Progress in the field

A number of component questions must be answered for us to understand how laminae develop. First, how is the laminar fate of a neuron determined? In the retina and cerebral cortex, a combination of cell-intrinsic competence and environmental cues present when the cell enters its last mitosis specify a cell’s laminar fate, and that cell subsequently migrates to its lamina (Desai and McConnell 2000; Livesey and Cepko 2001). The molecular mechanisms of lamina formation are best understand in the spinal cord, where a gradient of *Sonic hedgehog* defines the spatial limits of expression of homeodomain proteins, which in turn define cell fate by a combinatorial code (Jessell 2000). Once a neuron has associated with a lamina, it must polarize its neurites toward their targets, a process that may include designating one neurite as the axon. Neurite extension follows, which in some cases requires the growth of a long axon to a completely different brain region. The question of how neurons polarize their neurites and pathfind to their target regions has been studied extensively, and genetic players, particular guidance ligands and receptors, have been identified in forward genetic screens and in biochemical assays (Tessier-Lavigne and Goodman 1996; Dickson 2002). An intriguing study published during my time in graduate school described a role for intracellular cyclic nucleotide levels in determining whether a soluble cue is attractive or repulsive to axons (Nishiyama et al. 2003). Thus the field has seen significant progress in identification of relevant cell-surface and signal transduction molecules, and a full picture of axon pathfinding, from surface receptor to cytoskeleton, is feasible in the near-term. The third question, that of how a neurite knows when to begin branching within its target lamina, is the focus of this study. Considerable progress on this question has been made in the fly visual system, where distinct photoreceptors project to signature laminae in the optic lobe. In particular, a number of cell-surface molecules required for proper lamination, including the protein tyrosine phosphatase receptor LAR, and cell adhesion molecules N-cadherin, Flamingo, and Capricious, have been discovered in forward genetic screens. In addition, glial migration mutants showed that glia in the optic lamina (in this case, lamina is the specific name for a target region in the optic lobe) function as intermediate targets for some photoreceptor axons. The glia seem to provide a stop signal, because in their absence these axons traverse their target and extend to a deeper optic lobe region, the medulla (Ting and Lee 2007). These screens in *Drosophila* have uncovered both genetic and cellular mechanisms of lamination-- the molecules identified suggest that neurite-neurite signaling is of greater importance than cell-intrinsic mechanisms in developing laminar projections, and the glial migration mutants revealed an unexpected function for glia. By accretion of these mechanisms from various model systems, we may eventually draw conclusions about the essential components of lamination, which in turn may shed light on why we see this motif so often in the nervous system.

The visual system as a model

In this thesis work, I characterized the laminar organization of two structures in the zebrafish visual system—the retina and the optic tectum. I investigated the role of activity in the formation of these layers, and conducted a forward genetic screen for mutants that could be informative to the development of laminae. Of the two structures, the retina comes with far more groundwork from prior studies examining its development. My studies of the retina augment existing data, while my work in the tectum is largely exploratory. For this reason, I will focus here on what is known about the development of the retina.

In the retina, five laminae, each comprising a unique complement of cell bodies or synapses, arise from a uniform neuroepithelium. The larval zebrafish retina is shown here in a section, with cartoon drawings of the major cell types (Goldsmith and Harris 2003). The outermost layer, the outer nuclear layer (ONL) contains the photoreceptors, the rods (pink) and cones (orange) that convert photons into a change in neurotransmitter output from their terminals. Photoreceptor terminals innervate the next lamina, the outer plexiform layer

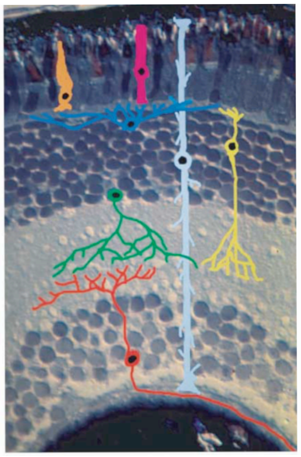

(OPL), where they synapse with bipolar cell (BC, yellow) and horizontal cell (HC, dark blue) dendrites. The photoreceptor to BC connection is the fundamental path of information, but those connections are modulated by HCs. Lateral inhibition by HCs is responsible for the enhancement of edges between light and dark surfaces in the visual field—edges appear to us to have greater contrast then they actually do. BCs, HCs, and amacrine cells (ACs, green) make up the inner nuclear layer (INL). BCs transmit light information to retinal ganglion cells (GCs, red) in the inner plexiform layer (IPL), the larger neuropil of the retina where BCs, ACs, and GCs form heterogeneous synapses. The many synapses of the IPL are responsible for the varied response properties of GCs; for example, a wide-field AC called the starburst cell integrates the signals from a moving light stimulus and relays this information to direction-selective GCs. The detailed organization of the IPL is discussed in Chapter 2. The innermost layer of the retina is the ganglion cell layer (GCL), which contains all the GCs and some ACs. Each GC projects an axon into the optic nerve, which traverses out through the IPL, INL, OPL, and ONL and out of the retina to the brain. The light blue cell shown in the above diagram is a Müller glial cell, a late differentiating cell that spans most of the neural retina.

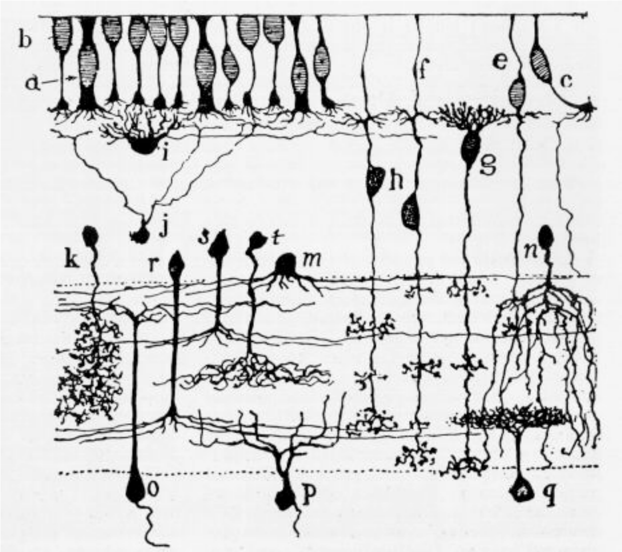

My interest is not in the generation of cellular laminae, but in the sublamination of neurites within the IPL. The highly specific projection patterns of IPL neurites caught the attention of Ramon y Cajal—his sketch is shown here. The IPL is the wide synaptic region making up most of the bottom half of the drawing. Some neurites ramify broadly across sublaminae, but others, as in cells o, r, s, t, and h, project specific arborizations into sublaminae. A popular hypothesis posits that each sublamina is part of a labeled line, transmitting a specific aspect of the visual scene to the GCs. One instance where this is clearly the case is the subdivision of the IPL into the ON and OFF portions. The outer, or OFF portion of the IPL is innervated by bipolar cells responsive only to the offset of light, while the inner, ON, portion is innervated by the class of BCs that responds to light onset (Nelson and Kolb 2003). In this way, at any given moment, dark regions of the visual scene are represented in the outer IPL, and light regions, in the inner IPL. In mammals, 90% of GCs eventually restrict their dendritic projections to either the ON and OFF IPL (Famiglietti and Kolb 1976; Chalupa and Gunhan 2004). In zebrafish, the majority of GCs maintain bi- or multistratified dendritic arbors into adulthood (Mangrum et al. 2002; Mumm et al. 2006). These different outcomes suggest that the GCs of the different species use different developmental strategies.

Within the brain of lower vertebrates, the major retinorecipient structure is the optic tectum, which has been studied mostly for its topographic map of visual space. The tecta of fish and frogs has been shown to be important for tracking and catching prey (Gahtan et al. 2005; Behrend et al. 2006). In mammals, the major retinorecipient structure is the lateral geniculate nucleus of the thalamus, but the tectum retains its function in tracking moving objects and is called the superior colliculus (Sewards and Sewards 2002). The topographic map of the tectum is in the plane defined by the rostro-caudal and medio-lateral axes. Orthogonal to the map, along the dorsal-ventral axis, the tectum is also a laminated structure, which has been characterized by NISSL and Golgi stains. In adult fish, the laminae of the tectum correspond to those described in the chick, which are designated based on their fiber and cell body content. In particular, the major retinorecipient lamina, the *stratum fibrosum et griseum (SFGS)*, contains both neurites and cell bodies in the adult. By contrast, in larval fish, the tectum is divided simply into a cell body region and a neuropil. A time series of tectal development from the larva to the adult has never been undertaken, so we do not know how the neuropil and gray matter are merged into the adult pattern. However, we do know that the larval and adult retinotectal projections both subdivide into four branches upon innervating the tectum. Therefore, the four divisions of the larval retinotectal projection are named according to their presumed counterparts in the adult. The laminae of optic tectal neurites, with their proper names, are described in Chapter 3.

Tools available in the zebrafish visual system

The zebrafish is a tractable model for the study of visual function; by 5 days post fertilization (dpf), larvae have a well developed retina and brain, and a number of visually dependent behaviors. At 68 hours post fertilization (hpf), larvae respond to a sudden dark stimulus with a characteristic startle swimming movement (Easter and Nicola 1996). By 80 hpf, two responses to a moving grating of black and white stripes—the optomotor response (OMR) and optokinetic response (OKR)—are established (Brockerhoff et al. 1995; Easter and Nicola 1996, 1997). In the OMR, larvae will swim in the direction that the stripes of the grating move. In the OKR, fish embedded in media that prevents swimming but allows eye movements will track individual stripes with their eyes (Neuhauss 2003). By 4 dpf, larval zebrafish respond to ambient light by distributing pigment in their skin cells such that they blend with the environment; this response is retina-dependent (Kay et al. 2001). This repertoire of behaviors can be exploited with assays to test whether mutants retain these abilities. As has been well advertised, one advantage of the zebrafish as a model system is its amenability to chemical mutagenesis, which has been exploited for the study of the visual system (Brockerhoff et al. 1995; Neuhauss et al. 1999; Muto et al. 2005; Xiao et al. 2005). Using the behavioral assays described above, the Baier laboratory completed a large scale screen of approximately 1700 mutagenized genomes and identified roughly 200 mutants deficient in one or more of these behaviors (Muto et al. 2005). Since that time, members of the laboratory have used the pool of mutants in secondary, or "shelf," screens, in search of mutations affecting a particular aspect of neural development or behavior.

There are a growing number of tools for studying the details and causes of a mutant phenotype. Injection of lipophillic dyes into the retina labels the retinofugal projections, and has been used successfully to identify mutants with aberrant axon pathfinding (Baier et al. 1996). A few transgenic lines have been generated labeling subsets of retinal cells, using the enhancer elements of the transcription factors *Pax6* and *Brn3c* (Kay et al. 2004; Xiao et al. 2005). In these lines, subpopulations of ACs and GCs, respectively, express a membrane-targeted GFP, which brightly labels axons and dendrites. Additional transgenic founders have been made from each of these constructs, some of which express GFP in a variegated manner and therefore label individual cells which can be imaged by confocal microscopy (Godinho et al. 2005; Xiao and Baier 2007). Unfortunately, imaging in the eye has proven difficult due to reflective pigments, which is why many of the figures in this work show cryostat sections of the retina.

Functional studies of neurons are becoming more common as activity dependent Calcium imaging (Niell and Smith 2005) and electrophysiology (Smear et al. 2007) are adapted to the zebrafish. The identification of the lesioned gene in a mutant remains a bottleneck for researchers, but the situation is improving as the genome assemblies become more complete and more polymorphic markers for positional mapping are identified.

Observations of zebrafish IPL development

Time course studies of zebrafish retinal development have laid the groundwork for this research. Most significantly, light and electron microscopic analyses of the embryonic and larval retina, and more recent *in vivo* time lapse observations of growing ACs and GCs, describe IPL development in tandem with the changes occurring in the retina (Schmitt and Dowling 1994, 1999; Godinho et al. 2005; Mumm et al. 2006). The summary here is drawn from the confluence of these studies.

The eye begins as an outgrowth of the forebrain, an undifferentiated, log-shaped epithelium extending laterally from the neural keel (the teleost neural “tube” is so called because it is a solid mass of cells—ventricles develop later). Over the next ten hours, this outgrowth morphs into the shape of an eye. First, the log-shaped epithelium grows laterally, until the eye primordium becomes a wing-shaped appendage to the brain, connected by the optic stalk at its anterior pole. The primordium then rotates relative to the brain such that the original dorsal surface of the “wing” becomes lateral. At this point, the lateral surface begins to differentiate into retina and lens precursors, while the medial surface begins to form the pigment epithelium that will surround the retina. Subsequently, the lateral (formerly dorsal) surface invaginates, until at 24 hpf the eye primordium can be described as the optic cup. During invagination, the retinal primordial cells are proliferating, such that by 24hpf the retina is a pseudostratified epithelium approximately 4 cell bodies thick from the pigment epithelium to the lens. Regions of the retina closer to the pigment epithelium are referred to as outer or scleral because of their proximity to the hard coating that will eventually cover the retina. The inner regions of the retina are referred to as vitreal, in reference to the gel-like substance that fills the lens cavity. By 24hpf, retinal cells are undergoing interkinetic nuclear migration—the cell bodies transit from the scleral to the vitreal edges of the retina in phase with their cell cycles (Baye and Link 2007). A neuron is said to differentiate when it exits its final mitosis and migrates to its position in the developing laminae.

The development of the IPL is intrinsically linked to the differentiation of retinal neurons; both are described here in a compilation of published observations from electron microscopic and time lapse confocal imaging (Schmitt and Dowling 1999; Godinho et al. 2005; Mumm et al. 2006). The neurons of the retina differentiate in a roughly vitreal to scleral order. GCs differentiate first—the earliest at 32 hpf—followed by ACs, HCs, photoreceptors, and lastly, BCs. The first suggestion of an IPL appears after ACs differentiate and migrate to their positions in the inner INL. A few hours after arriving, ACs exhibit directed growth of neurites toward the GCL, and these neurites form a thin plexus in the nascent IPL. This plexus appears at approximately 42hpf. A subset of ACs, identifiable by shape and position at the vitreal edge of the INL, begin to extend neurites *away* from the GCL and toward the INL. As they do so, they begin to migrate through the nascent IPL towards the GCL—they will eventually join the GCL and are referred to as displaced ACs. The function of displaced ACs in development is unknown, but they appear to form a temporary barrier to GC dendrites at these early stages of IPL development. AC and GC neurites begin the innervate the IPL at about the same time, but the population of future displaced ACs temporarily separates the two classes of neurite. The purpose of this initial separation, if there is one, is unclear, and the GC dendrites eventually bypass these ACs while the cells are still in the IPL.

By 50 hpf, EM studies show an IPL with many AC and GC neurites, immature conventional synapses, scattered ACs (presumably transiting to the GCL), and intercellular spaces. The IPL may form as a result of innervating neurites, which may be attracted to cells in the adjacent laminae. On the other hand, extra spaces in the IPL suggest that a spatial separation of INL and GCL occurs independent of the growth of neurites. BC terminals appear in the IPL ten hours later, at 60hpf, and form a small number of synapses with ACs and GCs by 70hpf. The number of conventional synapses—between ACs and GCs—is growing rapidly at this point, while accumulation of the ribbon synapses made by BCs is slow. However, there are enough complete vertical pathways from photoreceptors to BCs to GCs to enable some visual responses at this stage. Sublamination becomes apparent after all three cell types have innervated the IPL. The class of ACs labeled in the *Pax6:mGFP* transgenic line label the ON and OFF portions of the IPL by 70 hpf, and BC terminals are arranged into 4 sublaminae by 74hpf. Very rough sublamination of GC dendrites has been observed at 72 hpf; GC dendrites labeled in the *Brn3c:mGFP* transgenic line are subdivided into three sublaminae by 84 hpf. The entire population of AC dendrites is subdivided into five sublaminae by 76 hpf. In brief, there is an extended period of development—from 42hpf until 70hpf—when AC, GC, and lastly BC neurites share the IPL, ending with the formation of BC ribbon synapses and the appearance of ON and OFF sublaminae. After these events, multiple aspects of IPL sublamination become apparent in the next 6 hours.

These observations give rise to three key questions: 1) why do GCs wait for the differentiation of ACs to innervate the IPL, 2) how are these neurites interacting and changing in the 28 hour period before BC synapses form, and 3) what changes after 70 hpf create the windfall of sublamination. One possibility that is gaining experimental evidence is that ACs, or a subclass of ACs, create the IPL and form a scaffold which sets the pattern for the other neurites (Stacy and Wong 2003; Bytyqi et al. 2004; Kay et al. 2004; Godinho et al. 2005; Mumm et al. 2006). This scenario is especially plausible given observations of single ACs and GCs, imaged during IPL development. Though the gross sublamination of the population of *Pax6:mGFP+* AC neurites appears at 70 hpf, these neurites innervate their target sublaminae directly upon IPL innervation at roughly 55 hpf—they do not follow the exuberant growth, followed by refinement, pattern of development attributed to many neurites. Thus the *Pax6+* AC neurites choose their sublaminae prior to innervation by BCs. The gross appearance of the ON and OFF sublaminae depends on the lateral extension of these neurites, which creates the brightly labeled bands (Godinho et al. 2005). In contrast, individual *Brn3c:mGFP* labeled GCs use a variety of strategies to innervate the IPL. These include a biased projection to a region of the IPL that is further refined with time, direct targeting of one sublamina followed by outgrowth into another, non-adjacent sublamina, and, in a minority of cases, exuberant growth followed by modest refinement (Mumm et al. 2006). This circumstantial evidence can only be used to form hypotheses, in this case that ACs are an organizing force for GCs. More direct evidence has come from two mouse mutants—a *pancreatic transcription factor 1a (ptf1a)* mutant (Nakhai et al. 2007) and an *acetylcholinesterase (AChE)* knockout (Bytyqi et al. 2004). The *ptf1a* transcription factor is required for pancreatic differentiation, but also for the development of GABAergic cells in the mouse brain. In the retina of mouse *ptf1a* mutants, ACs fail to differentiate, and no IPL develops. A *ptf1a* mutant has since been identified in zebrafish and has the same phenotype (Duc Dong and Didier Stainier, unpublished results). This mutant provides direct evidence of the importance of ACs in initiating IPL formation. *AchE* knockout mice have the full complement of retinal neurons, but a subset of ACs which are cholinergic lack this molecule, and IPL sublamination is delayed and incomplete. Cholinergic ACs and the *Pax6*+ ACs described above are an overlapping population; both innervate the IPL early and define the first ON and OFF sublaminae. Based on the hypothesis that ChAT+ ACs act as a scaffold for IPL organization, two groups have tried to eliminate these cells with genetic techniques (Bansal et al. 2000; Reese et al. 2001). Neither saw significant changes, however, neither study eliminated these cells prior to their expression of *Choline acetyltransferase (ChAT),* which seems to be expressed after ON and OFF sublaminae have been established. *AChE* is expressed prior to *ChAT* in these cells, and, according to the phenotype of the knockout, is an important instructive cue for IPL sublamination.

These loss of function studies are valuable because they can lend both cellular and molecular insights, particularly when the mutated gene is expressed in a restricted subset of retinal cells. The time lapse observations published, and our own, unpublished observations, are not very informative because much sublamination appears to occur at roughly the same time and place. The truth is likely that the interactions defining sublaminae happen well before we can observe sublaminae, and so our best course to identifying mechanisms is to disrupt the system in single genes and assess the results.

References

Baier H, Klostermann S, Trowe T, Karlstrom RO, Nusslein-Volhard C et al. (1996) Genetic dissection of the retinotectal projection. Development 123: 415-425.

Bansal A, Singer JH, Hwang BJ, Xu W, Beaudet A et al. (2000) Mice lacking specific nicotinic acetylcholine receptor subunits exhibit dramatically altered spontaneous activity patterns and reveal a limited role for retinal waves in forming ON and OFF circuits in the inner retina. J Neurosci 20(20): 7672-7681.

Baye LM, Link BA (2007) Nuclear migration during retinal development. Brain Res.

Behrend O, Branoner F, Zhivkov Z, Ziehm U (2006) Neural responses to water surface waves in the midbrain of the aquatic predator Xenopus laevis laevis. Eur J Neurosci 23(3): 729-744.

Brockerhoff SE, Hurley JB, Janssen-Bienhold U, Neuhauss SC, Driever W et al. (1995) A behavioral screen for isolating zebrafish mutants with visual system defects. Proc Natl Acad Sci U S A 92(23): 10545-10549.

Bytyqi AH, Lockridge O, Duysen E, Wang Y, Wolfrum U et al. (2004) Impaired formation of the inner retina in an AChE knockout mouse results in degeneration of all photoreceptors. Eur J Neurosci 20(11): 2953-2962.

Chalupa LM, Gunhan E (2004) Development of On and Off retinal pathways and retinogeniculate projections. Prog Retin Eye Res 23(1): 31-51.

Desai AR, McConnell SK (2000) Progressive restriction in fate potential by neural progenitors during cerebral cortical development. Development 127(13): 2863-2872.

Dickson BJ (2002) Molecular mechanisms of axon guidance. Science 298(5600): 1959-1964.

Easter SS, Jr., Nicola GN (1996) The development of vision in the zebrafish (Danio rerio). Dev Biol 180(2): 646-663.

Easter SS, Jr., Nicola GN (1997) The development of eye movements in the zebrafish (Danio rerio). Dev Psychobiol 31(4): 267-276.

Famiglietti EV, Jr., Kolb H (1976) Structural basis for ON-and OFF-center responses in retinal ganglion cells. Science 194(4261): 193-195.

Gahtan E, Tanger P, Baier H (2005) Visual prey capture in larval zebrafish is controlled by identified reticulospinal neurons downstream of the tectum. J Neurosci 25(40): 9294-9303.

Godinho L, Mumm JS, Williams PR, Schroeter EH, Koerber A et al. (2005) Targeting of amacrine cell neurites to appropriate synaptic laminae in the developing zebrafish retina. Development 132(22): 5069-5079.

Goldsmith P, Harris WA (2003) The zebrafish as a tool for understanding the biology of visual disorders. Semin Cell Dev Biol 14(1): 11-18.

Jessell TM (2000) Neuronal specification in the spinal cord: inductive signals and transcriptional codes. Nat Rev Genet 1(1): 20-29.

Kay JN, Finger-Baier KC, Roeser T, Staub W, Baier H (2001) Retinal ganglion cell genesis requires lakritz, a Zebrafish atonal Homolog. Neuron 30(3): 725-736.

Kay JN, Roeser T, Mumm JS, Godinho L, Mrejeru A et al. (2004) Transient requirement for ganglion cells during assembly of retinal synaptic layers. Development 131(6): 1331-1342.

Livesey FJ, Cepko CL (2001) Vertebrate neural cell-fate determination: lessons from the retina. Nat Rev Neurosci 2(2): 109-118.

Mangrum WI, Dowling JE, Cohen ED (2002) A morphological classification of ganglion cells in the zebrafish retina. Vis Neurosci 19(6): 767-779.

Mumm JS, Williams PR, Godinho L, Koerber A, Pittman AJ et al. (2006) In vivo imaging reveals dendritic targeting of laminated afferents by zebrafish retinal ganglion cells. Neuron 52(4): 609-621.

Muto A, Orger MB, Wehman AM, Smear MC, Kay JN et al. (2005) Forward genetic analysis of visual behavior in zebrafish. PLoS Genet 1(5): e66.

Nakhai H, Sel S, Favor J, Mendoza-Torres L, Paulsen F et al. (2007) Ptf1a is essential for the differentiation of GABAergic and glycinergic amacrine cells and horizontal cells in the mouse retina. Development 134(6): 1151-1160.

Nelson R, Kolb H (2003) ON and OFF pathways in the vertebrate retina and visual system. In: Chalupa LM, Werner JS, editors. The Visual Neurosciences. Cambridge, MA: MIT Press. pp. 260-278.

Neuhauss SC (2003) Behavioral genetic approaches to visual system development and function in zebrafish. J Neurobiol 54(1): 148-160.

Neuhauss SC, Biehlmaier O, Seeliger MW, Das T, Kohler K et al. (1999) Genetic disorders of vision revealed by a behavioral screen of 400 essential loci in zebrafish. J Neurosci 19(19): 8603-8615.

Niell CM, Smith SJ (2005) Functional imaging reveals rapid development of visual response properties in the zebrafish tectum. Neuron 45(6): 941-951.

Nishiyama M, Hoshino A, Tsai L, Henley JR, Goshima Y et al. (2003) Cyclic AMP/GMP-dependent modulation of Ca2+ channels sets the polarity of nerve growth-cone turning. Nature 423(6943): 990-995.

Reese BE, Raven MA, Giannotti KA, Johnson PT (2001) Development of cholinergic amacrine cell stratification in the ferret retina and the effects of early excitotoxic ablation. Vis Neurosci 18(4): 559-570.

Schmitt EA, Dowling JE (1994) Early eye morphogenesis in the zebrafish, Brachydanio rerio. J Comp Neurol 344(4): 532-542.

Schmitt EA, Dowling JE (1999) Early retinal development in the zebrafish, Danio rerio: light and electron microscopic analyses. J Comp Neurol 404(4): 515-536.

Sewards TV, Sewards MA (2002) Innate visual object recognition in vertebrates: some proposed pathways and mechanisms. Comp Biochem Physiol A Mol Integr Physiol 132(4): 861-891.

Smear MC, Tao HW, Staub W, Orger MB, Gosse NJ et al. (2007) Vesicular glutamate transport at a central synapse limits the acuity of visual perception in zebrafish. Neuron 53(1): 65-77.

Stacy RC, Wong RO (2003) Developmental relationship between cholinergic amacrine cell processes and ganglion cell dendrites of the mouse retina. J Comp Neurol 456(2): 154-166.

Tessier-Lavigne M, Goodman CS (1996) The molecular biology of axon guidance. Science 274(5290): 1123-1133.

Ting CY, Lee CH (2007) Visual circuit development in Drosophila. Curr Opin Neurobiol 17(1): 65-72.

Xiao T, Baier H (2007) Lamina-specific axonal projections in the zebrafish tectum require the type IV collagen Dragnet. Nat Neurosci 10(12): 1529-1537.

Xiao T, Roeser T, Staub W, Baier H (2005) A GFP-based genetic screen reveals mutations that disrupt the architecture of the zebrafish retinotectal projection. Development 132(13): 2955-2967.

Chapter 2: Activity-independent assembly of retinal synaptic layers by cell-cell interactions

Linda M Nevin, Jeremy N Kay, Michael R Taylor, Herwig Baier

Abstract

The shape of neurite arbors is integral to the development of the nervous system—form influences function, and the placement of neurite endings determines partner choice. We have used genetics and pharmacology to uncover mechanisms regulating neurite arbor morphology in the developing zebrafish (*Danio rerio*) retina. We first characterized in detail a synaptic region—the inner plexiform layer (IPL)—in which the cell-type specific branching patterns of amacrine cell (AC), bipolar cell (BC), and ganglion cell (GC) neurites generate a stack of at least nine sublaminae. We next investigated the role of visual experience and neural activity in IPL development. *brudas,* an *N-maleimide sensitive factor (NSF)* mutant lacking photoreceptors, shows wildtype IPL sublamination, as do larvae reared in the dark or with a pharmacological blockade to BC signaling (APB). Indeed, complete elimination of synaptic transmission with Botulinum toxin B (BtTxB) does not effect IPL organization. To identify relevant players, we completed a mutagenesis screen and found five mutations—*notorious (noto), spellbound (spel), moonraker (mra), asphalt jungle (asph),* and *cape fear (cfe)*—affecting IPL development. In *noto* and *mra*, sublamination errors are shared across classes of neurites; we show that shared phenotypes result in part from cross-talk between neurons. In *noto* mutants, poorly

sublaminated GCs provide aberrant cues which alter the sublamination of AC and BC neurites—demonstrating that GCs can instruct other IPL neurites. In *mra*, mutated in *DEAD-box protein 19 (ddx19),* the sublamination of many GC and AC neurites is lost completely. *ddx19* may be important for mRNA nuclear export; *mra/*wildtype chimeras suggest that a global signaling loss, from within neurons and from neighbors, cause *mra* neurites to branch nonspecifically. Together, these data support a model in which IPL sublamination requires activity-independent intercellular signaling.

Introduction

Laminar arrays of neurites are a common motif in nervous system organization, from the *Drosophila* visual system to the mammalian cortex. The true purpose of arranging neurites into laminae is subject to conjecture, but is likely an organizational strategy to appropriately pair pre- and post-synaptic neurites. In cases where individual neurons innervate more than one lamina, the spatial separation between arborizations may be important for the functional properties of the neuron. We are interested in the development of synaptic laminae because of their prominence in neural systems and because they are a tractable proxy for the development of proper neurite morphology and appropriate synaptic connections.

The vertebrate retina is a strictly laminated structure, and follows the same basic organizational plan from teleosts to primates (Pujic and Malicki 2004). In a cross section of the inner plexiform layer (IPL) of the retina, amacrine cell (AC), bipolar cell (BC), and ganglion cell (GC) neurites are organized into a stack of as many as ten sublaminae. The neurites innervating the IPL are organized based on functional properties; for example, BCs have been shown to select their target sublaminae in the IPL based on whether they respond to light onset or offset, and whether they receive input from rods or cones (Connaughton 2001; Nelson and Kolb 2003). The sublaminar choice of a neurite may be an important factor in preserving the ‘labeled lines’ required to transmit distinct visual signals. If so, the development of intact vision requires tight regulation of IPL sublamination.

The cellular interactions that assemble IPL synaptic layers are just beginning to be elucidated. Three recent time-lapse imaging studies in the larval zebrafish have demonstrated that developing ACs, BCs, and GCs use diverse strategies to locate their appropriate sublamina. A subset of ACs innervate the IPL early, and project straight to their target sublaminae, in a process that may depend, at least transiently, on signals from GCs (Kay et al. 2004; Godinho et al. 2005). A subset of BCs was shown to sublaminate in by overgrowth and refinement (Schroeter et al. 2006). Finally, a labeled subset of GCs employed a number of sublamination strategies, including direct innervation of a target sublamina, overgrowth and refinement, and switching from one specific sublamina to another in the course of imaging (Mumm et al. 2006). This is in contrast to the strategy used in all mammals studied to date, in which early GC dendrites elaborate across the IPL and are subsequently refined to sublaminae in an activity dependent manner (Bodnarenko and Chalupa 1993; Bodnarenko et al. 1995; Chalupa and Gunhan 2004).

It has not previously been clarified what role, if any, visual experience and retinal activity play in zebrafish IPL development. We explored the role of retinal activity in shaping IPL sublaminae using pharmacological tools and *brudas (bru)*, which lacks photoreceptors and which we identified as an *N-maleimide sensitive factor (NSF)* mutant. NSF is a cytosolic ATPase important for vesicle fusion with the plasma membrane—and hence, synaptic transmission. Though zebrafish retinal neurites rely on intercellular signals to select sublaminae (see below), these signals do not depend on visual experience nor synaptic transmission. Most convincingly, injection of Botulinum toxin type B (BtTxB) completed eliminated transmission in the retina, but did not affect IPL sublamination.

The molecular mechanisms underlying IPL development are not yet known, although certain cell adhesion molecules are known to mediate sublayer formation. N-cadherin (Cdh-2) and R-cadherin (Cdh-4) are important for overall retinal organization and IPL neurite sublamination in the zebrafish, and sidekick1 and -2 have been shown to mediate sublaminar selection in the chick IPL (Yamagata et al. 2002; Masai et al. 2003; Babb et al. 2005). A mouse knockout has demonstrated that acetylcholinesterase, expressed by an AC class known as the starburst cells, is required to maintain the timing of IPL sublamination and to prevent the formation of spurious sublaminae (Bytyqi et al. 2004). These identified factors do not account for the number of sublayers observed in the vertebrate IPL, nor do they speak to the diverse strategies that retinal neurons use to sublaminate.

To uncover the cellular and genetic mechanisms that govern IPL sublamination in the zebrafish, we conducted a forward mutagenesis screen. The forward genetic approach has proved extremely useful for uncovering the molecular mechanisms that guide axons to their broader target area (Tessier-Lavigne and Goodman 1996; Dickson 2002). More recent work in *Drosophila* has now begun to yield insights into synaptic choices within a target area (Clandinin and Zipursky 2002; Ting and Lee 2007). These prior studies provide ample precedent that neurite development can be elucidated using forward genetics.

To create an enriched pool of mutants, families carrying random (ENU induced) mutations were screened for altered visual background adaptation (VBA), a retina-dependent response in which zebrafish camouflage to ambient light. Fish that appear blind in this assay are likely, though not guaranteed, to show visual system anatomy defects (Muto et al. 2005). Here we asked whether any showed laminar targeting defects in the retina. The forty VBA-deficient mutants were sectioned and immunostained to label the neurites of molecularly distinct sublaminae—our panel of markers allowed us to distinguish nine sublayers in the IPL of 5 days post fertilization (5 dpf) larvae. We report here the discovery of three mutants with IPL sublamination defects in an otherwise wildtype retina, and two mutants with retinal organization defects which lend insight into the mechanisms of IPL development. In each case, we have characterized the mutant phenotype and exploited the mutant as an experimental tool. We show that IPL neurons rely on intercellular signals to shape their neurite arbors, and that these signals can maintain the relative organization of sublaminae in an altered IPL. Further, GCs have a privileged role in instructing the lamination of other retinal neurites. In addition, we identify *DEAD-box 19 (ddx19),* the mutated gene in *mra,* as an important player in IPL development.

Results and Discussion

Cell type specific markers demonstrate precise stratification of synaptic connections in the IPL

The antibodies used in this study were selected from known retinal cell type markers in the mouse and other vertebrate models. As previous zebrafish studies have shown, the zebrafish retina is organized quite similarly to that of other vertebrates (Yazulla and Studholme 2001; Goldsmith and Harris 2003) (Fig 1). As has been documented in the adult zebrafish (Yazulla and Studholme 2001), PKC, ChAT, and parvalbumin antisera label a population of BCs and two populations of ACs, respectively, in the INL (Fig 1 B, G, L). PKC+ neurons are identifiable as BCs because they extend processes to both the outer plexiform layer and the IPL. Based on position and size, Yazulla and Studholme (2001) have identified these as the ON-responsive BCs, and their projections are a good marker of the ON portion of the IPL. ChAT antiserum brightly labels a small, presumably cholinergic population of INL ACs. Many of the ChAT+ ACs have a characteristic elongated shape with a wide, labeled process extending from the cell soma to the IPL. Parvalbumin positive ACs are more numerous and have a rounder shape than the ChAT+ cells. As in rodents (Sanna et al. 1993), the zebrafish has a population of parvalbumin positive neurons in the ganglion cell layer; these cells have not been definitively established as GCs or ACs, but are likely to be ACs because parvalbumin immunoreactivity is not seen in GC axons. Zrf3, a monoclonal antibody from the ZFIN collection, is a reported marker of glial and neurite fibers (ZFIN). While this antibody labels the entire IPL, four sublaminae stain more brightly (Fig 1H). We do not know the cell type origin of the brightly-staining fibers. In addition to immunolabeling, we crossed some mutants into transgenic backgrounds to label specific retinal cell types. The *Brn3c*^{273} *(Brn3c)* transgene insertion labels about 50% of GCs (Xiao et al. 2005) (Fig 1C); *Pax6 (Pax6)* is another transgenic line in which a small population of ACs are labeled (Fig 1M). Some *Pax6*+ ACs co-express ChAT (Kay et al. 2004), and some co-express parvalbumin.

Each of these labeled cell types projects neurites to two or more sublaminae of the IPL. To determine which neurites share IPL sublaminae, we performed double-labeling experiments with our pool of markers. In addition, we measured the positions of sublaminae relative to the IPL edges. Sublamina position can be described as a percentage of the total IPL width. By this convention, the innermost edge of the IPL is at 0%, and the outermost at 100%. Mumm *et al* characterized the five *Brn3c*+ sublaminae as s10 (the sublaminae located 10% of the IPL width from the innermost edge), s40, s55, s70, and s90 (2006) (Fig 1C). These sublaminae are not as distinct as the others described here, probably because many zebrafish GC dendrites ramify broadly across the IPL rather than restricting to sublaminae (Mangrum et al. 2002; Mumm et al. 2006). Figure 2 is a schematic of the 5 dpf retina, including the cell types we examined and the nine IPL sublaminae which are their projection targets. For example, parvalbumin positive neurons of the INL and GCL project to three IPL sublaminae—two in the inner and one in the outer IPL (Fig 1A-E). Based on their position, we refer to these parvalbumin+ bands as s25, s45, and s85 (percentages are means based on 9 measurements from 3 larvae; standard deviations <= 3, rounded to the nearest 5). This co-localization study enables us to infer which neurons might form synapses in the various sublaminae of the IPL. ChAT+ and parvalbumin+ ACs may synapse in sublaminae s25 and s85, and *Brn3:mGFP+* GCs may synapse with ChAT+ ACs in s40 and s70. The ChAT+ starburst ACs of the mammalian retina are known to synapse with GCs and other ACs to mediate direction selectivity (Famiglietti 1983; Voigt 1986; Millar et al. 1987; Brandon 1991; Sandmann et al. 1997; Cuenca et al. 2003). PKC+ bipolar cells likely synapse with *Brn3c*+ GCs in s10 and s55. The BC/GC synapse is the fundamental conduit of light information from outer to inner retina. In each case, these putative connections are consistent with the known wiring of the vertebrate retina.

In some sections, closely apposed bands of one type may appear as one; this is often the case for ChAT, zrf3, and *Pax6*+ sublaminae. The fine sublamination of ChAT, zrf3, and *Pax6* positive bands can be seen under higher magnification in some images. In addition we show the IPL localization of neurites from tyrosine hydroxylase (TH) positive ACs, a sparse class of neurons not used in our screen (Supp Fig 1). These innervate the very edges of the IPL, targeting s10 and s90.

By sectioning and immunostaining, we can see whether each cell type's neurites have developed appropriately, such that they have found homotypic neurites, co-localized with heterotypic partner neurites, and nested properly between neighboring sublaminae. The clear sublamination of neurites into bright bands enables us to assess the effects of single gene mutations on laminar targeting of developing axons and dendrites.

Lamination of IPL does not require visual experience nor bipolar cell signaling

Data from mammals indicate that GC dendrites require visual input and BC signaling to target the appropriate sublaminae. By adulthood, 90% of mammalian GCs are monostratified—projecting to either the ON or OFF portion of the IPL, but not both. In mice, dark rearing alters the distribution of GC dendrites and compromises their ability to sublaminate in the OFF IPL (Xu and Tian 2007). In cats, treatment with the bipolar-cell mGluR6 antagonist amino-phophono-butyrate (APB) leaves GC dendrites unrefined, and bistratified to the ON and OFF IPL (Gunhan et al. 2002). Morphological studies of GC dendrites in adult zebrafish revealed a surprising species difference: most zebrafish GC dendrites are bi- or multistratified, arborizing in both the ON and OFF portions of the IPL (Mangrum et al. 2002). Further, a developmental time course study has established that most zebrafish GC dendrites do not follow the expected growth/refinement pattern of development. Many target their destination sublaminae directly, others add branches to new sublaminae and retract branches from other sublaminae as they develop (Mumm et al. 2006).

We have tested the role of activity in IPL development in several ways. First, we simulated the mammalian experiments by dark rearing, and by blocking ON bipolar cell activity with APB added to the embryonic media. Neither of these treatments alter IPL sublamination of *Brn3c*+ GC dendrites, or parvalbumin+ and PKC+ neurites (Fig 3). Dark-rearing blocks the develop of the VBA; dark reared fish returned to the light fail to condense pigment granules in the skin for several hours, though the OKR is intact. Five dpf APB-reared fish have an intact VBA and OKR, but fish treated with APB at 7dpf are VBA and OKR negative (data not shown). Some change in the vision system between 5 and 7 dpf must account for the changes in behavioral response to APB. Both dark-reared and APB-treated fish are active swimmers and have an intact acoustic startle response. In a previous study from our group, and subsequently confirmed by us (data not shown), our APB treatment is sufficient to block the majority of the B-wave of the electroretinogram (ERG) recorded from the 5 dpf larvae (Page-McCaw et al. 2004).

To further examine the importance of visual input, we exploited the previously identified *bru* mutant. In 2002, Doerre and Malicki reported two alleles of *bru* in a study of mutants with photoreceptor loss. This study established that *bru*^{m148} mutant photoreceptors fail to develop proper inner or outer segments, and die quickly after exiting the cell cycle. In 2003, Goldsmith *et al* reported the discovery of an identical mutant, then called *ebony*, which has since been shown by complementation cross to be an allelic mutation. Our primary mutagenesis screen (see below) yielded four new alleles of *bru,* which are easily spotted due to dark pigmentation, progressive paralysis, and larval lethality (Doerre and Malicki 2002; Goldsmith et al. 2003). These mutants enabled us to determine whether functioning photoreceptors are required for the proper development of IPL sublaminae. Likely because of the increased cell death in the *bru* retina, many sections can show a slightly degraded IPL. However, by sectioning many mutants, for each of the cell type markers parvalbumin, PKC, and *Brn3c*, we identified at least one example with a perfectly wildtype IPL (Fig 4). Even in those sections with deterioration, gross morphology of sublaminae was preserved (Fig 5). From this we conclude that photoreceptor function is dispensable for the formation of IPL sublayers.

bru/NSF mutants and Botulinum toxin type B injections reveal synaptic transmission is not required for IPL sublamination

The *bru* locus was mapped to a small region of LG 3, which includes the full coding region of zebrafish *NSF*. Because *bru/eby* mutants share the phenotypes of two published *NSF* mutants (*st25* and *st53*) (Woods et al. 2006), we hypothesized that *bru,* too, encodes NSF. This was confirmed by complementation crosses. NSF's function as a regulator of membrane fusion is conserved from yeast (the yeast homolog is SEC18) to mammals (Wilson et al. 1989; Bennett and Scheller 1993). In its best understood role, NSF is required to disassemble SNARE complexes after membrane fusion, freeing the SNAREs to form new complexes (Kawasaki et al. 1998; Tolar and Pallanck 1998; Littleton et al. 2001). SNAREs (SNAP receptors) are membrane-associated proteins each with a cytosolic α-helix, which can associate with other SNAREs in a parallel, coiled-coil configuration to mediate membrane fusion. NSF associates with membranes by interaction with assembled SNARE complexes which are bound to its partner, SNAP (soluble NSF attachment protein) (Sollner et al. 1993). An NSF-induced conformational change in the bound SNAREs may cause the dissolution of the complex (Zhao et al. 2007). To identify mutations in *bru/NSF*, we sequenced the *NSF* coding regions for three of the four alleles found in our recent screen (*s364, s501,*and *s300)* and a *bru* allele identified by another group (*tw212*) (Doerre and Malicki 2002). Our new alleles had no coding region mutations, but *bru*^{tw212} mutant *NSF* was shown to lack exons 4 and 5 of the 20 exon cDNA (Fig 6). The polypeptide sequence for the two excised exons was compared to the published sequence of *Cricetulus griseus NSF* (NCBI Accession P18708), which has been structurally characterized by X-ray crystallography. Exons 4 and 5 correspond to residues 83 through 171 of the *Cricetulus* published sequence (84% protein identity). The excision eliminates 74% of N-terminal subdomain N_B; the groove between subdomains N_A and N_B is the putative binding pocket for SNAP (Yu et al. 1999).

Gene identification elucidates the failure of *bru* photoreceptors to develop properly; photoreceptors require massive NSF-dependent transport of opsin-containing vesicles from the Golgi to the outer segment (Besharse and Pfenninger 1980; Papermaster et al. 1985). Though it is not clear why, the failure of opsin transport to the outer segment has previously been shown to induce apoptosis (Tam and Moritz 2007). Of course, were there a complete knockout of NSF function, the larvae should fail to develop at all. The zebrafish genome contains two *NSF* orthologs (Woods et al. 2006), likely due to a genomic duplication which occurred after the divergence of class Actinopterygii (the ray finned fishes, including zebrafish) from class Sarcopterygii (lobe-finned fishes, amphibians, reptiles, and mammals) (Taylor et al. 2001). We suspect that *bru* mutants are viable and motile in the early larval stages due to maternal RNA contributions or compensation by NSFb.

As attested by progressive paralysis in the mutants, synaptic transmission in *bru* is likely impaired. Because *NSF* is expressed throughout the retina (Woods et al. 2006), we suspect that it is important for synaptic communication between retinal cells. Due to the lack of photoreceptors, we cannot test this hypothesis directly by electroretinogram (ERG) recording. However, the *bru* phenotype was a compelling hint that perhaps synaptic transmission of any kind is irrelevant to IPL development. We tested this possibility by injection at the single cell stage of BtTxB, a clostridial toxin which eliminates synaptic vesicle fusion by cleaving the v-SNARE synaptobrevin (Pellegrini et al. 1995). BtTxB injected larvae are immobile throughout development, and most die by 5 dpf. Those that survive tend to develop edema. From surviving larvae at 5 dpf, we sorted those with zero motility from those that could show a slight startle movement when probed. These paralyzed larvae were tested for light responses by ERG recordings, alongside uninjected controls. Fig 7 shows an example of an injected larva with an intact photoreceptor response, known as the A-wave, but a complete elimination of the B-wave, which is representative of BC activity. As shown in Fig 3, IPL organization of parvalbumin+, PKC+, and *Brn3c*+ neurites is unaltered in treated larvae (n = 15, including the larva recorded in Fig7B). This finding, along with the dark-rearing and APB results, is surprising in light of data from mammalian systems, in which activity appears to be an important regulator of IPL refinement.

brudas/NSF ***and eternal sunshine mutants aberrantly localize the zrf3 antigen to cell bodies of the INL***

In addition to the loss of photoreceptors, cell bodies of the *bru* INL strongly express zrf3 immunoreactivity, which is confined to the IPL in 5 dpf wildtype larvae. Our VBA screen uncovered a second mutant, *eternal sunshine (eter)*, with phenotypes very similar to *bru,* including inviability by 8 dpf, lack of a swimbladder, the absence of photoreceptors, increased neuronal cell death, and this ectopic localization of zrf3 immunoreactivity (Fig 8). *eter* mutants are distinct from *bru* in that the increase in cell death is more pronounced, and the eyes are small by 5 dpf, yet the motility phenotype is less severe—*eter* mutants are sluggish but do not become paralyzed (data not shown). It is possible that the *eter* gene product shares a pathway with NSF.

We suspected that the extra zrf3 immunoreactivity might represent a change in the expression profile of Müller glia, which are known to de-differentiate into stem cells when photoreceptors are damaged (Bernardos et al. 2007). However, we observed no change in the expression of glutamine synthetase (a marker of differentiated Müller glia) in INL neurons in the *bru* retina (Fig 8D,E). To test the possibility that photoreceptor loss upregulates INL zrf3 expression without affecting glutamine synthetase, we investigated the zrf3 phenotype of *modern times (moti)*, a mutant discovered in our group's screen for mutants with optomotor behavioral deficits. *moti* shows a severe loss of photoreceptors by 7 dpf and is non-responsive to both the OMR (optomotor response) and OKR stimuli (M Orger, M Smear, H Baier, unpublished results). Five dpf *moti* larvae show photoreceptor cell death by TUNEL but no INL expression of zrf3 (Fig 9A,E). Based on the *moti* phenotypes, we conclude that photoreceptor loss does not lead inevitably to zrf3 misexpression. Additionally, *moti* provides evidence that dying photoreceptors do not cause a disintegration of the organized IPL (Fig 9B-D, F-H). Based on *bru* and *moti,* neither the development of functioning photoreceptors nor their survival influence IPL organization.

We next speculated that the zrf3 immunoreactivity could be the mark of an immature retina; however, labeling of 3 and 4 dpf retina did not support this hypothesis. Zrf3 immunoreactivity is restricted to the IPL at these earlier ages (data not shown). As it is not known what the true antigen of zrf3 antisera is, we can only conjecture that the *bru* and *eter* mutations cause a change in cell type specific expression or the failure of transport of the labeled protein from INL cell bodies to their neurites. As NSF is important for the transport of molecules to the synapse, the compromise of transport function is a likely explanation.

A behavior-based mutagenesis screen uncovers five loci essential for IPL neurite sublamination and/or retinal development

We hypothesized that mutations affecting visual performance would, in some cases, also affect the anatomy of the visual system. We first pre-screened all VBA-impaired mutants to exclude those with gross defects in retinal organization (see methods). These were not characterized in detail, with the exception of *asph*, which was kept for its intriguing phenotype of ectopic plexiform regions. We next used our panel of antibodies to screen for mutants with perturbed IPL sublayers. Of forty VBA-impaired mutants screened by immunohistochemistry, three—*noto, spel,* and *mra*—were identified with defects in IPL sublamination in an otherwise well-organized retina. In addition to the VBA phenotype, all three of these mutants have no OKR (data not shown), suggesting that the defects in connectivity we observe are relevant to visual function. New alleles of the *bru/NSF* mutant, which lacks photoreceptors, were identified, and explored in detail to assess the role of photoreceptor and NSF function in IPL development (see above). In addition, one mutant (*cfe)* was identified in which neuronal cell body positioning in the retina was altered without perturbing IPL organization. With the exception of *cfe*, for which 5 alleles were found, only a single allele of each new gene was uncovered in our screen. The phenotypes of all mutants are summarized in Tables 1 and 2.

notorious ***is required for fine IPL sublamination of all GCs, ACs, and BCs examined***

In *noto* mutants, the IPL is of normal width, and grossly sublaminated, as shown in Figure 10. *Brn3c* expressing GCs project dendrites to approximately the right place, but the separation between layers is compromised—five sublaminae are blurred into three fatter bands (Fig 10A,B). Parvalbumin positive neurites are also grossly targeted to the correct space, but the inner two bands are indistinct, creating one thick band (Fig 10C,D). PKC+ BC terminals cover the inner portion of the IPL, but are not well divided into sublaminae—at best, two rows of terminals can be distinguished (Fig 10G,H, Fig 12F). It appears that the outermost sublamina of PKC+ terminals, s55, is sparsely populated, which can be seen in co-labeling with *Pax6* (Fig 11B,D,F)*.* On close inspection, the finer separation of *Pax6* labeled sublaminae is lost in *noto,* and the two pairs of ChAT sublaminae are condensed to two single bands (Fig 10M,N and Supp Fig 2). As the IPL continues to develop after 5 dpf, the sublamination defects in *noto* mutants become more pronounced (Fig 11). In wildtype, the space between bands grows wider while sublaminae appear to maintain their width. In the 7dpf *noto* IPL, parvalbumin and *Pax6* labeled sublaminae have grown more diffuse, and AC neurites have spread exuberantly into the space between their innermost sublamina and the GCL. PKC+ terminals appear somewhat more segregated, but the outermost band, s55, still has few terminals. These defects are not the result of increased cell death (mean number of TUNEL+ cells per section: *noto*, 1 +/- 1.24 using the 95% confidence interval, n = 5 larvae, wildtype, 0, n=4 larvae).

Mistargeted GCs, ACs, and BCs can maintain local relative positioning

Our double-labeling experiments revealed that while the *noto* gene is required for the confinement of many neurites to sublaminae, neurites maintain their relative positions independent of *noto* function. As shown in Fig 10A-F, parvalbumin+ and *Brn3c+* neurites are closely apposed, but not overlapping, in both the wildtype and *noto* IPL. This preservation is striking because two bands of *Brn3c+* neurites (s40 and s55), which flank a parvalbumin+ band (s45) in wildtype, are merged in *noto,* yet the two types of neurites do not overlap. The parvalbumin+ sublaminae are rearranged in a complementary fashion, such that a single merged band of parvalbumin+ neurites in the proximal IPL lies between two diffuse bands of *Brn3c+* neurites. Double-labeling at 7dpf also demonstrate this principle with PKC+, *Pax6+,* and parvalbumin+ neurites—even as the sublaminae become more diffuse, neighbor neurites maintain their separation, indicating that some synaptic positional information does not rely on the *noto* gene (Fig 11J). The mutation in *noto* thus appears to cause chronic dysfunction in the neurites' ability to confine to sublaminae, yet some cues—perhaps attractive or repulsive signals between neurites—are strong enough to maintain relative positioning.

The **notorious** *mutation reveals an instructive role for GCs in IPL sublamination*

Subsequent experiments with the *noto* mutant demonstrated that GCs can act instructively to alter the sublamination of other neurites. We reasoned that if the gene acts to alter the sublamination of GC neurites, which in turn alter the organization of other retinal neurites, the removal of GCs from the mutants would rescue the remaining sublamination phenotypes. This hypothesis is testable because of the available *lakritz (lak)* mutant, one of the first VBA mutants studied. *lak* mutants show a very specific loss of all GCs, due to a null mutation in the bHLH transcription factor Ath5, which is required for GC neurogenesis (Kay et al. 2001). In *lak* mutants, the remaining IPL neurites are delayed in sublamination by one day, but recover the wildtype pattern with some disruptions along the IPL (Kay et al. 2004). *noto/lak* double mutants were generated, in effect genetically removing GCs from *noto*. Double mutants were identified by dark pigmentation, loss of GCs (visualized using *Brn3c),* and the absence of a swimbladder (*lak* single mutants have a swimbladder; *noto* mutants do not). In the ten 6 dpf *noto/lak* double mutants sectioned, all neurites examined, parvalbumin+, ChAT+, PKC+, and zrf3+, sublaminate as in *lak*—that is, in a wildtype pattern with disrupted regions. Figure 12 shows the contrast between *noto* mutant sections at 6 dpf and *noto/lak* mutant sections at the same stage (ChAT not shown). Unlike in *noto* single mutants, the *noto/lak* IPL sublaminae are crisp and well separated. The experiment demonstrates that the *noto* phenotypes of these classes of ACs and BCs result from the influence of aberrant GCs. To our knowledge, this is the first non-circumstantial evidence the GCs are able to instruct other IPL neurites.

The* spellbound *gene is required for parvalbumin+ and PKC+ neurite sublamination in the retina

spel has the most subtle layering defects of any mutant found in the screen. Mutant parvalbumin+ neurites project to three refined sublaminae, as in wildtype, but the middle band (s45) appears faint and discontinuous rather than smooth (Fig 13A,D). This phenotype might be caused by neurites that fail to branch within the sublamina, or by a change in the expression level or protein distribution of parvalbumin. As shown in Fig 13G,J, the s40/45 bands of *Pax6* GFP immunoreactivity are brightly and smoothly labeled in *spel* mutants, as in wildtype. However, the fine subdivision of the two bands is lost in *spel* (Fig 13H,K), suggesting that the *spel* phenotype is not specific to parvalbumin protein, but rather reflects a defect in the s40/s45 layers of the IPL. PKC+ BC terminals are poorly organized into bands despite appearing as numerous as their wildtype counterparts (Fig 13B,E). These findings indicate that the *spel* gene is required for targeting of neurites to specific sublaminae, and possibly a broader region of the ON IPL where the PKC+ BCs terminate. The reasons for the targeting defects seen in this mutant are not yet clear; one possibility is that lack of s45 innervation by parvalbumin+ ACs leads to defects in *Pax6*+ and PKC+ neurite targeting.

Although *spel* mutants have very subtle and specific defects in IPL sublaminar targeting, behavioral tests show them to be almost completely blind (data not shown). This raises the possibility that incorrect sublaminar choices by retinal interneurons may lead to a severe visual deficit. The only other retinal phenotype we were able to discern, aside from the lamination defects, was mild ectopic zrf3 localization to AC cell bodies (Fig 13F), which is unlikely to explain the vision phenotype. Further study will be necessary to determine whether the requirement of the *spel* gene for vision is due to its developmental role in sublamination.

Mislocalized neurons in* asphalt jungle *mutants project to ectopic plexiforms regions in the GCL

Sections of the *asph* eye at 5 dpf appear quite different from others in this study because the eye is small, lacks a lens, and has GCL organizational phenotypes. Some larvae show the double arc IPL phenotype seen in other small-eyed fish (Wehman et al. 2005). GCL neurons show dysplastic growth into the anterior chamber, where the lens resides in wildtype. Parvalbumin, PKC, and *Pax6* positive neurons are present in the overgrown GCL, and many project to ectopic IPL-like regions, labeled with zrf3 in Fig 14A,B. Ectopic plexiform regions were observed in the GCL of 10 out of 11 mutant fish, versus 0 out of 5 wild type siblings, and not seen in any other fish. Ectopic plexiform layers exist as branches from the native IPL, nested inside and parallel to the native IPL, or as island patches within the GCL. In some cases, the native IPL is disrupted as neurites exit and join an ectopic plexiform region (Fig 14F-J).

The division of cell body from neuropil regions is not limited to the *asph* retina, and is therefore not likely a result of the lost lens. In the mutant tecta shown in Supp Fig 3, a patch of ectopic neuropil appears in the cell body region of one larva, and a group of cell bodies invades the neuropil in another. A wild type section has a clear distinction between the neuropil and the cell body region. The phenotype of disorganized neuropil localization occurs less often in the tectum (2 out of 6 mutant fish, versus 0 out of 3 wild type siblings) than in the retina, but has never been seen in any other sectioned larva.

The phenotypes of *asph* are quite reminiscent of those of the “dwarf” mutants, which carry known mutations in various laminins (Semina et al. 2006; Zinkevich et al. 2006; Biehlmaier et al. 2007; Lee and Gross 2007). The fourteen known laminin (lam) proteins are key components of the basement membranes of epithelial structures. The retina has a number of basement membranes separating cells into distinct layers, including the lens capsule (surrounding the lens), the inner limiting membrane (between the GCL and the vitreum), and the outer limiting membrane (between photoreceptors and pigment epithelium) (Biehlmaier et al. 2007; Lee and Gross 2007). In the published *bashful(bal)/lama1* mutant, the lens capsule and inner limiting membrane fail to form properly, causing inner retinal defects similar to those of *asph* (Biehlmaier et al. 2007). *asph* mutants share the short, curved body phenotype of the "dwarf" mutants. Therefore we strongly suspect that the *asph* mutation lies in a component of the basement membrane, and may well be allelic to a previously published laminin mutation.

The *asph* mutant provides an interesting extension to our prior study of IPL sublamination in *lak* mutants. In the absence of GCs, AC neurites first form a flawed, jagged IPL too close to the inner limiting membrane. As the *lak* retina matures, some ACs migrate into the GCL and the IPL repositions to its correct location; many of the flaws in its shape and order are corrected by 6 dpf (Kay et al. 2004). This *lak* data establishes that GCs have a transient role in IPL localization, perhaps by creating a barrier preventing AC neurites from extending to the inner limiting membrane. In *asph*, the GCL is dysplastic, and contains aberrant neurons of various types. In a number of cases shown, AC neurites of the IPL dive *en masse* into the GCL, leaving an interruption in the native IPL (e.g., Fig 14F). In others, the inner band of *Pax6* immunoreactivity diverges from the IPL, while the outer band stays the course; in these cases, the IPL appears 'unzipped' (e.g., Fig 14G,H). This suggests that the organization of the GCL, not simply its very presence, is necessary to direct AC neurites to the native IPL. The synaptic layering of the native mutant IPL is normal, so clearly the gene mutation does not affect the ability of these neurites to sublaminate once they innervate the correct region. However, the ectopic plexiform layers appear not to be at all organized with respect to any of our markers (Fig 14D), though they represent the convergence of many homo- and heterotypic neurites. Perhaps these plexiform regions lack for the perfect combination of neurites to build a sublaminated IPL. Alternatively, they may be something unique about the position of the native IPL that drives its sublamination.

Mislocalized neurons in **cape fear** *mutants do not disrupt the sublamination of the IPL*

We include mention of *cfe* here, despite its wildtype IPL, because in these mutants an altered retina develops perfect or near perfect sublamination. As discussed above, *bru*, which lacks photoreceptors, can develop intact IPL bands. The partial recovery of *lak* sublamination in the absence of GCs is an indication that IPL sublamination has a number of compensatory mechanisms which can overcome grave changes in the retina. In *cfe*, parvalbumin+ neurons of the GCL are scattered toward the lens, rather than closely apposed to the IPL as in wildtype. Despite this organizational defect, parvalbumin+ neurites are properly confined to the three wildtype sublaminae (Supp Fig 4). PKC+ bipolar cell neurite sublamination is also normal (data not shown). The formal possibility that neurons of the retina project neurites a pre-determined distance, which coincides with the proper IPL band, is most plausible to the parvalbumin neurons of the GCL. In wildtype, these neurons are in a stereotyped position—always closely apposed to the IPL. However, *cfe* establishes that these neurons can compensate for a change in position, and likely use positional cues in the IPL and/or cell-cell interactions to sublaminate.

Compromised **ddx19** *function leads to a failure of IPL sublamination in* **moonraker** *mutants*

In contrast to *noto,* in which aberrantly sublaminated neurites maintain their relative positioning, *mra* mutant neurites make varied sublamination errors that undo the exclusive co-localization of partner neurites. Parvalbumin+ and PKC+ neurites maintain their refined projections to thin IPL bands, but the pattern of projection is altered—the parvalbumin+ ACs project to two sublaminae, instead of three, while PKC+ BCs project to a single sublamina instead of three (Fig 15C-F). These neurite defects are consistent with the most obvious *mra* phenotype, which can be seen in a simple nuclear stain; the IPL is strikingly thin. In contrast to the PKC+ and parvalbumin+ neurites, *mra Pax6+* and *Brn3c+* neurites show a profound loss of IPL sublamination—the GFP immunoreactivity fills the IPL (Fig 15G-J). We suspected that the phenotype of *Pax6+*and *Brn3c+* neurites resulted from exuberant branching outside of target sublaminae. To examine individual cells, we generated chimeras by blastula-stage transplantation from *Pax6* transgenic donors into unlabeled hosts. *Pax6+* neurons are more tractable than *Brn3c+* GCs for assessing neurite arbor morphology because, in wildtype, their neurites are more tightly confined to sublaminae (Kay et al. 2004; Godinho et al. 2005; Mumm et al. 2006). We generated a set of 82 chimeras, representing each possible combination of wildtype and *mra* donors and hosts. To compare *mra* and wildtype neurite arbors in the IPL, we cryosectioned fixed chimeras for which the donor and host were of the same genotype. As shown, wildtype *Pax6+* neurites (in a wildtype host, Fig 17A-C) clearly sublaminate, while equivalent *mra* neurites (in a mutant host, Fig 17F) are spread across several sublaminae. In these neurons, a reduction of *ddx19* function results in an overgrowth of neurites, outside the bounds within which they are usually confined. Thus, the *mra* mutation has distinct effects on different retinal neurons. For parvalbumin+ ACs and PKC+ BCs, the IPL sublamination pattern is different, but still refined to single bands, while for *Pax6+* ACs and *Brn3c+* GCs, IPL sublamination is lost. The *mra* gene product must therefore meet several criteria. First, it is likely expressed in multiple, or all, retinal cell types, in order to influence the different types distinctly. Second, the gene must have a molecular role that is upstream of varied aspects of neurite targeting, such that its loss of function might cause altered sublaminar choice or exuberant branching. And finally, the gene's function must occlude the mechanisms that IPL neurites in *noto* use to respond to aberrant targeting and maintain relative positioning in the IPL.

We used positional cloning and gene sequencing to identify the *mra* locus. *mra* carries a a T→A transversion in the coding sequence of the RNA-binding ATPase *DEAD-box protein 19 (ddx19,* (NCBI BC044541). The mutation results in the substitution of asparagine (N) for the native isoleucine (I) at residue 143 of the 487 amino acid protein, a position which is conserved from yeast to vertebrates (Fig 16). DEAD-box proteins share a number of sequence motifs, numbered I through VI, some of which have known functions. These motifs are mapped onto the schematic of the Ddx19 protein in Fig 16. Motif IV was not found in the protein sequence of zebrafish Ddx19. Though the mutation is not within one of these short motifs, it is immediately adjacent to motif I, which makes part of the ATP binding pocket (Rocak and Linder 2004). We verified the identity of our *ddx19* allele by complementation cross to *ddx19*^{hi1464}*,* a lethal mutant allele discovered in an insertional mutagenesis screen (Amsterdam et al. 1999). Prior to death at 55 hpf, *ddx19*^{hi1464} mutants have small, curved bodies and small eyes. *ddx19*^{hi1464}*/ddx19*^{mra} trans-heterozygotes survive to 5 dpf, but also have small curved bodies and small eyes, and share the dark pigmentation phenotype with *mra*. *mra* mutants can survive to 8 dpf, and have straighter bodies and normal sized eyes. TUNEL staining at 5 dpf did not reveal any increase in cell death in *mra* mutants or *ddx19*^{hi1464}/*ddx19*^{mra} trans-heterozygotes, while *ddx19*^{hi1464} mutants show widespread TUNEL staining by 48 hpf (Supp Fig 5). We conclude that *ddx19*^{mra} is a hypomorphic mutation.

The yeast homolog of *ddx19, DBP5p,* has been shown to interact genetically and physically with components of the nuclear pore complex, and to facilitate the detachment of mRNA from the nuclear protein *Mex67,* allowing the mRNA to translocate the pore (Snay-Hodge et al. 1998; Hodge et al. 1999; Schmitt et al. 1999; Lund and Guthrie 2005). Notably, a known human *ddx19* mutation in the ATP-binding domain inhibits mRNA export when expressed in *Xenopus laevis* oocytes (Schmitt et al. 1999). Given the conservation of this gene's sequence between zebrafish and *Xenopus laevis* (NCBI NP_001080632, 84% protein identity, Expect = 0.0) and the apparent absence of a duplicate *ddx19* ortholog in the zebrafish genome, we posit that zebrafish *ddx19* replicates the function of its homologs, and that protein expression is reduced non-specifically in mutants due to failed mRNA transport. Consistent with this interpretation, expression levels of transgenic GFP are reduced in mutants; in fact, mutants can be sorted from their wildtype siblings by the brightness of transgenic GFP even at 48 hpf, which is prior to the appearance of any anatomical defects. The putative global function of *ddx19* is further supported by expression data. We performed whole mount *in situ* hybridization with a *ddx19* RNA probe, and found that *ddx19* is expressed in all cells as early as 24 hpf (Fig 16). We did not observe any cell-type specific expression in the retina or tectum. In later stages (up to 4 dpf), the expression pattern continues to be non-specific, and appears to decrease with time, particularly in the retina (Supp Fig 6). No differences were observed between wildtype and *mra* larvae.

The diverse phenotypes of *mra* can be better understood in light of the cloned mutation. *ddx19* is expressed in all retinal cells during IPL development, and is likely nonspecifically important for the generation of proteins. The effect of the mutation on neurite morphology may vary depending on the individual requirements of each cell type. For example, *Pax6*+ neurites may tend to branch exuberantly, and require strong intrinsic expression of a particular Rho GTPase, or strong expression of a repulsive cue by neighboring neurites, to block excess branching. Conversely, PKC+ axons may require a strong molecular signal to develop bulbous terminals—if that signal is not received, the axons may default to extending a single terminal. What determines the tendencies of each cell type is a matter of great cell biological interest, and may depend on intrinsic properties of the cell, or on the stage of development that cell has achieved once *ddx19* becomes limiting. The putative nonspecific role of *ddx19* signaling in mRNA transport also elucidates why *mra* neurites cannot compensate for the disruptions to maintain relative positioning. These compensatory mechanisms likely require localization of attractive, repulsive, and/or adhesive molecules to the neurite surface—a bottleneck at the nuclear pore complex would severely disrupt the localization of these signals.

ddx19 ***is required for the differentiation of starburst-like ACs***

The importance of *ddx19* is most pronounced in the loss of starburst morphology ACs in *mra* derived clones. The *Pax6* population comprises neurons with three basic arbor shapes: small and symmetric, small and asymmetric, and starburst-like (Kay et al. 2004). Fig 17A shows a fixed, immunostained chimeric fish in wholemount with one labeled starburst-like AC from a donor clone. Like mammalian starburst ACs, zebrafish starburst-like ACs have multiple processes extending radially in all directions from the cell body; these processes are targeted to a single IPL sublayer (Fig 17B). Starburst-like cells are also commonly found in transplanted clones—but only in clones derived from a wildtype donor. In almost all chimeras with wildtype donors (33 of 34), transplanted clones gave rise to at least one starburst-like AC, independent of the genotype of the host. In contrast, no transplanted *mra* clones gave rise to ACs with starburst morphology, even within a wildtype host (n = 22). This result may indicate an absence of particular cell type from *mra* mutant clones, or perhaps dendrite morphogenesis defects render the cells unrecognizable by shape.

mra/*wildtype chimeras establish the importance of cell non-autonomous signals in Pax6+ neurite sublamination*

As mentioned above, the *mra* sublamination defects could result from failure of intrinsic regulation of branching, cell-environment interactions, or both types of signaling. As *ddx19* is expressed in all retinal cells, the phenotypes alone cannot establish whether cell autonomous or cell non-autonomous *ddx19* function is important for IPL sublamination. We anticipated that both types of signaling would be important, which seems intuitive—adhesion molecules and guidance molecules function as pairs, interacting when two membranes are in close proximity. However, due to the sparse data on mechanisms governing IPL development, a purely cell intrinsic mechanism of outgrowth has remained a possibility, especially for *Pax6*+ ACs. A descriptive developmental study of *Pax6*+ neurites demonstrated that these choose the ON or OFF region of the IPL early and directly, without appearing to probe the environment. Once the neurite arbor has reached its target, additional branches extend laterally along the sublamina—never into neighboring sublaminae (Godinho et al. 2005). One possibility is that *Pax6+* neurites innervate the IPL by a purely cell intrinsic mechanism—in which case a wildtype cell would show wildtype sublamination in a *mra* host. We used our set of chimeras to assess the roles of cell autonomous and non-autonomous signaling in *Pax6+* neurite sublamination.

We assessed the fine sublamination of *Pax6+* neurites in these chimeras by cryosectioning. We found that intrinsic and extrinsic *ddx19* function are both necessary for sublamination of these neurites, but neither is sufficient alone. As shown in Fig 17D, a wildtype *Pax6+* AC (white arrow), transplanted into a *mra* host, branches diffusely across more than one sublamina—some neurites even exit the IPL (yellow arrow). Wildtype starburst-like ACs are identifiable in serial sections by the length of their unbranched processes, which adhere faithfully to single sublaminae. In the *mra* environment, the starburst-like AC shown in Fig 17I extends a long process along the IPL which is mostly unbranched, but a few short branches emerge from the shaft (arrows). *mra* ACs transplanted into wildtype hosts are difficult to distinguish from their *mra*→*mra* counterparts, but in some cases (3 of 6 cells, Fig 17E,G,H), partial sublamination rescue is evident. The labeled AC in Fig 17F has a basic bistratified arbor, while the ACs in Figs 17G,H confine their neurites to the outer and inner portions of the IPL, respectively. Electrophysiology studies have demonstrated that the inner third is the ON portion, and the outer two thirds, the OFF portion, of the IPL (Connaughton 2001). Perhaps the wildtype environment provides a physical scaffold upon which *mra* neurites grow, or wildtype neighbor neurons are able to compensate for compromised *ddx19* function with strong expression of adhesion or guidance molecules. In either case, cell non-autonomous cues are clearly important for the sublamination of *Pax6+* neurites.

Conclusions

The map of IPL sublaminae in the zebrafish retina has proven to be a tractable system for the study of neurite arbor morphology and targeting. We have shown that distinct retinal cell types project reliably to IPL sublayers, where they co-localize with potential synaptic partners in a reproducible fashion. Hundreds of wildtype retina sections examined showed the same pattern of IPL organization, and IPL-specific mutant phenotypes proved to be invariant from animal to animal as well. IPL sublaminae proved to be accurate indicators of the morphology of individual neurites in the study of the *mra* mutant, in which the loss of *Pax6*+ sublamination corresponds with a nonspecific projection pattern of individual *Pax6*+ ACs. Finally, because these IPL-defective mutants have impaired visual responses in the VBA and OKR assays, we can conclude the IPL organization is either directly important, or at least a worthy proxy, for visual system function.

We have begun to characterize the mechanisms governing development of IPL sublaminae. To our surprise, IPL development requires neither light experience, photoreceptor function, nor synaptic transmission between any retinal neurons. This result stands in contrast to data from other vertebrates, in which visual experience and bipolar cell signaling are required for the proper organization of GC dendrites (Chalupa and Gunhan 2004; Xu and Tian 2007). Zebrafish *Brn3c*+ GC dendrites differ vastly in their morphogenesis from documented mammalian GCs (Mumm et al. 2006); perhaps the prominent GC populations in zebrafish differ from those in mammals, and rely instead on activity-independent signals. This style of visual circuitry development might suit the zebrafish better than its mammalian relatives, as hard-wired mechanisms could function faster to create an effective defense system in the larvae. In support of this idea, the visual startle response, in which larvae quickly reverse course in response to a looming shadow, can be observed as early as 68 hpf (Easter and Nicola 1996).

Our nested screen strategy was successful in uncovering five mutants with defects informative to the process of IPL sublamination. The phenotypes we have observed are broad in scope; in *asph,* the localization of the IPL itself is compromised, as ectopic IPLs form in the GCL, while in *spel,* the observed defects are limited to the sublamination of the ON IPL. Notably, we found only one mutant, *mra,* in which IPL defects result in the failure of partner neurites to specifically co-localize, and of non-partner neurites to segregate. The *mra* mutation is a hypomorphic allele of a ubiquitous, essential gene, which we know by its expression pattern and the early death phenotype of the *ddx19*^{hi1464} mutant. If *ddx19* maintains its known function in nuclear export of mRNA in zebrafish, then it is likely that all protein expression is reduced in these mutants, resulting in pleiotropic defects in every cell. We suspect that protein expression is non-specifically hindered in *mra* mutants, and, therefore, that the only identified single gene mutation with severe effects on IPL sublamination affects many—or even all—expressed genes. Though the *mra* mutation did not lead us to a specific pathway involved in IPL sublamination, the mutant provided a valuable ‘test tube’ for the study of cell autonomy in the development of *Pax6*+ neurites. We show that even wildtype starburst-like ACs, which faithfully project to single sublaminae, are prone to branching errors within a *mra* host—demonstrating the importance of cell non-autonomous cues in keeping these neurites confined to their targets. Studies of the *noto* mutant also highlighted the role of cell-cell interactions in the development of the IPL. In particular, *lak/noto* double mutants establish that *noto* GCs are the aberrantly projecting neurites that instruct the sublamination defects of the other IPL neurites. However, the *lak* single mutant phenotype reveals that GCs are not ultimately required for wildtype IPL organization. It appears that some IPL neurites can follow two paths to sublamination—the first following the instruction of GCs, and the second GC-independent. The *noto* mutant establishes that the GC-dependent pathway can become dominant where GCs project aberrantly. The plasticity of AC and BC neurites may be rarely employed, but could serve to preserve retinal circuitry in the face of environmental or genetic perturbations.

Methods

Fish maintenance

Adult Tübingen Longfin (TL) and WIK zebrafish (*Danio rerio)* were maintained in 2, 4, or 6 Liter tanks with their siblings. The colony kept at a temperature of approximately 28°C, on a 14 /10 hour light/dark cycle.

Dark rearing and APB treatment

Larvae were raised from 12 hpf in dishes wrapped in aluminum foil, with or without addition of 1mM (final concentration) (+/-)-2-amino-4-phosphonobutyric acid (Sigma). At 5 dpf, larvae were removed from dishes and immediately fixed in 4% PFA in a dim room.

Botulinum toxin B injection

Brn3c transgenic embryos were injected at the one-cell stage with a solution 0.1ug/ul or 1.0ug/ul botulinum toxin B (EMD Biosciences, Darmstadt, Germany) in embryonic media labeled with rhodamine dextran (Molecular Probes, Eugene, OR). At 5 dpf, immobilized larvae were tested extensively for startle responses. Apparently paralyzed larvae were tested for retinal neural activity by electroretinogram (ERG) recording, and then sectioned and immunostained.

Electroretinogram recording

Uninjected control fish were tested at the beginning and end of the recording session to verify the function of the equipment. Larvae were presented with two series of light pulses of increasing power, at intensities of 70µW, 100µW, 500µW, 2.4mW, and 4.4mW. In the first series, larvae were shone 20ms flashes of light separated by dark intervals of

5s. These stimuli elicit the retinal ON response. Larvae were then presented with a series of 1s duration light steps, separated by 10s of darkness. These stimuli elicit a sustained ON response followed by an OFF response at light offset.

Primary screen

This VBA screen was part of the San Francisco visual behaviors screen, documented in Muto *et al* (2005). Adult TL zebrafish males were mutagenized using ENU and crossed with wildtype females. Fish from the F1 generation, populated with carriers of a number of different mutations, were crossed with wildtype fish to generate F2 families. F2 fish were inbred to yield F3 clutches, which were screened as larvae at 5 days post fertilization for an intact VBA response. Larvae were dark adapted first, then placed on a white surface under fluorescent light for at least 20 minutes to facilitate light adaptation. F2 fish carrying mutations of interest were then out-crossed to TL wildtype fish to create the next generation of each mutant family. Carriers of the mutation of interest were identified by in-crossing siblings of each generation. The immunohistochemical screening and analyses described here were performed on larvae that were descended three to four generations from the F2 heterozygotes of the primary screen. The out-crossing and re-identification of carriers ensures that the mutation of interest is preserved while regulating factors are exchanged in meiosis. We therefore can be confident that a single mutation causes the phenotypes we observed.

Prescreening

Our intent was to limit our study to mutants that could be informative to the development of synaptic laminae. To exclude mutations affecting the overall health of the eye, mutants with small eyes (likely due to poor growth or excess cell death) were excluded from the secondary screen. Also, all mutants were first sectioned and stained with DAPI to assess overall retinal organization. We limited the secondary screen to mutants with normal-sized eyes and intact retinal organization, with the exception of *eter* and *asph*, which were of interest based on prior observations.

Sectioning

For the secondary screen, larvae aged 5 dpf were fixed in 4% PFA (w/v, pH 7.4) overnight at 4°C, infiltrated in 30% sucrose (w/v) in PBS overnight at 4 °C, and embedded in molds containing OCT freezing medium (Sakura Finetech U.S.A., Inc., Torrance, CA). In all cases, mutant larvae were embedded beside wildtype siblings in reverse orientation for comparison. Blocks were then frozen at -20 °C and sectioned horizontally at 12µm on a Jung Frigocut 2800N cryostat (Leica Instruments, Nussloch, Germany). Sections were collected on Superfrost Plus slides (Fisher, Pittsburgh, PA), air dried for 30 minutes to overnight, and re-hydrated in PBS. For the fuller characterization of mutant phenotypes, 4, 6, and 7 dpf larvae were sectioned as well, where noted.

Immunohistochemistry

Sections were incubated with blocking reagent containing 3% (v/v) normal goat or donkey serum (Jackson ImmunoResearch Laboratories, Westgrove, PA) and 0.3% Triton X-100 (v/v; Fisher Scientific) in phosphate buffered saline (PBS, pH 7.4) for 30 minutes at room temperature. Primary antibodies were diluted in blocking solution and pipetted onto sections; slides were left overnight in primary antibody at 4ºC in a humidified chamber. The following day, sections were washed for 5 minutes in PBS three times and treated with fluorophore-conjugated secondary antibodies diluted 1:200 in blocking solution for 2 hours at room temperature. Finally, sections were washed in PBS as above, stained with DAPI nuclear marker (Sigma, St. Louis, MO), mounted in Fluoromount G (Southern Biotechnology Associates, Inc., Birmingham, AL) under microscope coverslips (Fisher Scientific, Pittsburgh, PA) and air dried in the dark from four hours to overnight.

Four primary antibodies to specific cell types of the retina were used in the screen: anti-choline acetyltransferase (ChAT) (1:50; Chemicon, Temecula, CA), anti-parvalbumin (parvalbumin) (1:1200; Chemicon, Temecula, CA), anti-protein kinase C β1 (1:800; Santa Cruz Biotechnology, Santa Cruz, CA), and zrf-3 (1:250; Oregon Monoclonal Bank, Eugene, OR). We completed our screen using the anti-PKCβ1 antibody, but subsequently used the more reliable anti-PKCα antibody. The staining patterns of these two antibodies are indistinguishable.

Phenotype analysis

The foci of the screen were the presence of each cell type, the placement of each cell type in the retina, and the proper sublamination of each marker in the IPL. For each fish on a slide, a center section of the retina was identified and used for comparison. We used the size of the lens as a marker of the eye's center; center sections have a full, round lens (or lens cavity) without overlapping cell bodies.

Once we identified mutants of interest, we crossed some of these into transgenic backgrounds (*Brn3c* and *Pax6*) to enable further evaluation. Sections taken from transgenic larvae were immunostained with either polyclonal rabbit antisera to GFP (1:4000; Invitrogen, Molecular Probes, Eugene, OR) or monoclonal mouse anti-GFP (MAB3580; 1:400; Chemicon International, Temecula, CA) to enhance the signal. All phenotypes presented in this study were confirmed in multiple mutant larvae from different crosses, always compared side by side on every slide with wildtype larvae from the same clutch. We limited our studies to mutations with approximately 100% penetrance, judged by the number of dark fish in a clutch (roughly 25%), and for which every dark fish manifests the IPL phenotypes we identified.

Imaging sections

Screening was performed using fluorescence microscopy (Ortholux fluorescence microscope, Leitz, Wetzlar, Germany). Wide field fluorescence images were collected from the same microscope using a Spot RT slider camera (Diagnostic Instruments, Inc.). Confocal images were taken using the Zeiss LSM 5 Pascal microscope and software. Confocal stacks were further processed using ImageJ software. In some cases, z-projections of a few slices were made; in others, single representative slices were selected. In all figures, comparisons are made between two images that were processed equivalently—slices compared to slices, and projections compared to projections of a similar number of slices. Images were adjusted in Adobe Photoshop using the brightness/contrast, levels, and curves functions in order to best represent the pattern of sublamination in the IPL. Images presented side-by-side for comparison underwent equivalent processing, but brightness should not be compared between non-adjacent images. In noted cases, as in the study of the *mra* mutant, images for comparison were taken under identical conditions and processed with identical look up tables (LUTs) in Photoshop, in order to qualitatively compare brightness.

Optokinetic response recording and analysis

Recordings were performed and analyzed as previously (Orger et al. 2004). Briefly, larvae were mounted in 2% methyl cellulose, and an image of moving stripes was projected onto a circular drum surrounded the fish. Two minute movies were collected at 1 frame per second (fps), and the orientation of the eye in each frame was measured using the moment calculator plugin in ImageJ. To smooth the function, the orientation at each timepoint was averaged with its two neighboring timepoints.

in situ hybridization

The 3’ end of the *ddx19* mRNA sequence was amplified by PCR and cloned into the PCRII-TOPO vector using the TOPO TA cloning kit (Invitrogen). This construct was used directly for transcription of antisense and sense probes. *in situ* hybridization to *ddx19* transcripts was performed following a common published method (Keegan et al. 2002). Whole, fixed fish were hybridized with antisense and sense probes at 65°C overnight. We examined larvae at 1dpf, 1.5dpf, 2dpf, 3dpf, and 4dpf.

Blastula-stage transplantation

Chimeras were generated for single cell analysis and studies of cell-autonomy using methods very similar to those developed originally in the zebrafish (Ho and Kane 1990; Halpern et al. 1993). Our studies benefit from the addition of transgenes to either donors or hosts. Small numbers (5-15) of cells were transplanted from GFP expressing donors into non-transgenic hosts, to isolate labeled cells in the host environment. Donor blastulae were labeled by injection with a mix of Alexa 555-dextran and biotin-dextran (both with MW 10,000, 1% w/v each, Molecular Probes, Eugene, OR). At 24 hpf, transplanted hosts were sorted for rhodamine fluorescent clones in the eye. Chimeras with retinal clones were raised to 5 dpf for phenotype analysis. The corresponding donors were raised to 5 dpf and identified as mutant or wildtype. To assess the sublamination of IPL neurites, chimerae with clones in the retina were fixed, cryosectioned, and stained by immunohistochemistry. The donor clones in sections were labeled with Avidin-conjugated fluorophore (Avidin 555, 1:200, Molecular Probes, Eugene, OR).

Gene identification

We used established methods to map the *bru* and *mra* mutations to small regions of the genome (Bahary et al. 2004). In each case*,* other researchers had reported mutants with lesioned genes within the identified region, and these seemed plausible candidates for our mutations (Amsterdam et al. 1999; Woods et al. 2006). A. Amsterdam generously provided carriers from the $ddx19^{hi1464}$ line, and we found that the mutation failed to complement *mra.* The mutation in *mra* was identified by gene sequencing of our allele. W. Talbot generously provided carriers for each of two *NSF* mutants, *st25* and *st53*, which failed to complement our *bru* alleles. Gene sequencing did not reveal any coding sequence mutations in our alleles, but we identified a missense mutation in the bru^{tw212} line, provided to us by ZIRC.

References

Amsterdam A, Burgess S, Golling G, Chen W, Sun Z et al. (1999) A large-scale insertional mutagenesis screen in zebrafish. Genes Dev 13(20): 2713-2724.

Babb SG, Kotradi SM, Shah B, Chiappini-Williamson C, Bell LN et al. (2005) Zebrafish R-cadherin (Cdh4) controls visual system development and differentiation. Dev Dyn 233(3): 930-945.

Bahary N, Davidson A, Ransom D, Shepard J, Stern H et al. (2004) The Zon laboratory guide to positional cloning in zebrafish. Methods Cell Biol 77: 305-329.

Bennett MK, Scheller RH (1993) The molecular machinery for secretion is conserved from yeast to neurons. Proc Natl Acad Sci U S A 90(7): 2559-2563.

Bernardos RL, Barthel LK, Meyers JR, Raymond PA (2007) Late-stage neuronal progenitors in the retina are radial Muller glia that function as retinal stem cells. J Neurosci 27(26): 7028-7040.

Besharse JC, Pfenninger KH (1980) Membrane assembly in retinal photoreceptors I. Freeze-fracture analysis of cytoplasmic vesicles in relationship to disc assembly. J Cell Biol 87(2 Pt 1): 451-463.

Biehlmaier O, Makhankov Y, Neuhauss SC (2007) Impaired retinal differentiation and maintenance in zebrafish laminin mutants. Invest Ophthalmol Vis Sci 48(6): 2887-2894.

Bodnarenko SR, Chalupa LM (1993) Stratification of ON and OFF ganglion cell dendrites depends on glutamate-mediated afferent activity in the developing retina. Nature 364(6433): 144-146.

Bodnarenko SR, Jeyarasasingam G, Chalupa LM (1995) Development and regulation of dendritic stratification in retinal ganglion cells by glutamate-mediated afferent activity. J Neurosci 15(11): 7037-7045.

Brandon C (1991) Cholinergic amacrine neurons of the dogfish retina. Vis Neurosci 6(6): 553-562.

Bytyqi AH, Lockridge O, Duysen E, Wang Y, Wolfrum U et al. (2004) Impaired formation of the inner retina in an AChE knockout mouse results in degeneration of all photoreceptors. Eur J Neurosci 20(11): 2953-2962.

Chalupa LM, Gunhan E (2004) Development of On and Off retinal pathways and retinogeniculate projections. Prog Retin Eye Res 23(1): 31-51.

Clandinin TR, Zipursky SL (2002) Making connections in the fly visual system. Neuron 35(5): 827-841.

Connaughton VP (2001) Organization of ON- and OFF-pathways in the zebrafish retina: neurotransmitter localization, electrophysiological responses of bipolar cells, and patterns of axon terminal stratification. Prog Brain Res 131: 161-176.

Cuenca N, Deng P, Linberg KA, Fisher SK, Kolb H (2003) Choline acetyltransferase is expressed by non-starburst amacrine cells in the ground squirrel retina. Brain Res 964(1): 21-30.

Dickson BJ (2002) Molecular mechanisms of axon guidance. Science 298(5600): 1959-1964.

Doerre G, Malicki J (2002) Genetic analysis of photoreceptor cell development in the zebrafish retina. Mech Dev 110(1-2): 125-138.

Easter SS, Jr., Nicola GN (1996) The development of vision in the zebrafish (Danio rerio). Dev Biol 180(2): 646-663.

Famiglietti EV, Jr. (1983) 'Starburst' amacrine cells and cholinergic neurons: mirror-symmetric on and off amacrine cells of rabbit retina. Brain Res 261(1): 138-144.

Godinho L, Mumm JS, Williams PR, Schroeter EH, Koerber A et al. (2005) Targeting of amacrine cell neurites to appropriate synaptic laminae in the developing zebrafish retina. Development 132(22): 5069-5079.

Goldsmith P, Harris WA (2003) The zebrafish as a tool for understanding the biology of visual disorders. Semin Cell Dev Biol 14(1): 11-18.

Goldsmith P, Baier H, Harris WA (2003) Two zebrafish mutants, ebony and ivory, uncover benefits of neighborhood on photoreceptor survival. J Neurobiol 57(3): 235-245.

Gunhan E, Choudary PV, Landerholm TE, Chalupa LM (2002) Depletion of cholinergic amacrine cells by a novel immunotoxin does not perturb the formation of segregated on and off cone bipolar cell projections. J Neurosci 22(6): 2265-2273.

Halpern ME, Ho RK, Walker C, Kimmel CB (1993) Induction of muscle pioneers and floor plate is distinguished by the zebrafish no tail mutation. Cell 75(1): 99-111.

Ho RK, Kane DA (1990) Cell-autonomous action of zebrafish spt-1 mutation in specific mesodermal precursors. Nature 348(6303): 728-730.

Hodge CA, Colot HV, Stafford P, Cole CN (1999) Rat8p/Dbp5p is a shuttling transport factor that interacts with Rat7p/Nup159p and Gle1p and suppresses the mRNA export defect of xpo1-1 cells. Embo J 18(20): 5778-5788.

Kawasaki F, Mattiuz AM, Ordway RW (1998) Synaptic physiology and ultrastructure in comatose mutants define an in vivo role for NSF in neurotransmitter release. J Neurosci 18(24): 10241-10249.

Kay JN, Finger-Baier KC, Roeser T, Staub W, Baier H (2001) Retinal ganglion cell genesis requires lakritz, a Zebrafish atonal Homolog. Neuron 30(3): 725-736.

Kay JN, Roeser T, Mumm JS, Godinho L, Mrejeru A et al. (2004) Transient requirement for ganglion cells during assembly of retinal synaptic layers. Development 131(6): 1331-1342.

Keegan BR, Feldman JL, Lee DH, Koos DS, Ho RK et al. (2002) The elongation factors Pandora/Spt6 and Foggy/Spt5 promote transcription in the zebrafish embryo. Development 129(7): 1623-1632.

Lee J, Gross JM (2007) Laminin beta1 and gamma1 containing laminins are essential for basement membrane integrity in the zebrafish eye. Invest Ophthalmol Vis Sci 48(6): 2483-2490.

Littleton JT, Barnard RJ, Titus SA, Slind J, Chapman ER et al. (2001) SNARE-complex disassembly by NSF follows synaptic-vesicle fusion. Proc Natl Acad Sci U S A 98(21): 12233-12238.

Lund MK, Guthrie C (2005) The DEAD-box protein Dbp5p is required to dissociate Mex67p from exported mRNPs at the nuclear rim. Mol Cell 20(4): 645-651.

Mangrum WI, Dowling JE, Cohen ED (2002) A morphological classification of ganglion cells in the zebrafish retina. Vis Neurosci 19(6): 767-779.

Masai I, Lele Z, Yamaguchi M, Komori A, Nakata A et al. (2003) N-cadherin mediates retinal lamination, maintenance of forebrain compartments and patterning of retinal neurites. Development 130(11): 2479-2494.

Millar TJ, Ishimoto I, Chubb IW, Epstein ML, Johnson CD et al. (1987) Cholinergic amacrine cells of the chicken retina: a light and electron microscope immunocytochemical study. Neuroscience 21(3): 725-743.

Mumm JS, Williams PR, Godinho L, Koerber A, Pittman AJ et al. (2006) In vivo imaging reveals dendritic targeting of laminated afferents by zebrafish retinal ganglion cells. Neuron 52(4): 609-621.

Muto A, Orger MB, Wehman AM, Smear MC, Kay JN et al. (2005) Forward genetic analysis of visual behavior in zebrafish. PLoS Genet 1(5): e66.

Nelson R, Kolb H (2003) ON and OFF pathways in the vertebrate retina and visual system. In: Chalupa LM, Werner JS, editors. The Visual Neurosciences. Cambridge, MA: MIT Press. pp. 260-278.

Orger MB, Gahtan E, Muto A, Page-McCaw P, Smear MC et al. (2004) Behavioral screening assays in zebrafish. Methods Cell Biol 77: 53-68.

Page-McCaw PS, Chung SC, Muto A, Roeser T, Staub W et al. (2004) Retinal network adaptation to bright light requires tyrosinase. Nat Neurosci 7(12): 1329-1336.

Papermaster DS, Schneider BG, Besharse JC (1985) Vesicular transport of newly synthesized opsin from the Golgi apparatus toward the rod outer segment. Ultrastructural immunocytochemical and autoradiographic evidence in Xenopus retinas. Invest Ophthalmol Vis Sci 26(10): 1386-1404.

Pellegrini LL, O'Connor V, Lottspeich F, Betz H (1995) Clostridial neurotoxins compromise the stability of a low energy SNARE complex mediating NSF activation of synaptic vesicle fusion. Embo J 14(19): 4705-4713.

Pujic Z, Malicki J (2004) Retinal pattern and the genetic basis of its formation in zebrafish. Semin Cell Dev Biol 15(1): 105-114.

Rocak S, Linder P (2004) DEAD-box proteins: the driving forces behind RNA metabolism. Nat Rev Mol Cell Biol 5(3): 232-241.

Sandmann D, Engelmann R, Peichl L (1997) Starburst cholinergic amacrine cells in the tree shrew retina. J Comp Neurol 389(1): 161-176.

Sanna PP, Keyser KT, Celio MR, Karten HJ, Bloom FE (1993) Distribution of parvalbumin immunoreactivity in the vertebrate retina. Brain Res 600(1): 141-150.

Schmitt C, von Kobbe C, Bachi A, Pante N, Rodrigues JP et al. (1999) Dbp5, a DEAD-box protein required for mRNA export, is recruited to the cytoplasmic fibrils of nuclear pore complex via a conserved interaction with CAN/Nup159p. Embo J 18(15): 4332-4347.

Schroeter EH, Wong RO, Gregg RG (2006) In vivo development of retinal ON-bipolar cell axonal terminals visualized in nyx::MYFP transgenic zebrafish. Vis Neurosci 23(5): 833-843.

Semina EV, Bosenko DV, Zinkevich NC, Soules KA, Hyde DR et al. (2006) Mutations in laminin alpha 1 result in complex, lens-independent ocular phenotypes in zebrafish. Dev Biol 299(1): 63-77.

Snay-Hodge CA, Colot HV, Goldstein AL, Cole CN (1998) Dbp5p/Rat8p is a yeast nuclear pore-associated DEAD-box protein essential for RNA export. Embo J 17(9): 2663-2676.

Sollner T, Bennett MK, Whiteheart SW, Scheller RH, Rothman JE (1993) A protein assembly-disassembly pathway in vitro that may correspond to sequential steps of synaptic vesicle docking, activation, and fusion. Cell 75(3): 409-418.

Tam BM, Moritz OL (2007) Dark rearing rescues P23H rhodopsin-induced retinal degeneration in a transgenic Xenopus laevis model of retinitis pigmentosa: a chromophore-dependent mechanism characterized by production of N-terminally truncated mutant rhodopsin. J Neurosci 27(34): 9043-9053.

Taylor JS, Van de Peer Y, Braasch I, Meyer A (2001) Comparative genomics provides evidence for an ancient genome duplication event in fish. Philos Trans R Soc Lond B Biol Sci 356(1414): 1661-1679.

Tessier-Lavigne M, Goodman CS (1996) The molecular biology of axon guidance. Science 274(5290): 1123-1133.

Ting CY, Lee CH (2007) Visual circuit development in Drosophila. Curr Opin Neurobiol 17(1): 65-72.

Tolar LA, Pallanck L (1998) NSF function in neurotransmitter release involves rearrangement of the SNARE complex downstream of synaptic vesicle docking. J Neurosci 18(24): 10250-10256.

Voigt T (1986) Cholinergic amacrine cells in the rat retina. J Comp Neurol 248(1): 19-35.

Wehman AM, Staub W, Meyers JR, Raymond PA, Baier H (2005) Genetic dissection of the zebrafish retinal stem-cell compartment. Dev Biol 281(1): 53-65.

Wilson DW, Wilcox CA, Flynn GC, Chen E, Kuang WJ et al. (1989) A fusion protein required for vesicle-mediated transport in both mammalian cells and yeast. Nature 339(6223): 355-359.

Woods IG, Lyons DA, Voas MG, Pogoda HM, Talbot WS (2006) nsf is essential for organization of myelinated axons in zebrafish. Curr Biol 16(7): 636-648.

Xiao T, Roeser T, Staub W, Baier H (2005) A GFP-based genetic screen reveals mutations that disrupt the architecture of the zebrafish retinotectal projection. Development 132(13): 2955-2967.

Xu HP, Tian N (2007) Retinal ganglion cell dendrites undergo a visual activity-dependent redistribution after eye opening. J Comp Neurol 503(2): 244-259.

Yamagata M, Weiner JA, Sanes JR (2002) Sidekicks: synaptic adhesion molecules that promote lamina-specific connectivity in the retina. Cell 110(5): 649-660.

Yazulla S, Studholme KM (2001) Neurochemical anatomy of the zebrafish retina as determined by immunocytochemistry. J Neurocytol 30(7): 551-592.

Yu RC, Jahn R, Brunger AT (1999) NSF N-terminal domain crystal structure: models of NSF function. Mol Cell 4(1): 97-107.

Zhao C, Slevin JT, Whiteheart SW (2007) Cellular functions of NSF: not just SNAPs and SNAREs. FEBS Lett 581(11): 2140-2149.

Zinkevich NS, Bosenko DV, Link BA, Semina EV (2006) laminin alpha 1 gene is essential for normal lens development in zebrafish. BMC Dev Biol 6: 13.

Figure Legends

Table 1: Body phenotypes of VBA mutants

All seven mutants discussed in this study are listed with their allele numbers. In some cases, more than one mutant allele for one gene was discovered (*bru, cfe).* VBA score was assessed by eye. Wildtype light adaptation is a score of 1; a larva that is completely dark after exposure to light is scored as 0. All mutants fail to develop a swimbladder and die by 8 dpf. Many have body curvature and/or swimming defects. The .7/1 VBA rating for *asph* reflects a variable phenotype.

Table 2: Retinal phenotypes of VBA mutants

For each phenotype, the number of 5 dpf mutant larvae assessed is noted in parentheses. Except where denoted by proportions (*asph* mutant only), phenotypes were 100% penetrant among dark larvae.

Figure 1: Cell type and IPL organization of the 5 dpf zebrafish retina

All images are horizontal sections stained by immunohistochemistry to markers of retina cells or with DAPI (nuclear dye), imaged by confocal microscopy. IPL sublaminae are labeled (s10, s25, etc.). A: DAPI stain shows basic organization of retina into ganglion cell layer (GCL), inner plexiform layer (IPL), inner nuclear layer (INL), and outer nuclear layer (ONL). B-E: Parvalbumin antisera and transgenic *Brn3c* expression label subset of ACs and GCs, respectively. These neurites are closely apposed but reside in distinct sublaminae. F-J: ChAT antisera labels a population of ACs in the INL. ChAT and zrf3 antisera brightly label the same sublaminae. K-O: PKC (protein kinase C) antisera labels a subset of BCs, which project terminals to three sublaminae in the inner IPL. Transgenic *Pax6* expression labels a subset of ACs with neurites in three sublaminae of the IPL. In many sections, the s40 and s45 bands of *Pax6* immunoreactivity are difficult to distinguish. PKC+ terminals and *Pax6*+ neurites are closely nested but not co-localized. Bottom left scale bar, for whole retina images, is 50μm, bottom right scale bar, for panels E,J,O, is 25μm.

Figure 2: Schematic of retinal cell types and IPL organization

Cell types are labeled according to the color code on the right; corresponding neurites are matched to their cell type. OPL: outer plexiform layer; HC: horizontal cell.

Figure 3: Dark-reared, APB-reared, and BtTx-injected 7 dpf larvae show wildtype IPL sublamination

In all 40X, zoomed images, the lens is to the lower right, the sclera is up and to the left. A-D: PKC+ BC terminals are confined to three inner IPL sublaminae in untreated larvae, dark-reared larvae, in larvae raised in 1mM APB, and in BtTx injected larvae. E-H: By 7 dpf, the outermost band of parvalbumin immunoreactivity has become two bands. The pattern of sublaminae is the same in all treatments. I-L: *Brn3c*+ dendrites sublaminate normally in all treatments. Scale bar is 50μm.

Figure 4: Lack of photoreceptors in *bru* does not alter neurite sublamination

A-E: Wildtype retinal sections showing photoreceptors and IPL organization. F-J: *bru* retinal sections showing absence of photoreceptors and wildtype IPL sublamination. A,F: DAPI stain shows that *bru* lacks photoreceptors (elongated cells in the outer retina, yellow arrows) and has a thin IPL. B,G: PKC terminals segregate into three rows in both wildtype and *bru* IPL. C,H: *Brn3c*+ neurites in five bands in both mutant and wildtype. D,I: Three parvalbumin+ sublaminae in both mutant and wildtype. E,J: Merged images of

DAPI and *Brn3c*+ and parvalbumin+ neurites, showing consistent organization. Scale bar 50μm..

Figure 5: *bru* has increased cell death in the retina and variable IPL phenotypes

Montage showing the increase in TUNEL+ cells in the *bru* retina and the variable IPL phenotypes seen in the mutants. In some case, PKC+ BCs appear to innervate a single sublamina, the inner two parvalbumin+ bands are not cleanly separated, and four or fewer *Brn3c*+ sublaminae can be distinguished. Scale bar 50μm.

Figure 6: *bru*^{tw212} mutants have a splice site mutation in *NSF*

A: Phylogram showing genetic distance between *Homo sapiens, Drosophila melanogaster,* and *Danio rerio* orthologs of *NSF.* Both *D. melanogaster* and *D. rerio* have two orthologs, but they are the result of separate duplications. *NSF,* the *bru* locus, is more closely related the *H. sapiens* NSF than the *NSFb* ortholog. B: Schematic of the *NSF* gene, showing functional domains. The *bru*^{tw212} mutation causes the excision of exons 4 and 5. C: Sequence chromotograms of cloned *NSF* genomic DNA purified from siblings and *bru*^{tw212} mutants. The mutant sequence has a G→A transition at the exon 5 donor splice site.

Figure 7: BtTxB injection blocks the ERG B-wave

A,B: Sample ERG recordings showing retinal responses to flashes of light of intensities 70μW, 100μW, 500μW, 2.4mW, and 4.4mW. A shows an uninjected control, with pronounced B-waves. B shows one injected larvae in which the B-wave was eliminated, even in response to the brightest flash. C: Quantified B-wave amplitudes are markedly reduced in BtTxB injected larvae. The amplitudes are the difference between the peak of the B-wave of each ERG recording and the corresponding trough of the A-wave, i.e. the interpeak distance, normalized to the uninjected mean. Interpeak distances were calculated from 2 uninjected and 5 injected larvae, using recordings from the brightest stimulus.

Figure 8: *bru* and *eter* mislocalize zrf3 to INL cell bodies

A,B,C: Wildtype, *bru,* and *eter* retinas immunostained with zrf3. The mutants have ectopic immunoreactivity in the INL. D,E: Glutamine synthetase stain in wildtype and *bru*. Mutants have a similar number and indistinguishable morphology of Müller glia. Scale bar 50μm.

Figure 9: Photoreceptor death in *moti* mutants does not effect zrf3 expression or IPL sublamination

A,E: zrf3 (red) and TUNEL (green) co-labeling in the 5 dpf wildtype and *moti* retina. Dying cells are visible in the *moti* ONL, INL, and GCL, but zrf3 misexpression does not appear in the INL, and zrf3 sublamination of the IPL is intact. B,F: Parvalbumin+ neurite sublamination is identical in wildtype and *moti.* C,G: PKC+ BC terminal sublamination is unchanged in *moti.* D,H: Merged images demonstrate the intercalation of parv+ and PKC+ sublaminae. Scale bar 50μm.

Figure 10: *noto* mutants have multiple defects in fine IPL sublamination

A,B: The five wildtype *Brn3c*+ sublaminae are indistinct in *noto;* neurites are in three coarse sublaminae. C,D: Parv+ neurites in *noto* fail to segregate into 3 sublaminae. The inner two bands are blurred into one band, or sometimes distinct but poorly separated (as in P). E,F: *Brn3c/*Parv merge shows that in the *noto* mutant, these two sets of neurites maintain their relative positions—they are nested but not co-localized. G-H: PKC+ BC terminals are poorly sublaminated in *noto,* but do co-localize with GC dendrites. K,L:

DAPI nuclear stain shows that overall retinal organization is maintained in *noto*. In this section the *noto* IPL appears thin, but this is not a trend. M,N: *Pax6*+ neurites are grossly normal, but the finer sublamination of s40/s45 is lost. O,P: The parvalbumin phenotype can be variable. In this case, the inner bands show some separation. Q,R: Merge of DAPI, *Pax6,* and parvalbumin stains. Parvalbumin and *Pax6*+ neurites maintain co-localization in s45 in *noto.* S,T: Schematic of PKC/Parv/*Brn3c*+ neurite organization in wildtype and in *noto.* Scale bar 50μm.

Figure 11: *noto* mutant sublamination defects become more pronounced by 7 dpf

A,B: PKC+ BC terminals are segregated into two sublaminae in 7 dpf *noto* mutants. A few terminals mark an incomplete s55. C,D,I,J: *Pax6*+ ACs sublaminate in two bands in both wildtype and *noto. noto* neurites fail to show the fine sublamination in s45, and project exuberantly between sublaminae. E,F: Merged image of *Pax6* neurites and PKC+ BC terminals. Coarse relative positioning is maintained—arrows show BC terminals flanking s45. G,H: Parvalbumin+ AC neurites are very coarsely sublaminated in *noto*. K,L: Merged image of parvalbumin and *Pax6*+ neurites shows overlap due to exuberant projections. Scale bar 50μm.

Figure 12: *noto* sublamination defects are rescued in *noto/lak* double mutants

Images from wildtype (A,E,I), *noto* mutants (B,F,J), *noto;lak* double mutants (C,G,K), and *lak* mutants (D,H,L). Parvalbumin+ AC neurites (A-D), PKC+ BC terminals (E-H), and zrf3+ neurites (I-L) show sublamination defects in *noto* which are not present in wildtype or *lak* and rescued in *noto/lak* double mutants. The outermost parvalbumin+ band (s85) is dim in C and D; this is a common variation in parvalbumin staining. Scale bar 50μm.

Figure 13: *spel* mutants have AC and BC sublamination defects in the inner IPL

A,D: *spel* mutants have a poorly labeled s45 band of parvalbumin immunoreactivity. B,E: PKC+ BC terminals are plentiful but poorly segregated in *spel* mutants. C,F: Ordering of zrf3+ sublaminae is faint in *spel* mutants, which also have increased zrf3 immunoreactivity in the INL (arrows). G,J: *Pax6* bands of the On and Off IPL are bright and clear in mutants. However, the finer subdivision of the s40/s45 *Pax6* bands is lost in *spel,* as shown in the magnified images in H and K. I,L: *Brn3c* sublamination is maintained in *spel* mutants. Scale bar 50μm; scale bars for H,K 25μm.

Figure 14: Mislocalized neurons in the GCL project to ectopic plexiform regions in *asph* mutants

A,B: zrf3/DAPI co-labeling shows the extensive ectopic plexiform regions in the section from an *asph* mutant (B). Note the absent lens and the overgrowth of cells in the GCL. C,D: *Pax6* and PKC+ (arrow) neurons appear in the GCL of *asph,* and innervate ectopic plexiform regions (circled). Wildtype sublamination of the native IPL is intact in the *asph* mutant. E-J: Images of *Pax6* neurons and neurites (green), counterstained with DAPI (blue). In wildtype, these neurons reside in the INL, and neurites project exclusively to the native IPL (E). F-J show various examples of ectopic AC cell bodies in the GCL (arrows), ectopic plexiform regions in the GCL (dashed circles), and cases where the native IPL, or half of the native IPL, veers from its course and into the GCL (arrowheads). Scale bar for A-F is in E, scale bar for G-J is in I. Scale bars 50μm.

Fig 15: *mra* is essential for IPL sublamination

A,B: A DAPI stain shows the thin *mra* IPL. C,D: PKC+ BC terminals innervate one sublamina in *mra* instead of three. E,F: The three parvalbumin+ IPL bands are reduced to two in *mra* mutants. *Brn3c*

(G,H) and *Pax6* (I,J) expressing neurites fail to form sublaminae in *mra* mutants. Scale bar 50μm.

Fig 16: *mra* carries a missense mutation in *ddx19,* a ubiquitously expressed RNA helicase

A,B: Sequencher chromatogram files showing missense mutation in *ddx19*^{mra}. The T-->A transversion changes the amino acid isoleucine (I) to asparagine (N). C: The structure of the 487 amino acid Ddx19 polypeptide, showing the site of the mutation (residue 143) in the DEAD-box helicase domain. DEAD-box proteins have two helicase domains, labeled with green and blue 'bullets.' Functional sites, which are conserved between DEAD-box proteins and have been implicated in either ATP binding, ATP hydrolysis, or RNA unwinding (helicase activity), are shown below each domain. Motif IV was not found in the sequence. The *mra* mutation is quite near motif I, also know as the Walker A motif, which is required for ATP-binding. D: The mutated isoleucine is highly conserved from yeast to humans. Though it is not within a known functional motif, it is adjacent to the 'GTGKT' motif I. E,F: 24 hpf embryos stained by *in situ* hybridization using antisense and sense control riboprobes to *ddx19.* G: Dorsal view of ubiquitous expression in eye and brain. H: Lateral view of ubiquitous expression in eye. The darker staining around the lens is a common artifact of whole mount *in situ* hybridization.

Fig 17: Cell autonomous and cell non-autonomous *ddx19* function are required for *Pax6*+ neurite sublamination

Images A-F show 5 dpf host larvae with transplanted *Pax6* expressing clones. Nuclei are labeled blue with a DAPI stain, GFP+ ACs are green, and transplanted cells are red from rhodamine dextran labeling of donors. All GFP-expressing cells are from the donor. A: A single wt starburst-like AC in a wt-->wt chimera, shown from dorsal in whole mount. Scale bar 50μm. B: A cryostat section of a different wt-->wt chimera, showing the IPL in cross-section and processes from starburst-like cells (one process from the cell body shown, white arrows; process from neighbor starburst-like cell, yellow arrows). Note that each process appears confined to one sublamina. C: Another wt-->wt chimera shows sublamination of *Pax6*+ AC neurites. D: A wildtype cell (white arrow) innervates the IPL diffusely in a *mra* host; some neurites exit the IPL (yellow arrow). E: Individual *mra* ACs transplanted into a *mra* host do not sublaminate. F-H: These *mra Pax6*+ ACs are partially rescue in a wildtype host. In F, a neuron is grossly bistratified. In G,H, neurites appear confined to either the ON or OFF portion of the IPL. I: A wt starburst-like AC process crosses between sublaminae (see arrows) in a *mra* host. Approximate scale bar for B-I, lower left, 50μm.

Supplementary Figure 1: Tyrosine hydroxylase neurites innervate the edges of the IPL

Sectioned retina immunostained to tyrosine hydroxylase (TH) shows small processes at the IPL edges (arrows). The photoreceptor autofluorescence is particular high in this image; the photoreceptors are not TH immunopositive. Scale bar 50μm.

Supplementary Figure 2: *noto* fails to develop fine sublamination of ChAT+ neurites

ChAT staining of wildtype and *noto* mutant retina. Wildtype has four ChAT+ IPL sublaminae: *noto* has two. Scale bar 50μm.

Supplementary Figure 3: Altered neuropil organization in the *asph* tectum

Horizontal sections showing 5 dpf tectum. Cell bodies are labeled with DAPI, the neuropil is labeled with zrf3. A: In wildtype, the neuropil is confined to the anteriolateral portion of the tectum. B,C: In *asph* mutants, occasional gaps in the cell body region are filled with zrf3 immunoreactivity, suggesting that ectopic neuropils have formed. Scale bar 50μm.

Supplementary Figure 4: Parvalbumin+ neurons are scattered within the GCL of *cfe* mutants

A: Wildtype parvalbumin+ cell bodies of the GCL reside apposed to the IPL. B: In *cfe,* parvalbumin+ ACs are scattered throughout the GCL. Parvalbumin+ IPL sublaminae are unaffected in *cfe*. Scale bar 50μm.

Supplementary Figure 5: *mra* mutants and *mra/ddx19*^{hi1464} trans-heterozygotes show no increase in cell death at 5 dpf

Nuclei are labeled with DAPI (blue), dying cells are labeled with TUNEL (green). TUNEL staining of the skin may be artifactual. A: The wildtype retina and brain at 52 hpf has minimal TUNEL staining. B: The 52 hpf *ddx19*^{hi1464}-/- larvae is undergoing massive cell death. This larva was still alive when fixed but these mutants do not survive past this stage. C,D,E: 5 dpf wildtype, *mra* mutant, and *mra/ ddx19*^{hi1464} trans-heterozygotes show minimal TUNEL staining. The trans-heterozygote has a small eye, which may be due to developmental defects rather than cell death. Scale bar 50μm.

Supplementary Figure 6: *ddx19* expression time course

1, 2, 3, and 4 dpf larvae labeled by *in situ* hybridization with a *ddx19* riboprobe. The right column shows control staining with a sense probe. Strong, ubiquitous expression at 1 dpf tapers off with development. At later stages, the gain was increased to see the signal, which resulted in high background in the sense-probed larvae. By 4 dpf there is no *ddx19* expression in the eye.

Table 1: Body phenotypes of VBA mutants

Name	**Allele**	**VBA score**	**Body phenotype**	**Viability**
notorious (noto)	*s380*	.3	Sluggish, has variable body curvature, variable jaw defects, no swimbladder	Dies by 8 dpf
spellbound (spel)	*s308*	.3	Swims mostly upside-down, no swimbladder	Dies by 8 dpf
brudas (bru)	*s300, s364, s366, s501*	0	No movement by 4 dpf, no swimbladder	Dies by 8 dpf
eternal sunshine (eter)	*s383*	0	Sluggish, swims in circles, small eyes, no swimbladder	Dies by 8 dpf
asphalt jungle (asph)	*s166*	.7/1	Short body axis, curved body, no swimbladder	Dies by 8 dpf
cape fear (cfe)	*s322, s346, s347, s359, s360*	0	No swimbladder	Dies by 8 dpf
moonraker (mra)	*s135*	0	Curved body, lies on side, swims in circles, no swimbladder	Dies by 8 dpf

Table 2: Retinal phenotypes of VBA mutants

Name	Allele	Retinal morphology	TUNEL stain	PKC+ bipolar cell terminals in s10, s40, s55	Parv+ neurites in s25, s45, and s85	zrf3 immunoreactivity in s25, s40, s70, s85	*Brn3c:mGFP* dendrites in s10, s40, s55, s70, s90	*Pax6:mgfp* neurites in s40, s45, s70, s85
notorious (noto)	*s380*	Wildtype (66)	Wildtype (25 total at 3, 4, 6, and 7 dpf)	Terminals in two coarse bands (19)	Coarse sublaminae, inner two merged or poorly separated (50)	No IPL sublamination (19)	Dendrites in three coarse sublaminae (15)	Finer sublamination lost; s40/s45 and s70/s85 merged (18)
spellbound (spel)	*s308*	Wildtype (59)	Phenotype not established	Terminals poorly separated into sublaminae (32)	Middle sublamina dimly labeled (49)	Extra zrf3 label in INL, no IPL sublamination (26)	Wildtype (20)	Wildtype (6)
brudas (bru)	*s300,* *s364,* *s366,* *s501*	No photoreceptors, thin IPL (29)	Increased cell death, especially at the margins*	Variable, some sections wildtype	Variable, some sections wildtype	Variable, some sections wildtype	Variable, some sections wildtype	Variable, some sections wildtype
eternal sunshine (eter)	*s383*	Small eyes, no photoreceptors (36)	Increased cell death (4)	Phenotype not established	Neurons scattered in GCL, inner two IPL sublaminae poorly separated (32)	Extra zrf3 immunoreactivity in INL and GCL, no IPL sublamination (25)	Phenotype not established	Sublaminae crowded together, can only distinguish two bands, haze of extra immunoreactivity outside bands (7)
asphalt jungle (asph)	*s166*	Small eyes, no lens, disorganized retina (11)	Phenotype not established	Mislocalized cells in the GCL, terminals in ectopic IPLs (10/11)	Mislocalized cells in the GCL, terminals in ectopic IPLs (5/6)	Zrf3 labels ectopic IPLs (5/6)	Phenotype not established	Mislocalized cells in the GCL, terminals in ectopic IPLs (5)
cape fear (cfe)	*s322,* *s346,* *s347,* *s359,* *s360*	Wildtype (5)	Phenotype not established	Wildtype (5)	Neurons scattered in GCL, wildtype sublamination (5)	Wildtype (5)	Phenotype not established	Phenotype not established
moonraker (mra)	*s135*	Thin IPL (48)	Wildtype (18 total *mra/mra* and *mra/ddx19*muts, 5 dpf)	Reduced number of labeled cells, terminals in one thin band (22)	Neurites in two sublaminae (22)	No sublamination (21)	No sublamination (5)	No sublamination (5)

***Doerre and Goldsmith refs**

Figure 1: Cell type and IPL organization of the 5 dpf zebrafish retina

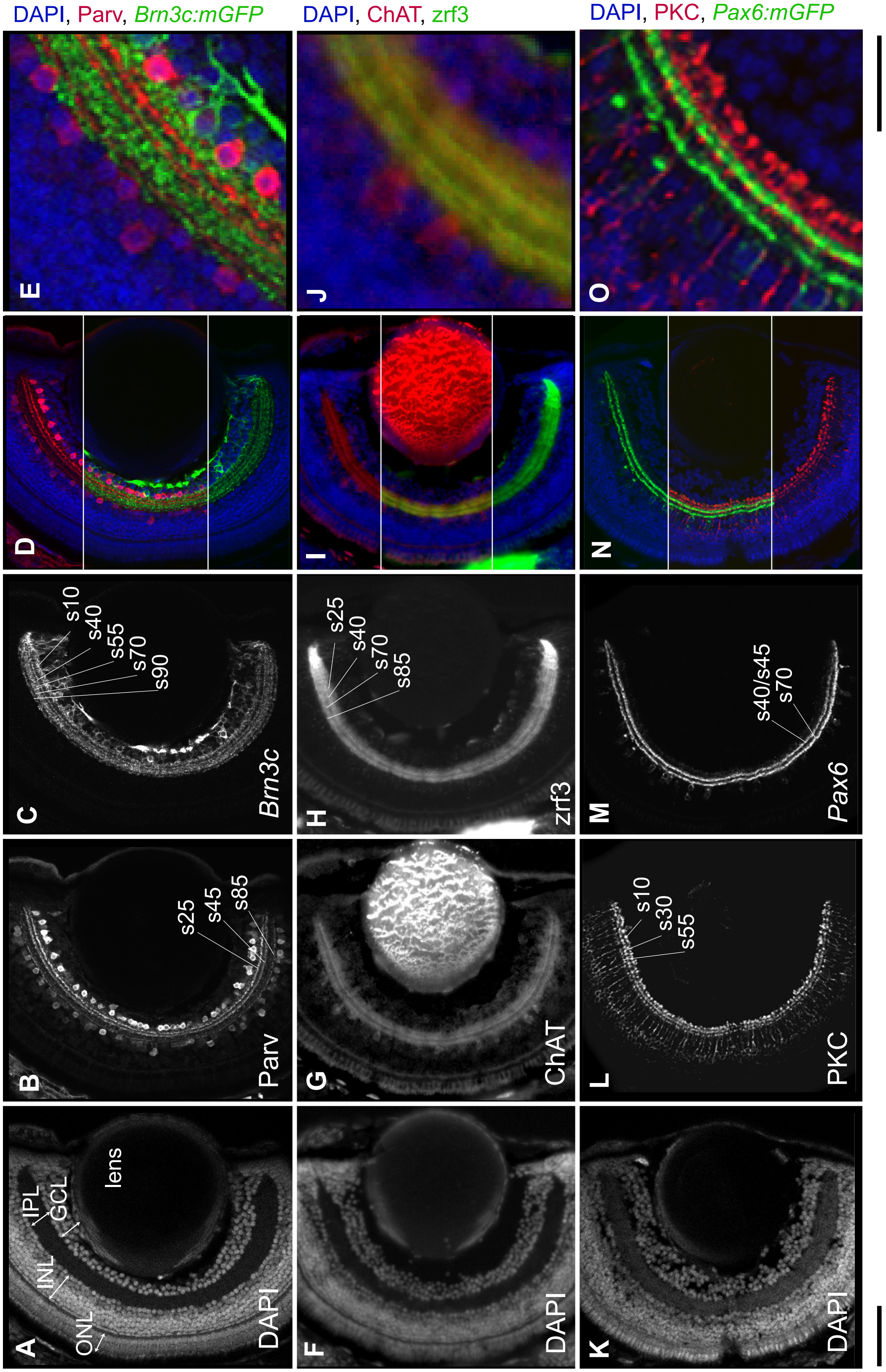
DAPI, Parv, *Brn3c:mGFP*
DAPI, ChAT, zrf3
DAPI, PKC, *Pax6:mGFP*
A
DAPI
lens
IPL
GCL
INL
ONL
B
Parv
s25
s45
s85
C
Brn3c
s10
s40
s55
s70
s90
D
E
F
DAPI
G
ChAT
H
zrf3
s25
s40
s70
s85
I
J
K
DAPI
L
PKC
s10
s30
s55
M
Pax6
s40/s45
s70
N
O

Figure 2: Schematic of retinal cell types and IPL organization

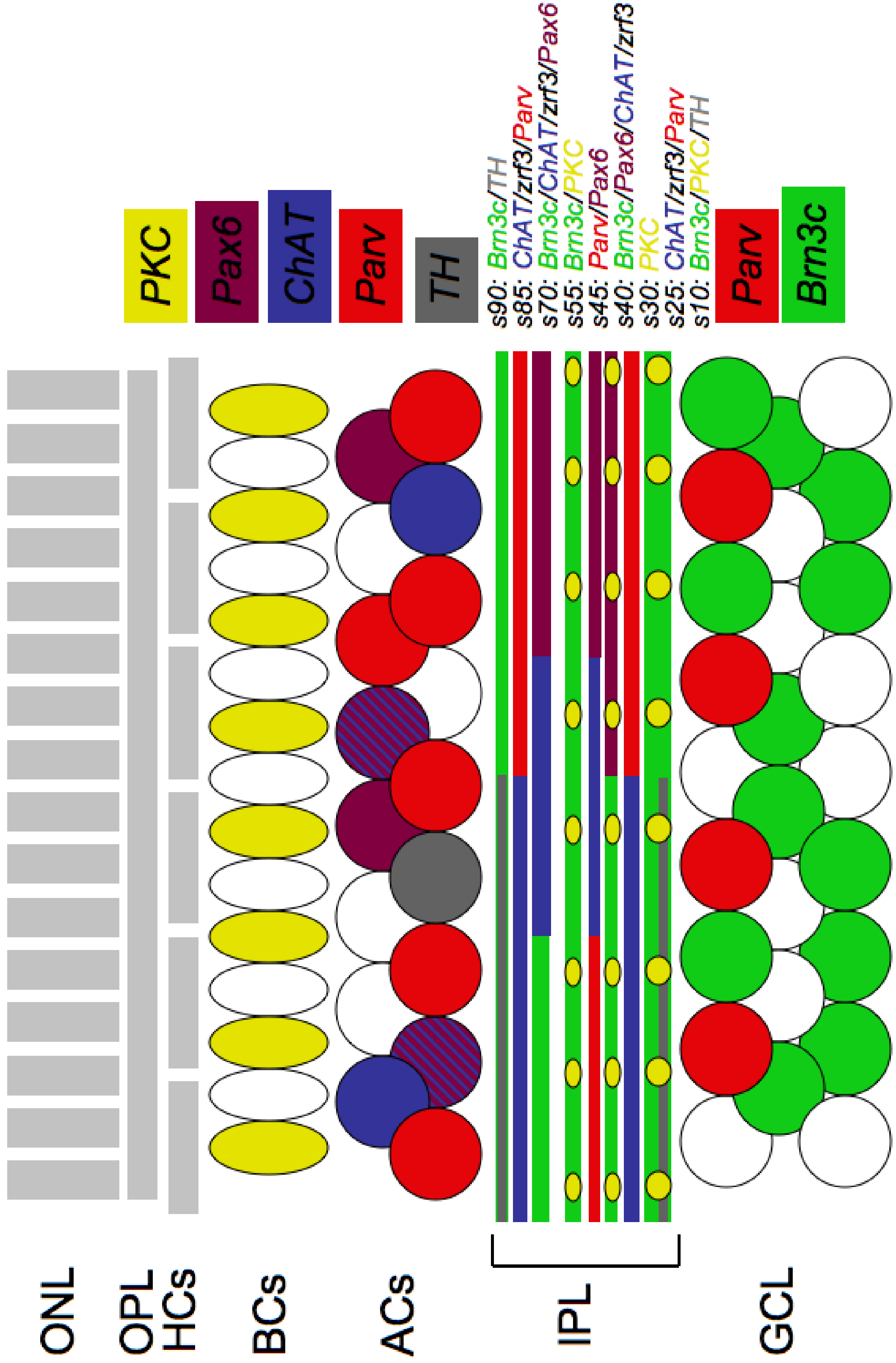
PKC
Pax6
ChAT
Parv
TH
s90: Brm3c/TH
s85: ChAT/zrf3/Parv
s70: Brm3c/ChAT/zrf3/Pax6
s55: Brm3c/PKC
s45: Parv/Pax6
s40: Brm3c/Pax6/ChAT/zrf3
s30: PKC
s25: ChAT/zrf3/Parv
s10: Brm3c/PKC/TH
Parv
Brm3c
ONL
OPL
HCs
BCs
ACs
IPL
GCL

Figure 3: Dark-reared, APB-reared, and BtTx-injected 7 dpf larvae show wildtype IPL sublamination

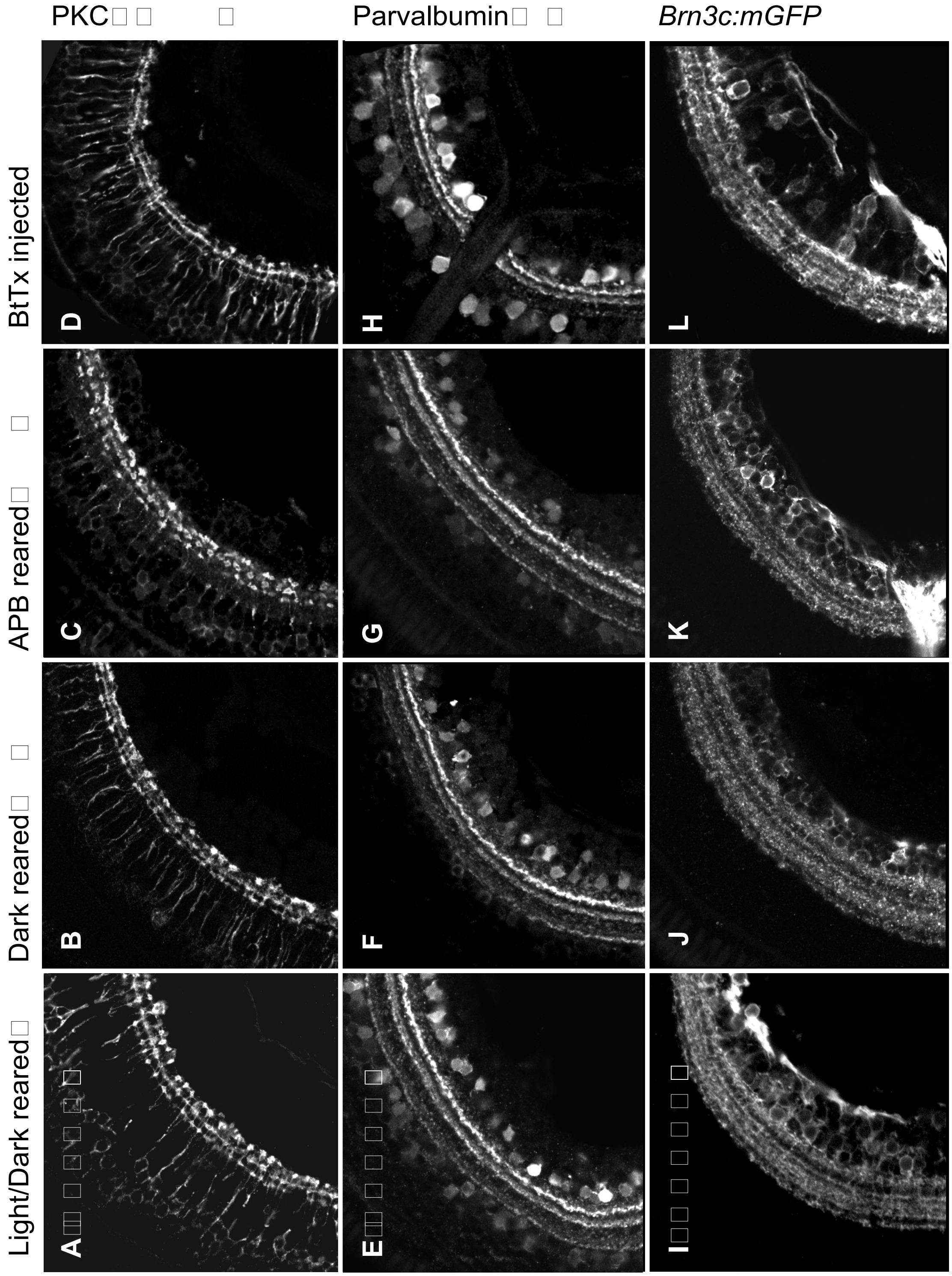
PKC
Parvalbumin
Brn3c:mGFP
BtTx injected
APB reared
Dark reared
Light/Dark reared
A
B
C
D
E
F
G
H
I
J
K
L

Figure 4: Lack of photoreceptors in *bru* does not alter neurite sublamination

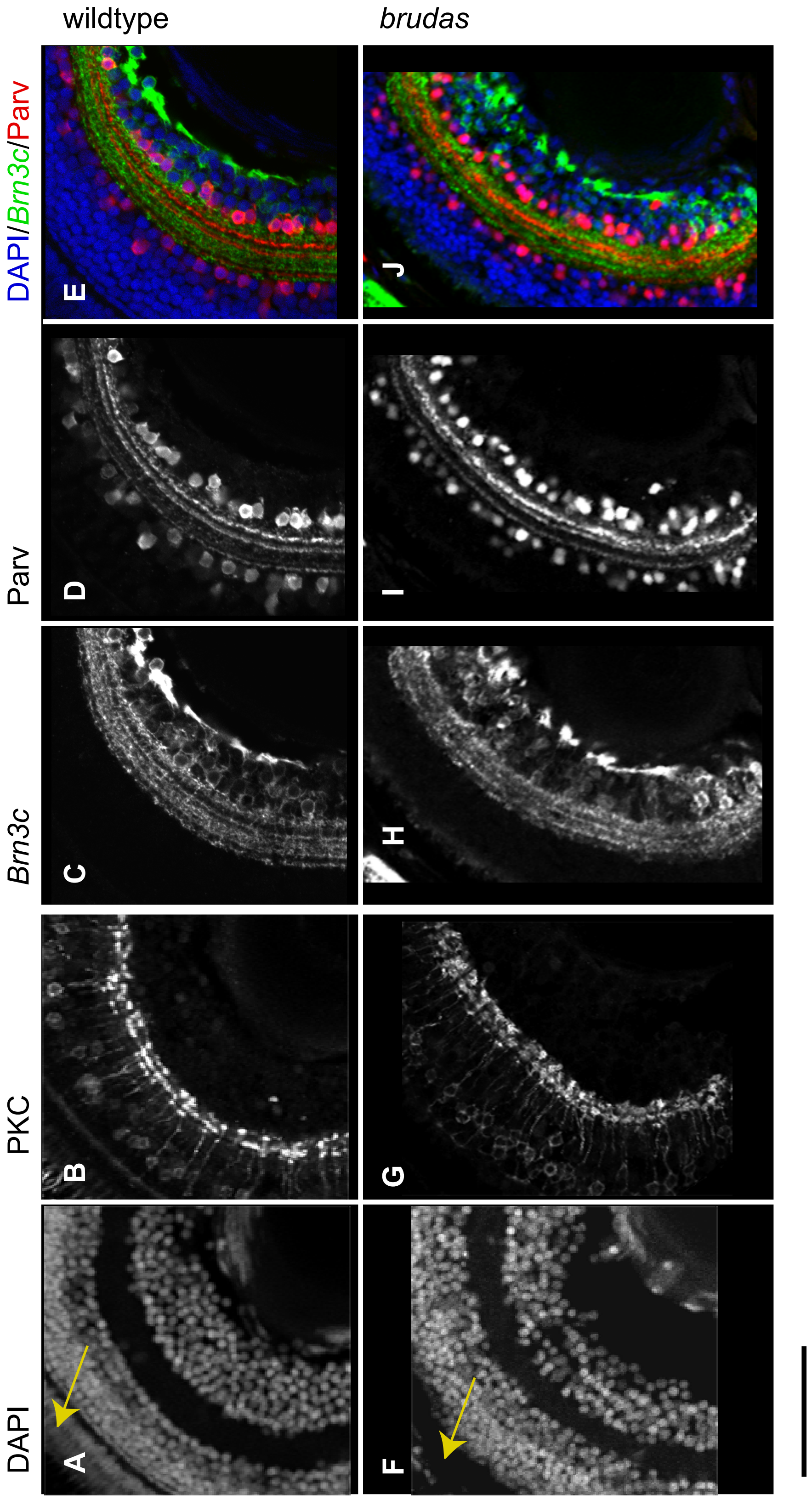
wildtype
brudas
DAPI/Brn3c/Parv
Parv
Brn3c
PKC
DAPI
A
B
C
D
E
F
G
H
I
J

Figure 5: *bru* has increased cell death in the retina and variable IPL phenotypes

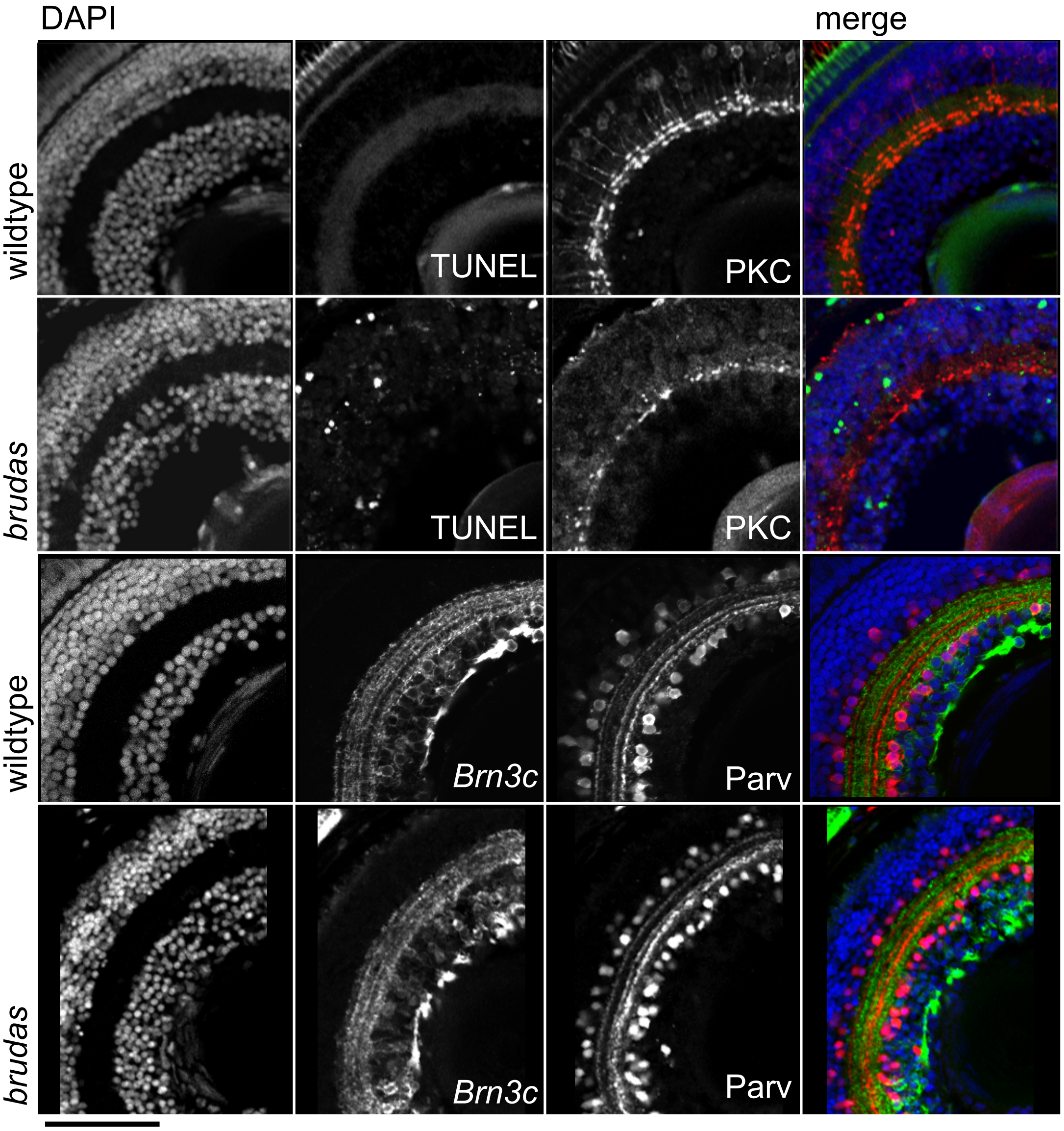
DAPI
merge
wildtype
TUNEL
PKC
brudas
TUNEL
PKC
wildtype
Brn3c
Parv
brudas
Brn3c
Parv

Figure 6: *bru*^{tw212} mutants have a splice site mutation in *NSF*

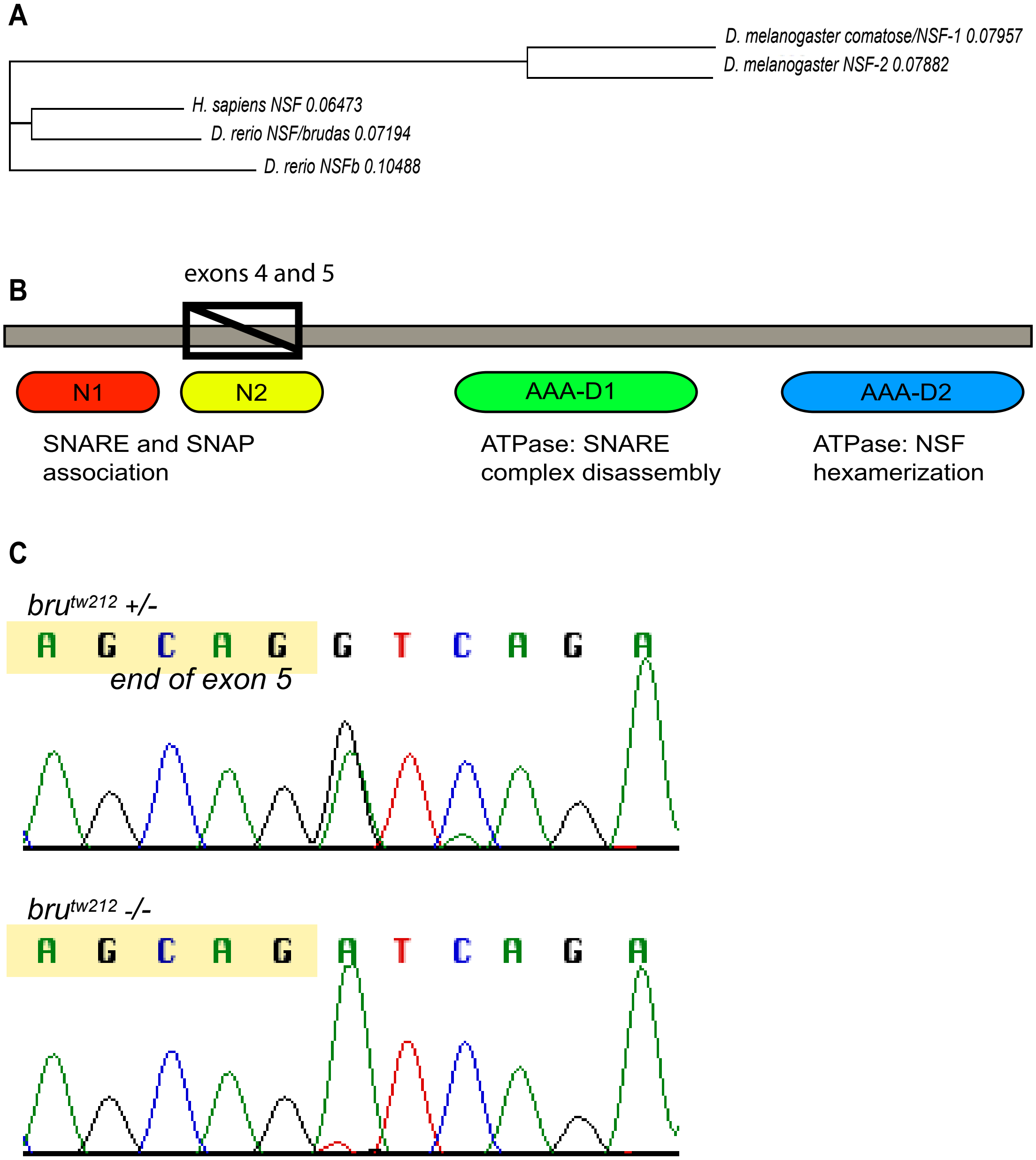
A
D. melanogaster comatose/NSF-1 0.07957
D. melanogaster NSF-2 0.07882
H. sapiens NSF 0.06473
D. rerio NSF/brudas 0.07194
D. rerio NSFb 0.10488
B
exons 4 and 5
N1
N2
AAA-D1
AAA-D2
SNARE and SNAP association
ATPase: SNARE complex disassembly
ATPase: NSF hexamerization
C
bru tw212 +/-
A G C A G G T C A G A
end of exon 5
bru tw212 -/-
A G C A G A T C A G A

Figure 7: BtTxB injection blocks the ERG B-wave

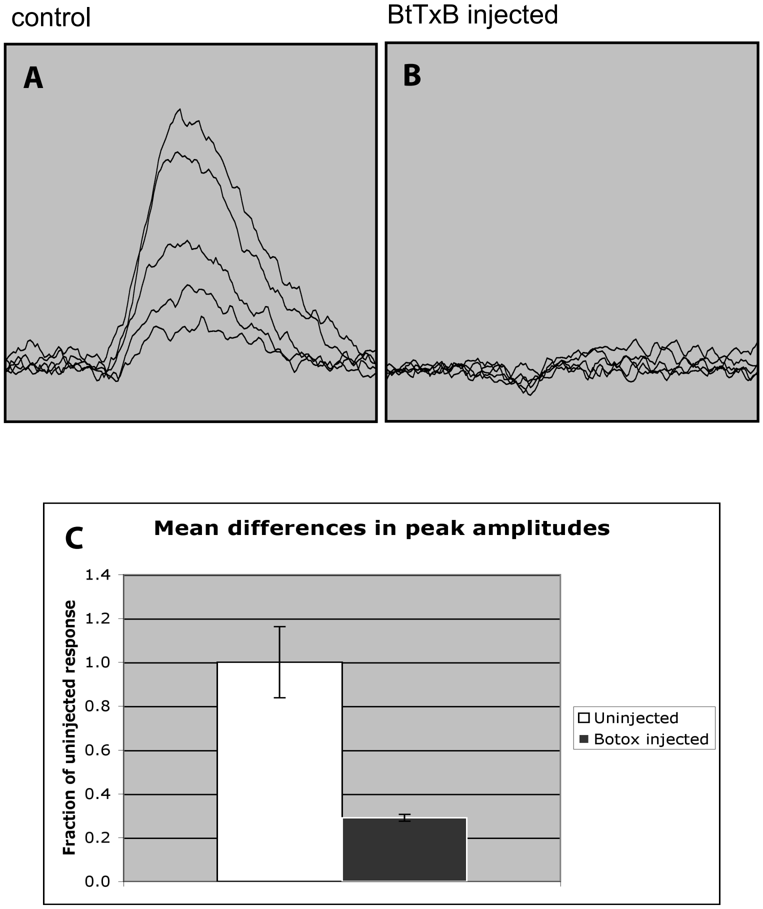

Figure 8: *bru* and *eter* mislocalize zrf3 to INL cell bodies

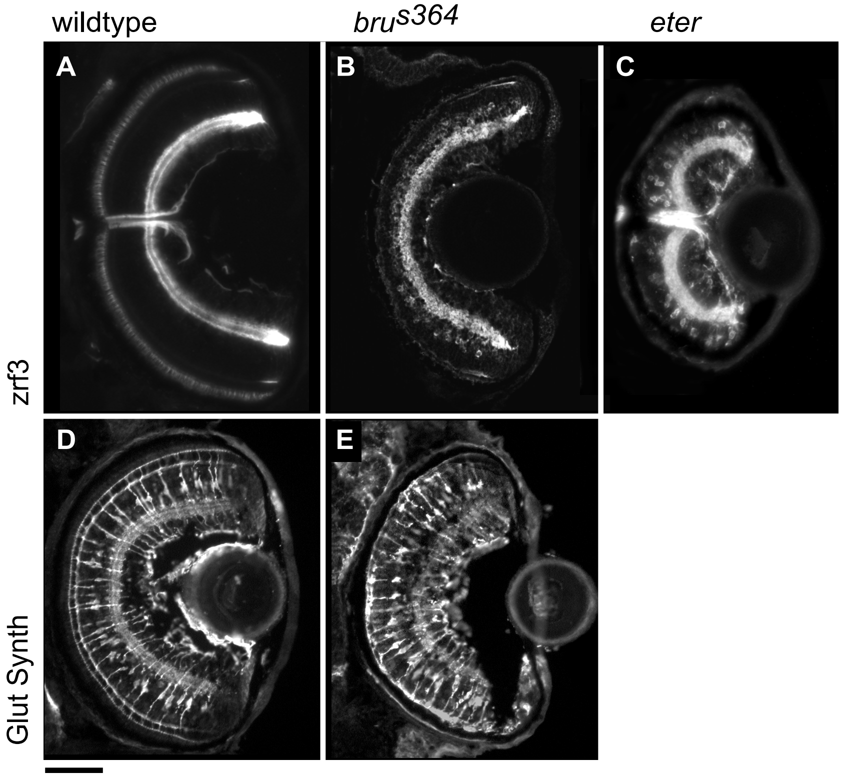
wildtype
bru^{s364}
eter
A
B
C
zrf3
D
E
Glut Synth

Figure 9: Photoreceptor death in *moti* mutants does not effect zrf3 expression or IPL sublamination

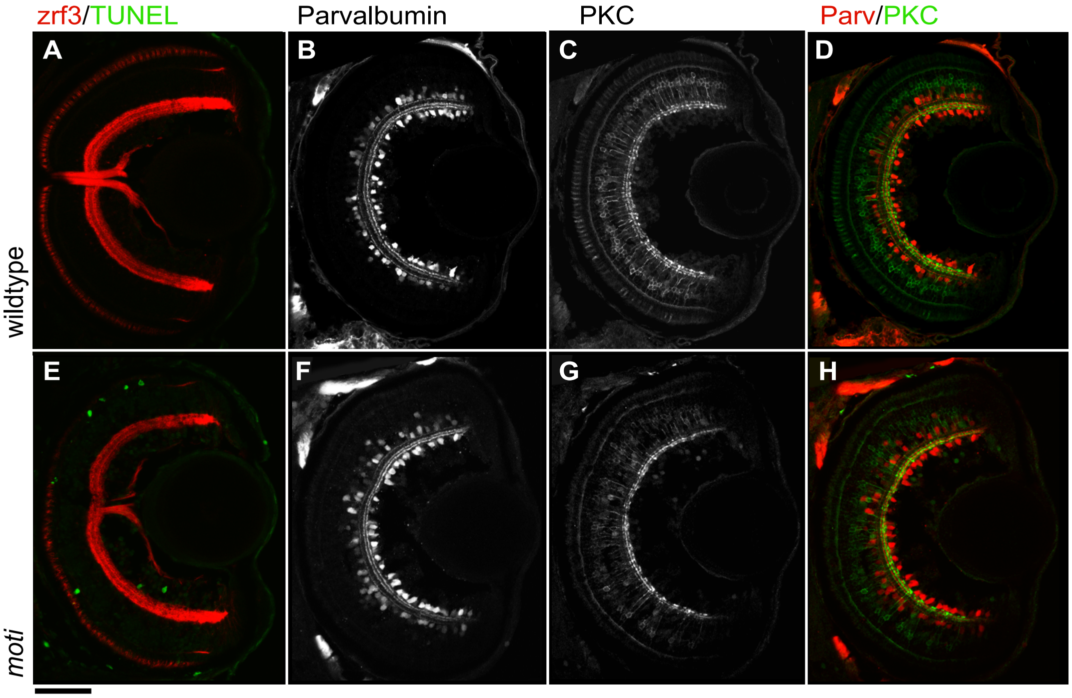
zrf3/TUNEL
Parvalbumin
PKC
Parv/PKC
A
B
C
D
wildtype
E
F
G
H
moti

Figure 10: *noto* mutants have multiple defects in fine IPL sublamination

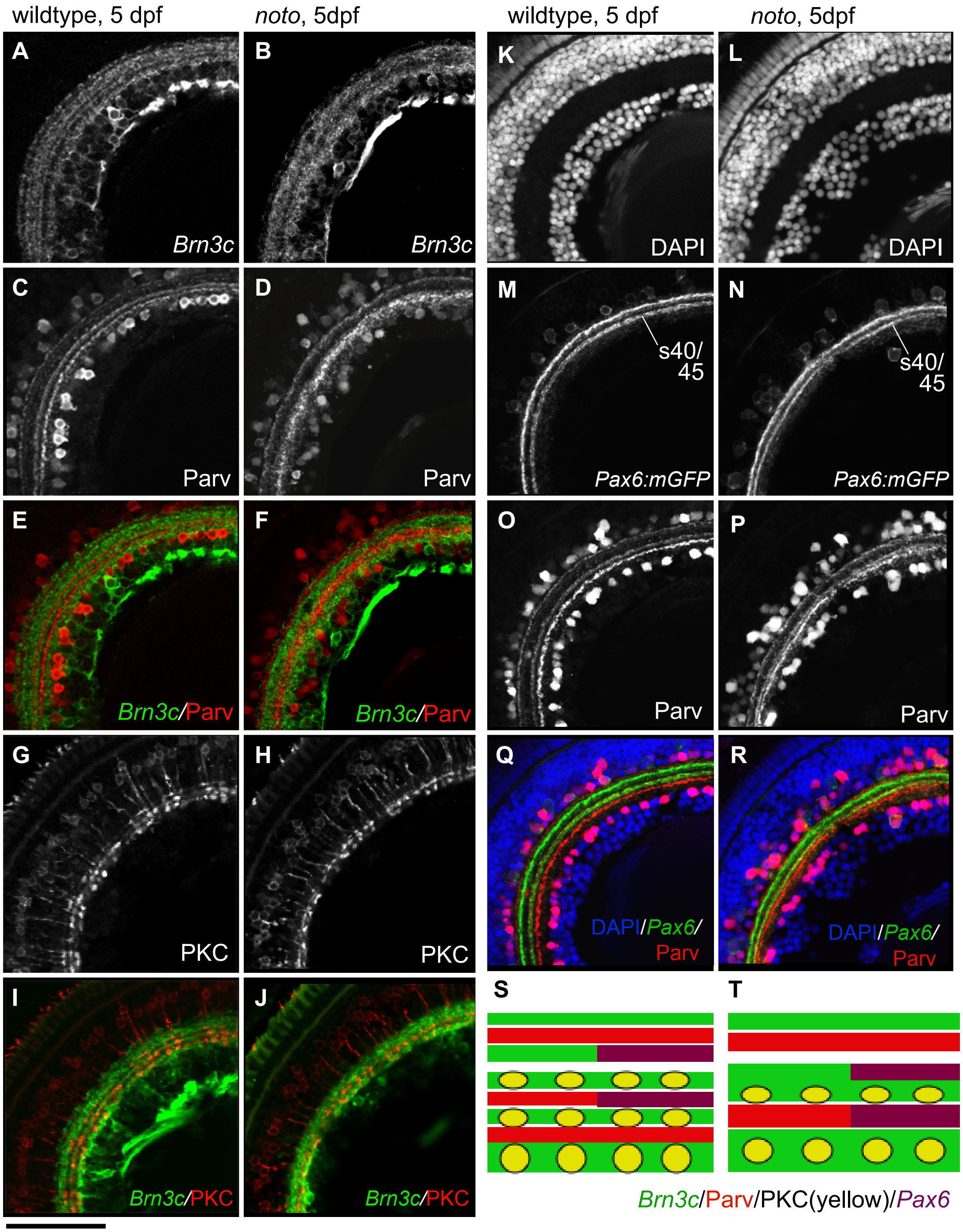
wildtype, 5 dpf
noto, 5dpf
wildtype, 5 dpf
noto, 5dpf
A
Brn3c
B
Brn3c
K
DAPI
L
DAPI
C
Parv
D
Parv
M
s40/
45
Pax6:mGFP
N
s40/
45
Pax6:mGFP
E
Brn3c/Parv
F
Brn3c/Parv
O
Parv
P
Parv
G
PKC
H
PKC
Q
DAPI/*Pax6*/
Parv
R
DAPI/*Pax6*/
Parv
I
Brn3c/PKC
J
Brn3c/PKC
S
T
Brn3c/Parv/PKC(yellow)/*Pax6*

Figure 11: *noto* mutant sublamination defects become more pronounced by 7dpf

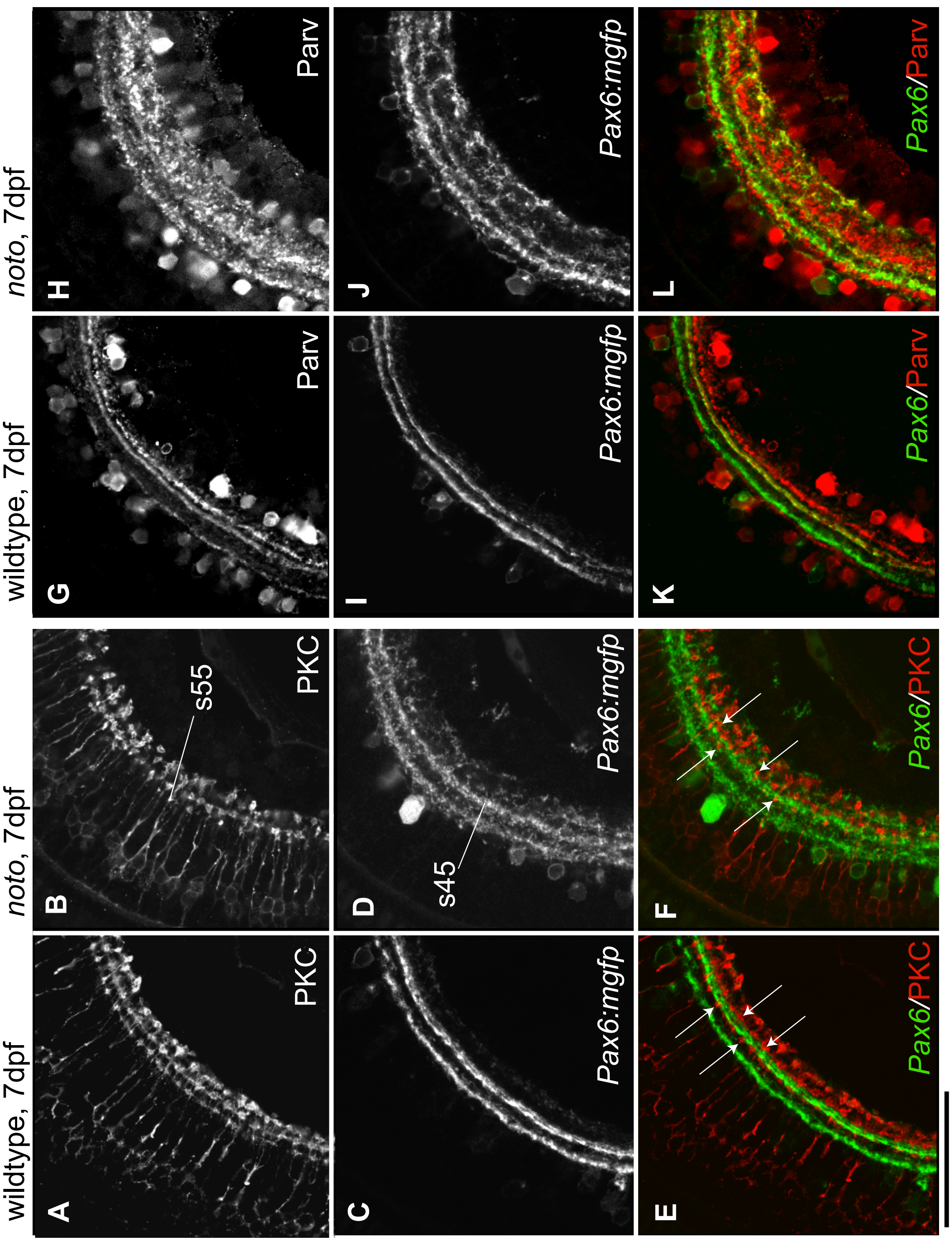
wildtype, 7dpf
noto, 7dpf
wildtype, 7dpf
noto, 7dpf
A
PKC
B
PKC
s55
C
Pax6:mgfp
D
Pax6:mgfp
s45
E
Pax6/PKC
F
Pax6/PKC
G
Parv
H
Parv
I
Pax6:mgfp
J
Pax6:mgfp
K
Pax6/Parv
L
Pax6/Parv

Figure 12: *noto* sublamination defects are rescued in *noto/lak* double mutants

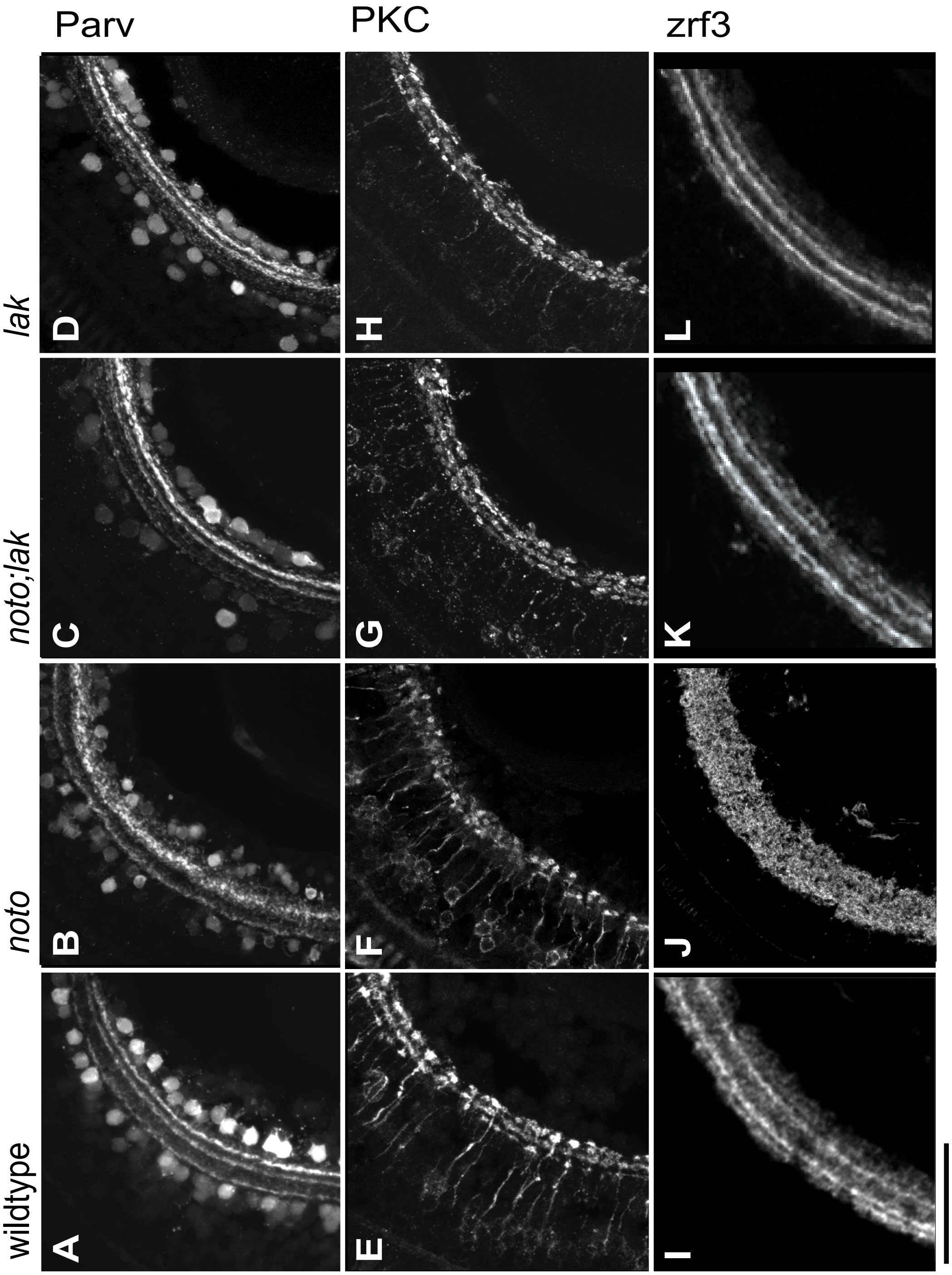
Parv
PKC
zrf3
lak
noto;lak
noto
wildtype
D
H
L
C
G
K
B
F
J
A
E
I

Figure 13: *spel* mutants have AC and BC sublamination defects in the inner IPL

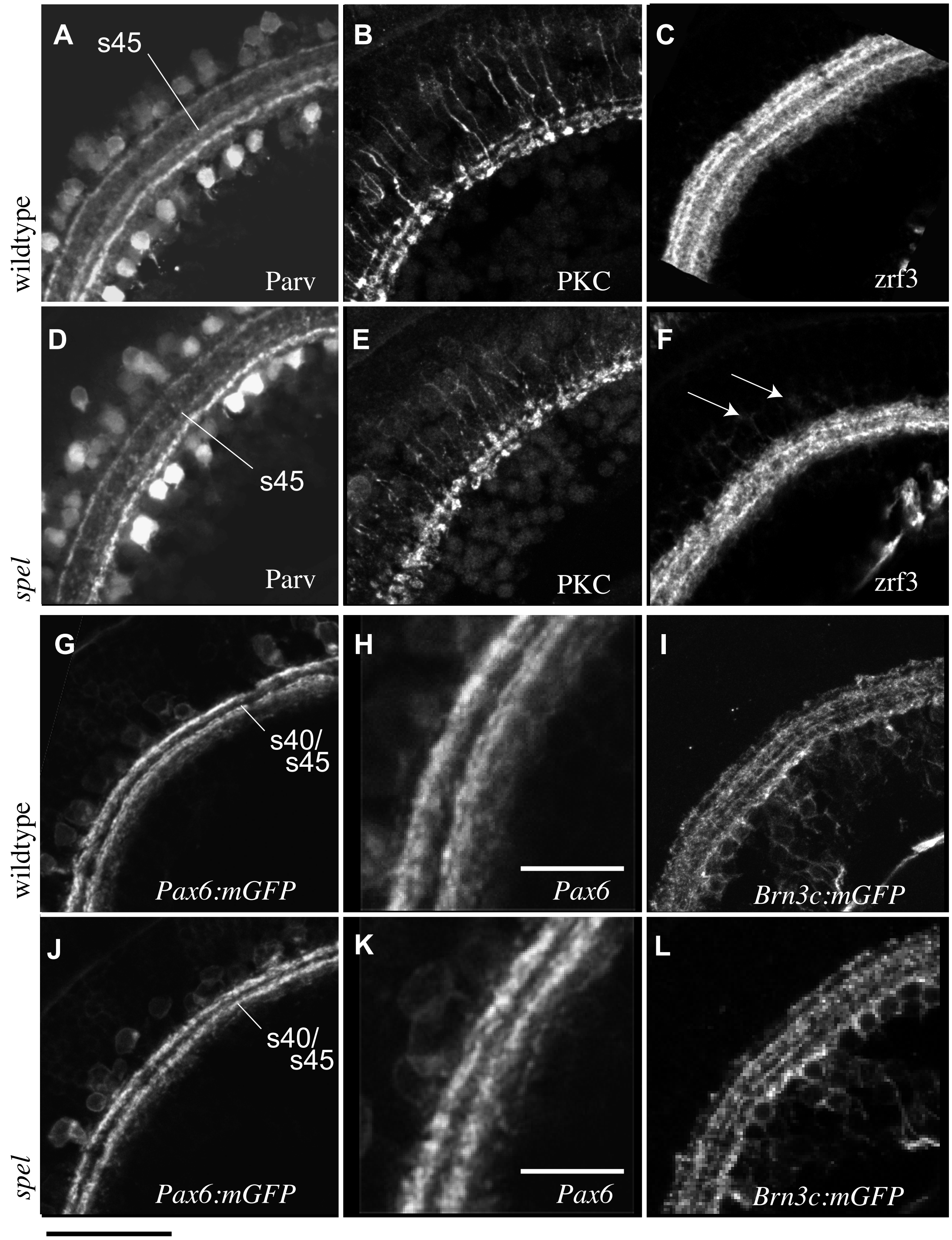
A
s45
B
C
wildtype
Parv
PKC
zrf3
D
E
F
s45
spel
Parv
PKC
zrf3
G
H
I
s40/
s45
wildtype
Pax6:mGFP
Pax6
Brn3c:mGFP
J
K
L
s40/
s45
spel
Pax6:mGFP
Pax6
Brn3c:mGFP

Figure 14: Mislocalized neurons in the GCL project to ectopic plexiform regions in *asph* mutants

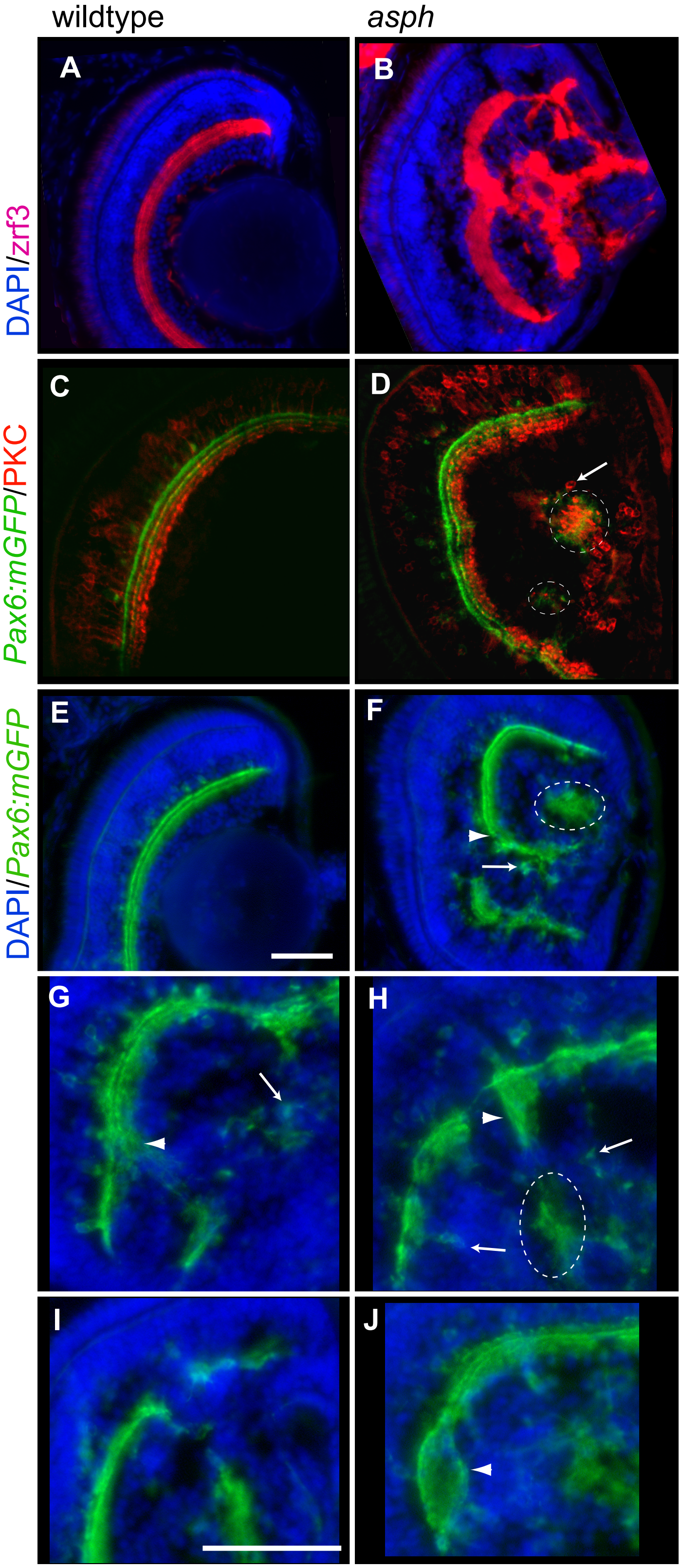
wildtype
asph
A
B
C
D
E
F
G
H
I
J
DAPI/zrf3
Pax6:mGFP/PKC
DAPI/Pax6:mGFP

Figure 15: *mra* is essential for IPL sublamination

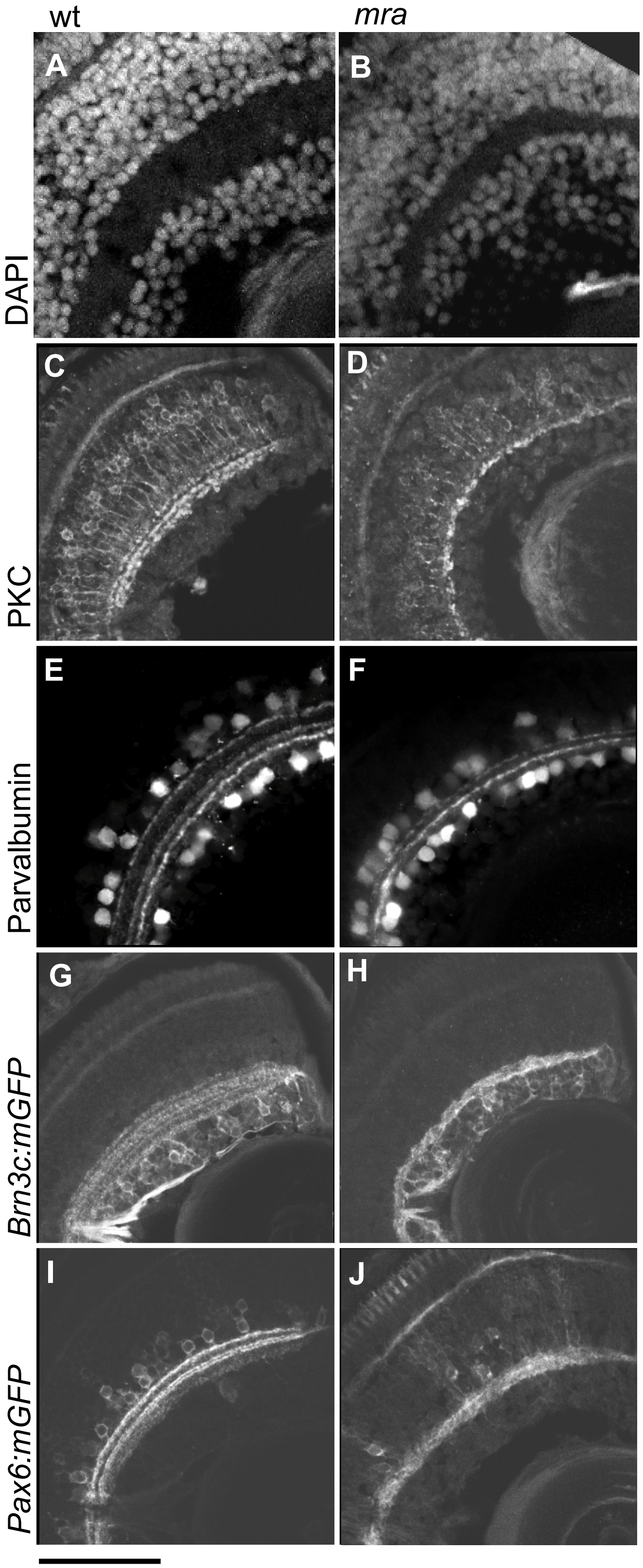
wt
mra
A
B
DAPI
C
D
PKC
E
F
Parvalbumin
G
H
Brn3c:mGFP
I
J
Pax6:mGFP

Figure 16: *mra* carries a missense mutation in *ddx19,* a ubiquitously expressed RNA helicase

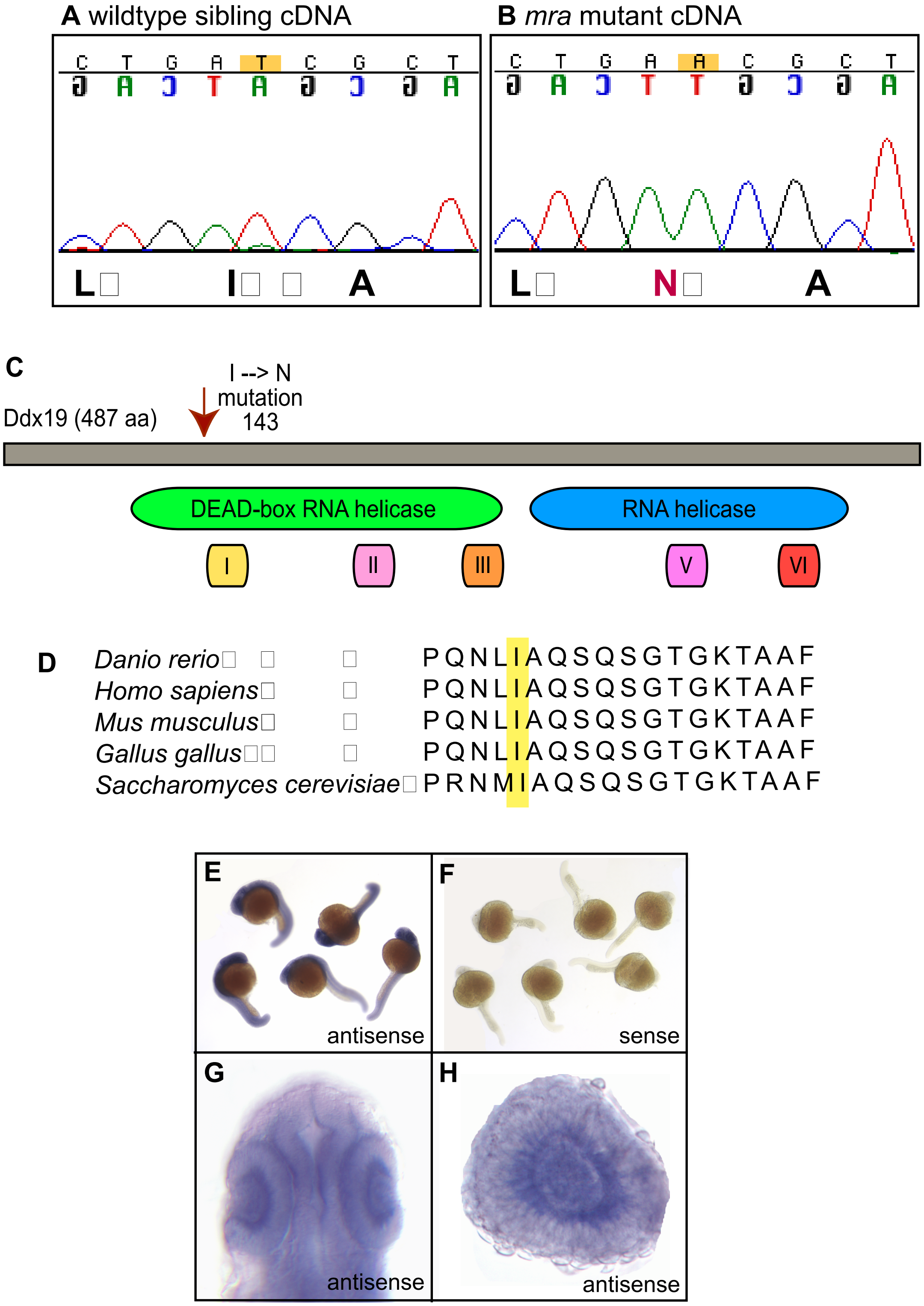

Figure 17: Cell autonomous and cell non-autonomous *ddx19* function are required for *Pax6:mGFP*+ neurite sublamination

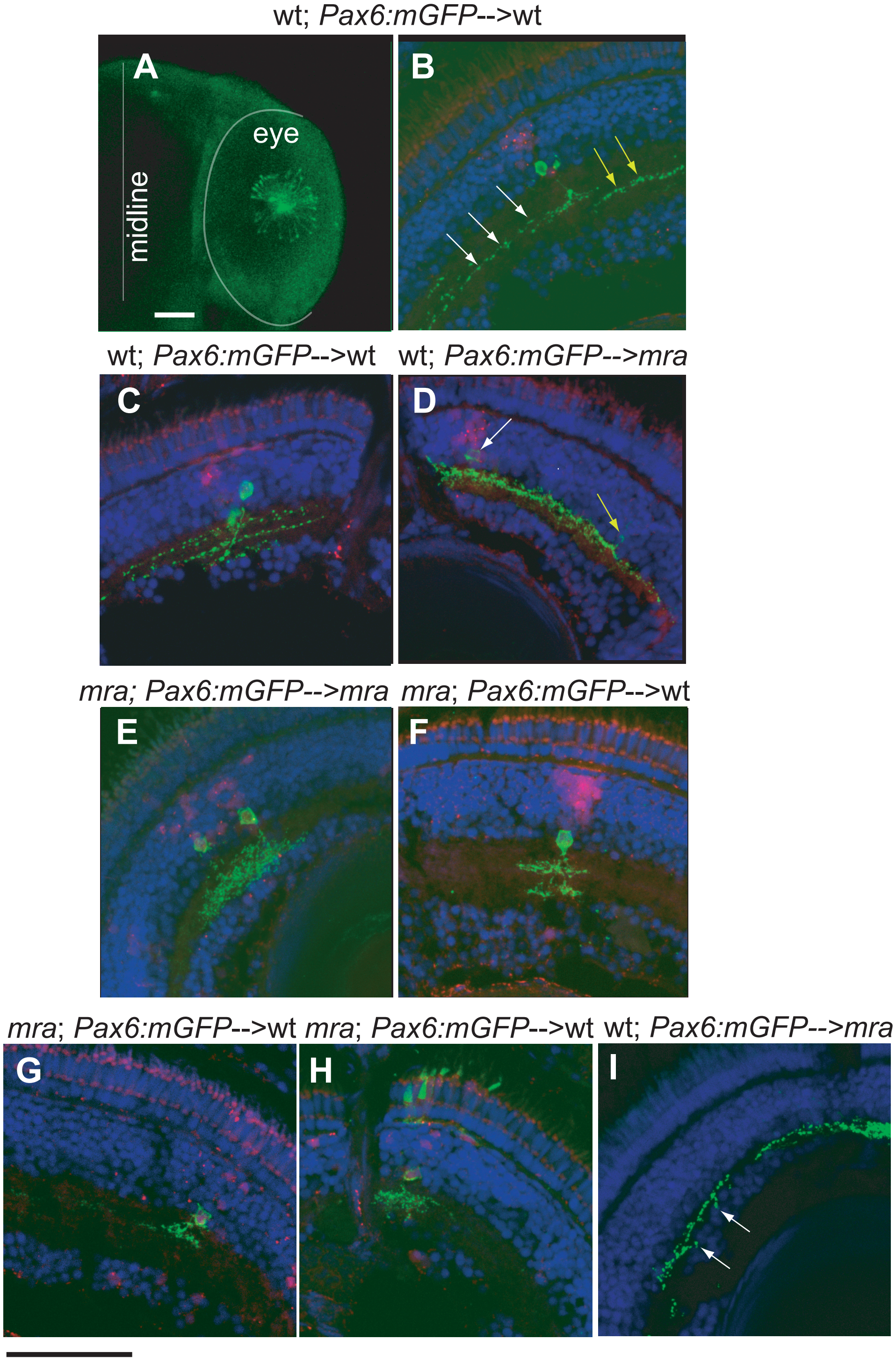
wt; *Pax6:mGFP*-->wt
A
eye
midline
B
wt; *Pax6:mGFP*-->wt
wt; *Pax6:mGFP*-->*mra*
C
D
mra; Pax6:mGFP-->*mra*
mra; *Pax6:mGFP*-->wt
E
F
mra; *Pax6:mGFP*-->wt
mra; *Pax6:mGFP*-->wt
wt; *Pax6:mGFP*-->*mra*
G
H
I

Supplementary Figure 1: Tyrosine hydroxylase neurites innervate the edges of the IPL

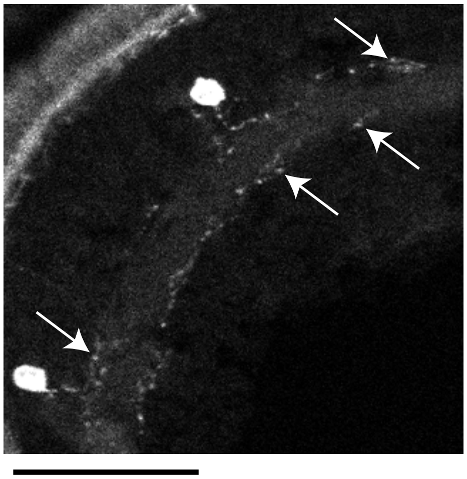

Supplementary Fig 2: *noto* fails to develop fine sublamination of ChAT+ neurites

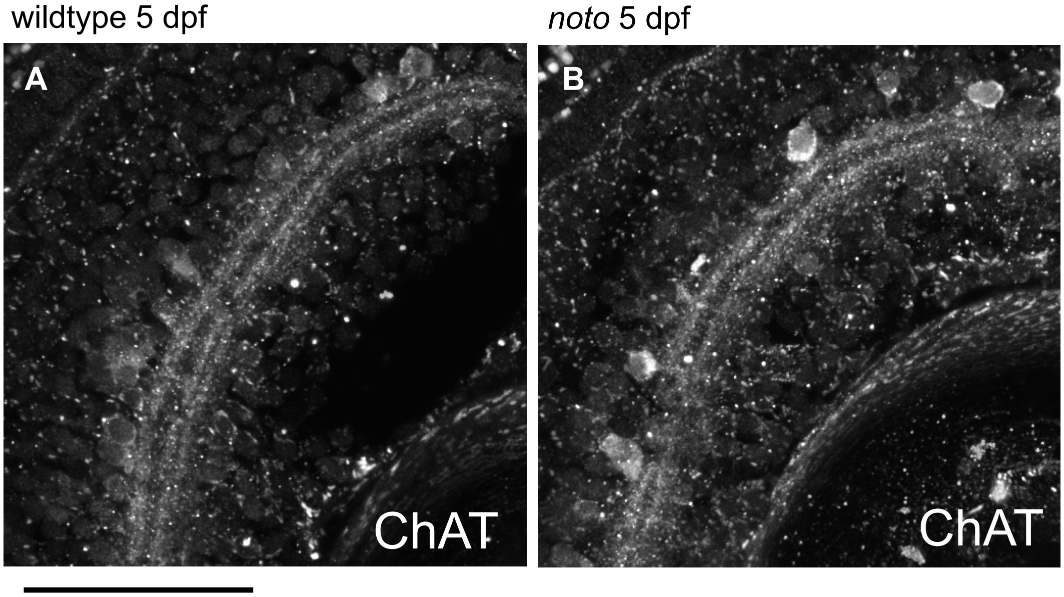
wildtype 5 dpf
noto 5 dpf
A
B
ChAT
ChAT

Supplementary Figure 3: Altered neuropil organization in the *asph* tectum

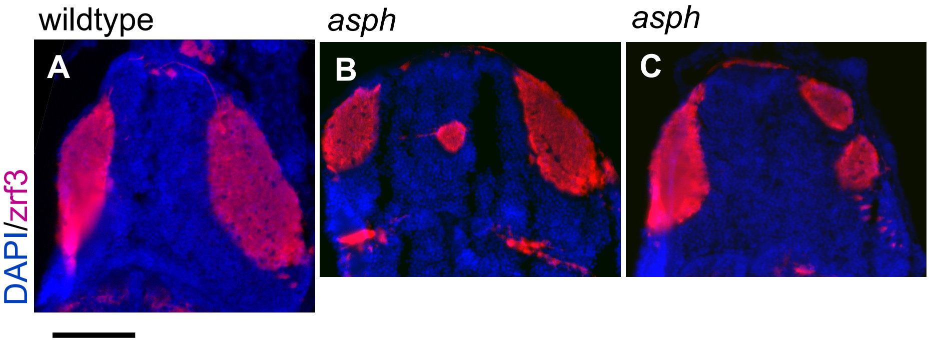
wildtype
asph
asph
A
B
C
DAPI/zrf3

Supplementary Figure 4: Parvalbumin+ neurons are scattered within the GCL of *cfe* mutants

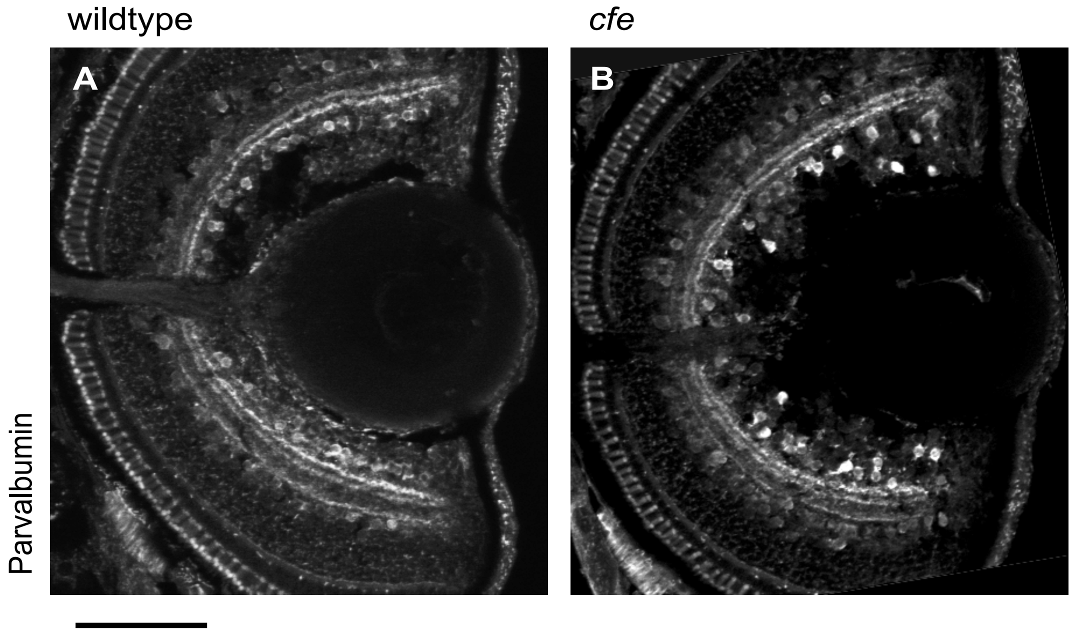
wildtype
cfe
A
B
Parvalbumin

Supplementary Figure 5: The *mra* mutation does not increase cell death measured by TUNEL

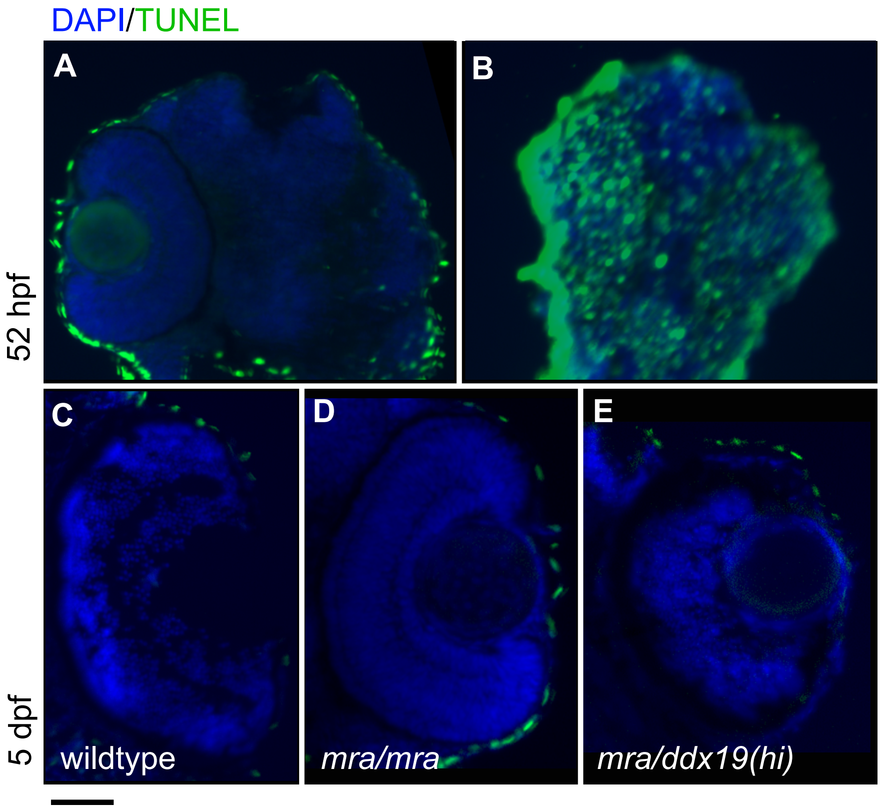
DAPI/TUNEL
A
B
52 hpf
C
D
E
5 dpf
wildtype
mra/mra
mra/ddx19(hi)

Supplementary Figure 6: *ddx19* expression time course

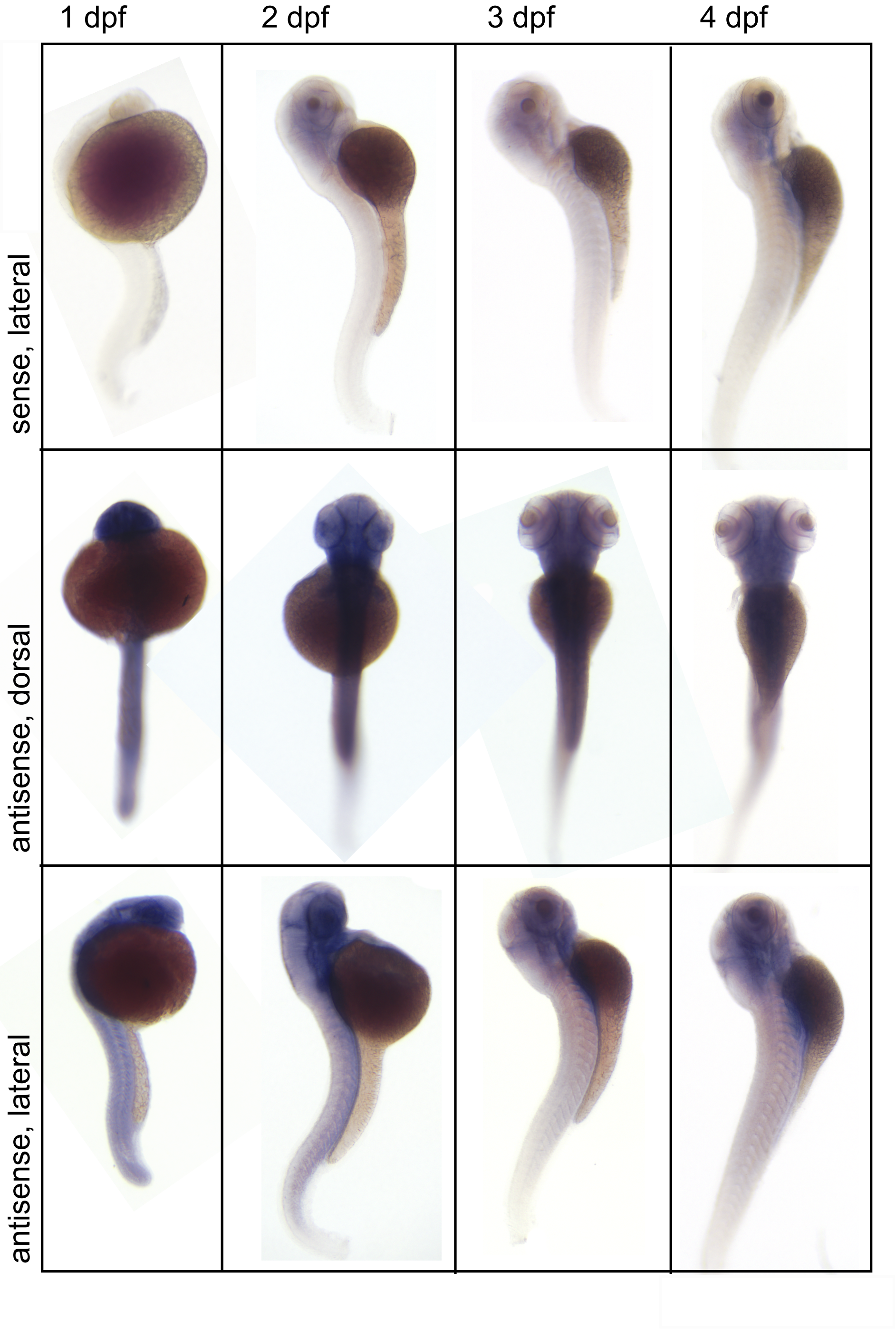
1 dpf
2 dpf
3 dpf
4 dpf
sense, lateral
antisense, dorsal
antisense, lateral

Chapter 3: Retinal ganglion cell axons arborize in inappropriate laminae and alter tectal dendrite projections in the *notorious* mutant

Linda Nevin and Herwig Baier

Abstract

The larval zebrafish optic tectum is a tractable region for the study of neurite targeting; GC axons and tectal dendrites are arranged into laminae, and forward mutagenesis can uncover molecular players in lamination. To better exploit the tectal neuropil as a model of neurite lamination, we have identified two antigens—parvalbumin and protein kinase C (PKC)—which specifically label distinct cell types in the tectum. Immunosera to these antigens labels dendrite projections to distinct laminae of the neuropil, such that immunostaining can easily reveal its laminar structure. Using these antisera in a forward genetic screen, we have identified a mutant—*notorious (noto)*—with aberrant targeting of parvalbumin+ tectal dendrites. The afferent ganglion cell (GC) axons, labeled in the *Brn3c:mGFP (Brn3c)* transgenic line, are also poorly targeted. Single cell imaging of GCs demonstrates that, while both wildtype and *noto* axons can extend short, club-like branches from one lamina to another, only *noto* GC axons can form branched arbors in more than one lamina. These observations suggest that the *noto* gene is involved in inhibited the branching of trespassing neurites in the tectum.

Introduction

Proper functioning of the nervous system depends on the formation of appropriate synaptic connections during development. Each developing axon or dendrite must recognize its appropriate synaptic partner, while avoiding connections with neurites belonging to inappropriate partners. The targeting of neurites to specific laminae of a synaptic region, such as the inner plexiform layer of the retina or one of the six layers of vertebrate cortex, is a common mechanism neurites use, ostensibly to find the correct partners. Laminar arrays of neurites are a tractable system for the study of neurite target choice because the pattern is often grossly visible. The optic tectum, the major retinorecipient structure in the zebrafish brain, is a laminated structure; tectal laminae have been described in adult goldfish (Meek and Schellart 1978), and more recently in the larval zebrafish, in which the tectum is organized into a medial cell body region and a lateral neuropil, which is further laminated based on the subdivision of the retinotectal projection (Xiao et al. 2005). The tectum has been exploited for studies of development since the 1960's because of its accessible location at the 'roof' of the midbrain, the topographic map resulting from organized projections of GCs axons, and its relevance to feeding behavior.

In the optically clear zebrafish *(Danio rerio)*, as in albino *Xenopus*, time lapse imaging of individually labeled neurons and electrophysiology have lent insight into the process of dendrite and axon morphogenesis (Sin et al. 2002; Ruthazer et al. 2003; Hua et al. 2005; Smear et al. 2007). Developmental studies exploiting the tectum often consider developing neurites independent of their target laminae. However, the branching dynamics of a GC axon or tectal dendrite may well depend on which lamina it has innervated, particularly if each lamina has a distinct complement of potential partners. Because the larval zebrafish tectum is a promising system for continued study of neuritogenesis, we endeavored to find immunohistochemical markers of tectal neurons and their dendrites. Our hope was to find a molecular signature for each tectal lamina, such that a simple antibody stain could identify them. We found that two antigens that label specific cell types in the retina, parvalbumin and protein kinase C (∝) (PKC), also label exclusive subsets of tectal neurons with different patterns of projection to the tectal neuropil. In addition, we show that GCs expressing *Brn3c:mGFP (Brn3c),* a molecular marker of about 50% of GCs (Xiao et al. 2005), co-localize with a signature complement of dendrites in each lamina. Not surprisingly, this lamination pattern suggests that the distinct laminar projections of GCs have distinct functions.

The factors contributing to the development of tectal laminae have become clearer in the past 12 years, beginning with the discovery of molecular markers of specific chick (*Gallus gallus)* tectal laminae (Yamagata et al. 1995; Yamagata and Sanes 1995a, 1995b). Co-cultures of GCs and tectal explants, as well as developmental studies using eye enucleation or tectal ablation, have suggested that cell surface or extracellular matrix signals, expressed in both tectum and retina, are important for guidance of GC axons to the correct laminae (Sanes and Yamagata 1999). For example, *cadherin7* is expressed by a subset of GCs and the interneurons of their single target tectal lamina. Homophilic cell adhesion may be responsible for the development of this connection (Yamagata et al. 2006). Studies of the chick retinotectal projection have yielded intriguing expression patterns of numerous molecules, and suggestive data from culture systems. However, in order to establish the roles of these molecules, *in vivo* loss of function studies are needed.

Though fewer molecular markers of GC subsets and tectal laminae are known in the larval zebrafish, this model system is amenable to forward genetics, and is therefore very tractable for learning which genes truly control the development of lamina-specific projections. The zebrafish tectum has a laminar structure similar to the chick's, and, as in chick, GC axons arborization in one lamina only. A previous forward genetic screen (Xiao et al. 2005) identifying several mutants with defects in the retinotectal projection led to the discovery that the extracellular matrix component Collagen 4(∝5) is required to restrict GC axons to single laminae (Xiao and Baier 2007). To identify additional mutations affecting tectal lamination, we conducted a forward genetic screen, using parvalbumin and PKC immunostaining as a proxy for tectal lamination. This screen was conducted in tandem with a screen for sublamination defects in the inner plexiform layer (IPL) of the retina, described in Chapter 2. We here report the identification of one mutant, *notorious (noto),* in which parvalbumin+ tectal laminae do not form properly. This phenotype corresponds to aberrant GC projections; many *noto* GC axons arborize in more than one lamina. In addition, as discussed in Chapter 2, *noto* mutants have analogous IPL sublamination phenotypes, which we have shown to be GC-autonomous. The *noto* gene therefore acts upon two distinct cellular compartments—the dendrite and the axon—to mediate arbor morphology. The mutation has not yet been identified, but we anticipate that the *noto* gene will introduce a novel pathway important for the restriction of GC axons to tectal laminae.

Results and Discussion

The laminated architecture of the tectum accommodates four layers of retinal afferents

The larval zebrafish optic tectum is divided into the cell body region and the neuropil, which is the arborization field for the majority of the optic tract (Burrill and Easter 1994). The *Sonic hedgehog:GFP (Shh:GFP)* transgenic line, in which all GCs express GFP (Neumann and Nuesslein-Volhard 2000), is a useful tool for locating these laminae, which have been described in the adult goldfish (Nieuwenhuys et al. 1998) and subsequently in zebrafish larvae (Roeser and Baier 2003). In a horizontal section, GC axons in *Shh:GFP* fish can be seen to innervate the SO (*stratum opticum)*, three different sublaminae of the SFGS (*stratum fibrosum et griseum superficiale)*, the SGC (*stratum griseum centrale)*, and the SAC (*stratum album centrale)*/SPV *(stratum periventriculare)* border. As previously reported, *Brn3c:mGFP+* axons project to two laminae in the neuropil—the SO and the SFGS. Finer division of *Brn3c:mGFP* axons into two SFGS sublaminae can be seen in some sections (Xiao et al. 2005).

The antibodies chosen for this study label specific cell types and synaptic layers in the retina; we found that two of these also have a lamina-specific pattern in the tectum. We immunostained the tectum with antisera to parvalbumin, a Calcium-binding molecule which tends to label subsets of interneurons (Baimbridge et al. 1992), PKC, a component of the G-protein coupled phosphoinositide signaling cascade (Stryer 1995), and choline acetyl-transferase (ChAT), an enzyme necessary for the synthesis of acetylcholine (Kandel et al. 2000). In addition, we labeled the tectum with the zrf3 antibody, which labels an unknown antigen present on radial fibers and some neurites (Trevarrow et al. 1990). Zrf3 proved informative to the development of retinal synapses because it brightly labels specific IPL sublaminae—we were interested to see if zrf3 might label specific tectal laminae as well. Figures 18 and 19 show the organization of parvalbumin, PKC, and zrf3 immunoreactivity in the tectum, with the *Brn3c:mGFP* and *Shh:GFP* retinotectal inputs as a reference for the laminae of the tectal neuropil. PKC and parvalbumin antibodies label two distinct populations of tectal neurons and their dendrites, which project into the tectal neuropil and arborize in six laminae. PKC+ and parvalbumin+ cell bodies have a rough spatial separation; more PKC labeled cells tend to be in the deeper portion of the SPV, and more parvalbumin+ cells abut the neuropil. PKC positive neurites label three bands in the tectal neuropil; these co-localize with inputs from the retina in the SO, the deeper half of the SFGS, and the SGC. Parvalbumin positive neurites arborize in four bands. In two of these, the SO, and the superficial half of the SFGS, the parvalbumin+ laminae are colocalized with *Brn3c*+ retinal input. Two additional parvalbumin+ laminae lie in the SGC and SAC, each between two arms of retinal inputs. ChAT antisera also labels a small population of neurons in the cell body region (approximately 15 per 12um section), with neurites that extend to the neuropil (data not shown). We did not use this marker for screening or phenotype analysis because the sublamination was quite indistinct and the antisera labeling was inconsistent. As previously reported, zrf3 labels the neuropil and radial glial processes perpendicular to the long axis of the neuropil. Unlike in the IPL, no lamination of zrf3 immunoreactivity is seen in the tectum.

The* notorious *gene is required for laminar axon targeting in the tectum

As described above, the zebrafish retinotectal projection is laminated into SO, SFGS, SGC, and SAC/SPV branches in the tectal neuropil. These laminae can be seen in a horizontal section of the tectum. Just as *noto Brn3c*+ dendrites are poorly confined to sublaminae in the IPL, the axons project aberrantly between laminae of the tectal neuropil. As shown in Fig 20, the *noto Brn3c+* projection fills the SO and SFGS most densely, but extends into the space between these laminae and into deeper tectal lamina. Correspondingly, the lamination of parvalbumin+ dendrites into four laminae is lost in *noto* (Fig 20C,D). PKC+ laminae appear wildtype in *noto* mutants (data not shown). We hypothesized that these GC axons arborize within wildtype laminae, but branch aberrantly between them. To determine whether individual GC axons cross aberrantly between tectal sublaminae, we crossed the *noto* mutation into a *Brn3c:Gal4;UAS:mGFP (BGUG)* transgenic line, in which variegated expression of *UAS:mGFP* results in sparsely labeled GCs. We examined the morphology of GC axons by imaging live, GFP-expressing fish at 5 dpf. As shown elsewhere, wildtype GC axons labeled in this line show a precise projection directly to one tectal lamina, in which they arborize exclusively (Xiao and Baier 2007) (Fig 21D,F). Fifteen of the 27 *noto* GC axons we observed laminated properly in either the SO or the SFGS, as in wildtype. In the remaining 12 cases, one or two branches from each axon exited one lamina, traversed to another lamina, and built a new, widely branched arbor in the second lamina (mean number of crossings per GC, with SEM—wildtype: 0, 0; *noto:* .53, .16. p-value < .006 by two tailed t-test for samples with unequal variance). The high percentage of GC axons crossing between sublaminae can explain the GFP labeling throughout the neuropil. It should be noted that wildtype and mutant GC axons occasionally project short, dead-end branches out of one lamina to another; however, in wildtype these extra-laminar branches never develop into arbors. We observed a non-significant increase in extra-laminar branches in *noto* mutants (p-value = .29). The graph in figure 21M shows the percentages of *Brn3c+* GC axons in wildtype and *noto* with multi-laminar arbors, found only in *noto,* and with dead-end extra-laminar branches, occasionally seen in both. Clearly, *noto* axons are distinguished from their wildtype counterparts not by the ability to branch out of one lamina but by the ability to arborize in a second lamina.

We suggest that each lamina contains cues, either from target neurons or from the extracellular matrix, which act permissively to allow appropriate axons to form branched arbors. We suspect that the *noto* gene is involved in this process. It may encode a ligand or receptor required for a repulsive interaction, or a downstream effector of such signaling, such as a Rho GTPase. Alternatively, it may encode a component of the extracellular matrix, which might function as a scaffold for repulsive cues. Indeed, a mutation in collagen IV(α5), an extracellular matrix component of the tectal neuropil, has been shown to develop a similar aberrant GC arborization phenotype (Xiao and Baier 2007). Positioning mapping with approximately 2900 mutants has failed to identify a closed region containing the gene. Unfortunately, the zebrafish genome assemblies are incomplete, and this region in particular has not been successfully assembled. Several candidate gene coding regions have been tested; none of these carries a mutation.

Conclusions

We have identified two populations of tectal neurons with distinct projection patterns to the neuropil. The parvalbumin+ and PKC+ neurons can be labeled by immunostaining, and were successfully used to identify a mutant with aberrant laminar organization in the tectum. With the establishment of these cell type markers, and the availability of transgenic lines labeling retinal inputs, the larval zebrafish neuropil is now a more tractable system for the study of neurite morphogenesis in the brain.

In *noto,* we found analogous defects in GC dendrites and axons, indicating that these two distinct cellular compartments use at least one common developmental mechanism. The most striking aspect of the *noto* phenotype is the elaborate arbors that GC axons can develop in inappropriate laminae. Prior to identification of this mutant, we imagined that tectal laminae might have strict barriers between them, preventing GC axons from trespassing with strong repulsive cues. However, as we examined single axons in wildtype and *noto*, we observed that small, club-like branches from GC axons do occasionally cross between laminae in both. In *noto,* as opposed to in wildtype, these branches can form branched arborizations. Based on these observations, we now interpret that each lamina has a distinct set of cues that promote branching of the appropriate axons, and prevent branching of trespassing axons. The identification of the *noto* gene should begin to elucidate this process.

Methods

Fish husbandry, sectioning, immunohistochemistry, and imaging of sections were performed as in Chapter 2.

Imaging live fish

In some cases, tectal lamination was assessed by imaging intact, live fish. Larvae were mounted in molten Seaplaque low melting temperature agarose (2% w/v in embryonic medium; Cambrex, Rockland, ME). Once the agarose solidified, a cube containing each live fish was excised and glued to the bottom of a petri dish. The petri dish was filled with embryonic medium, and approximately 2 ml Tricaine-S solution (.4% w/v, adjusted to pH 7; Western Chemical Inc., Ferndale, WA) was added to anesthetize the larva. In some cases, approximately 200 µl norepinephrine (1% w/v, adjusted to pH 7; Sigma-

Aldrich Co., St. Louis, MO) was also added to the dish to induce the larvae to contract the pigment granules in their melanosomes. Larvae were imaged with a 40X dipping lens on a Zeiss LSM 5 Pascal confocal microscope. Confocal stacks were rendered into 3D volumes in ImageJ, and rotated to best observe the cross section of neuropil laminae.

References

Baimbridge KG, Celio MR, Rogers JH (1992) Calcium-binding proteins in the nervous system. Trends Neurosci 15(8): 303-308.

Burrill JD, Easter SS, Jr. (1994) Development of the retinofugal projections in the embryonic and larval zebrafish (Brachydanio rerio). J Comp Neurol 346(4): 583-600.

Hua JY, Smear MC, Baier H, Smith SJ (2005) Regulation of axon growth in vivo by activity-based competition. Nature 434(7036): 1022-1026.

Kandel E, Schwartz J, Jessell T (2000) Principles of neural science. New York: McGraw-Hill, Health Professions Division.

Meek J, Schellart NA (1978) A Golgi study of goldfish optic tectum. J Comp Neurol 182(1): 89-122.

Neumann CJ, Nuesslein-Volhard C (2000) Patterning of the zebrafish retina by a wave of sonic hedgehog activity. Science 289(5487): 2137-2139.

Nieuwenhuys H, Donkelaar C, Nicholson C (1998) The Central Nervous System of Vertebrates. New York: Springer.

Roeser T, Baier H (2003) Visuomotor behaviors in larval zebrafish after GFP-guided laser ablation of the optic tectum. J Neurosci 23(9): 3726-3734.

Ruthazer ES, Akerman CJ, Cline HT (2003) Control of axon branch dynamics by correlated activity in vivo. Science 301(5629): 66-70.

Sanes JR, Yamagata M (1999) Formation of lamina-specific synaptic connections. Curr Opin Neurobiol 9(1): 79-87.

Sin WC, Haas K, Ruthazer ES, Cline HT (2002) Dendrite growth increased by visual activity requires NMDA receptor and Rho GTPases. Nature 419(6906): 475-480.

Smear MC, Tao HW, Staub W, Orger MB, Gosse NJ et al. (2007) Vesicular glutamate transport at a central synapse limits the acuity of visual perception in zebrafish. Neuron 53(1): 65-77.

Stryer L (1995) Biochemistry. New York: W.H. Freeman.

Trevarrow B, Marks DL, Kimmel CB (1990) Organization of hindbrain segments in the zebrafish embryo. Neuron 4(5): 669-679.

Xiao T, Baier H (2007) Lamina-specific axonal projections in the zebrafish tectum require the type IV collagen Dragnet. Nat Neurosci 10(12): 1529-1537.

Xiao T, Roeser T, Staub W, Baier H (2005) A GFP-based genetic screen reveals mutations that disrupt the architecture of the zebrafish retinotectal projection. Development 132(13): 2955-2967.

Yamagata M, Sanes JR (1995a) Target-independent diversification and target-specific projection of chemically defined retinal ganglion cell subsets. Development 121(11): 3763-3776.

Yamagata M, Sanes JR (1995b) Lamina-specific cues guide outgrowth and arborization of retinal axons in the optic tectum. Development 121(1): 189-200.

Yamagata M, Herman JP, Sanes JR (1995) Lamina-specific expression of adhesion molecules in developing chick optic tectum. J Neurosci 15(6): 4556-4571.

Yamagata M, Weiner JA, Dulac C, Roth KA, Sanes JR (2006) Labeled lines in the retinotectal system: markers for retinorecipient sublaminae and the retinal ganglion cell subsets that innervate them. Mol Cell Neurosci 33(3): 296-310.

Figure 18: Cell type and neuropil organization of the 5 dpf zebrafish optic tectum

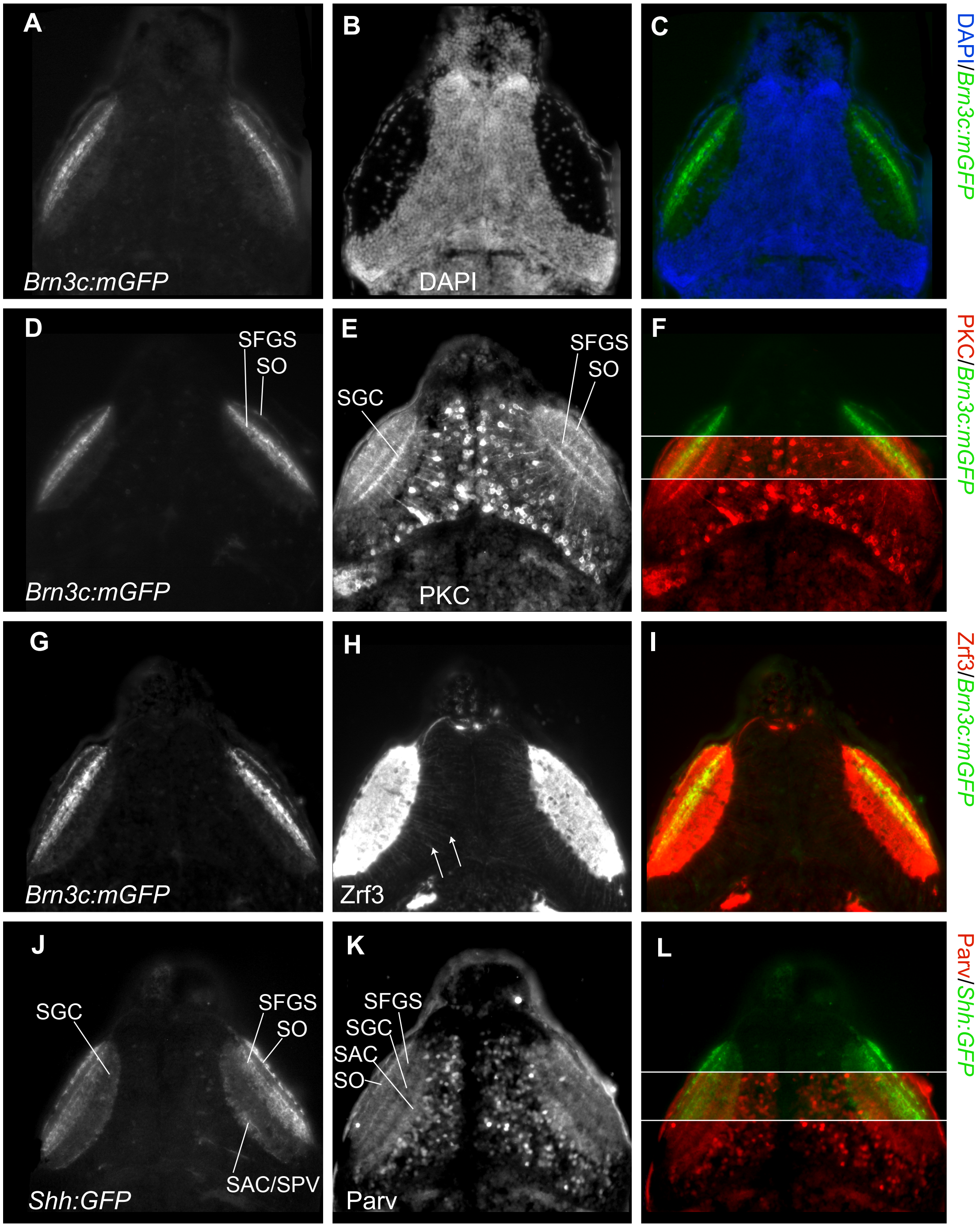
A
Brn3c:mGFP
B
DAPI
C
DAPI/Brn3c:mGFP
D
SFGS
SO
Brn3c:mGFP
E
SGC
SFGS
SO
PKC
F
PKC/Brn3c:mGFP
G
Brn3c:mGFP
H
Zrf3
I
Zrf3/Brn3c:mGFP
J
SGC
SFGS
SO
SAC/SPV
Shh:GFP
K
SFGS
SGC
SAC
SO
Parv
L
Parv/Shh:GFP

Figure 19: Magnified images of tectal laminations and schematic

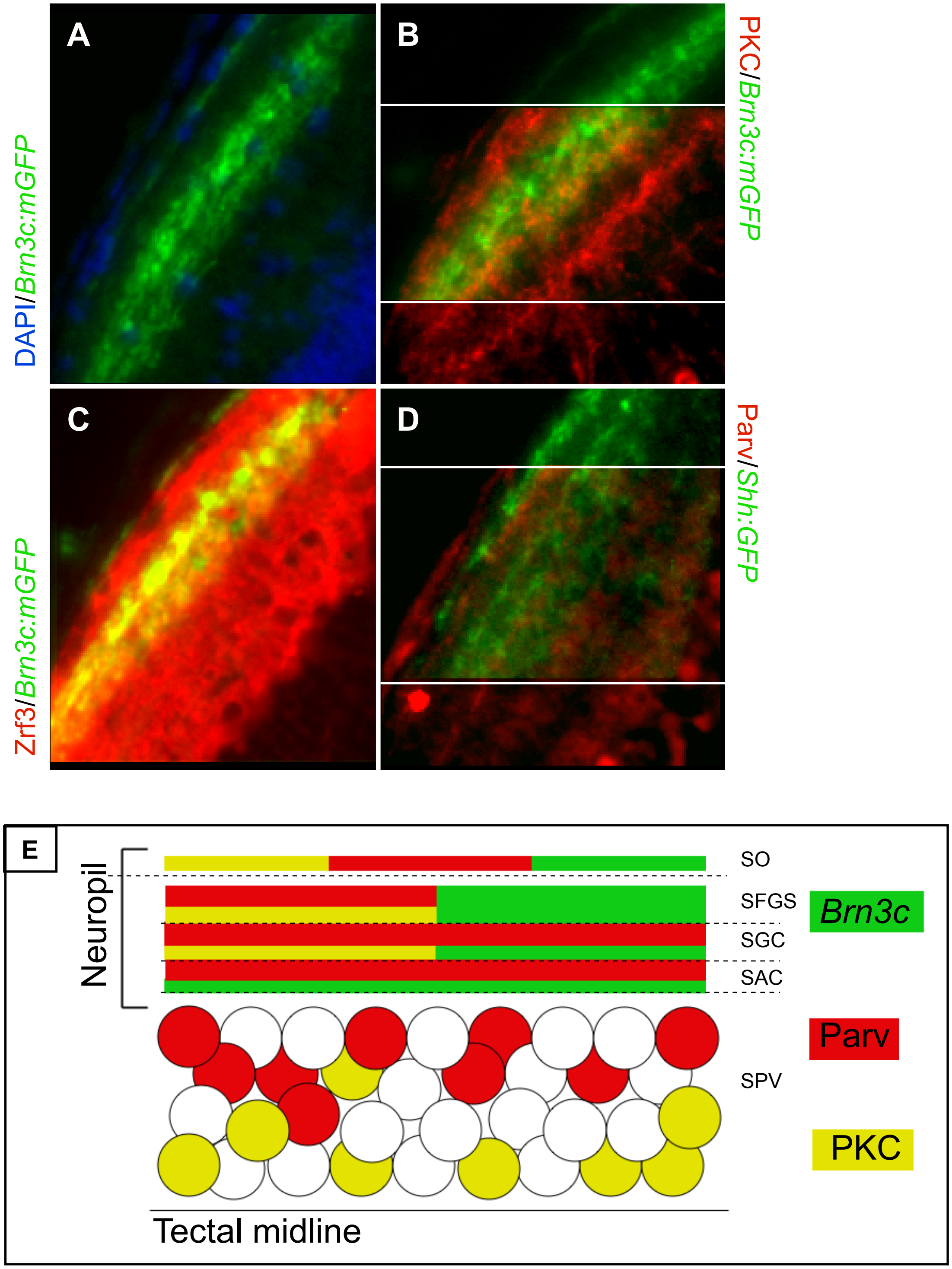
A
DAPI/*Brn3c:mGFP*
B
PKC/*Brn3c:mGFP*
C
Zrf3/*Brn3c:mGFP*
D
Parv/*Shh:GFP*
E
Neuropil
SO
SFGS
SGC
SAC
SPV
Tectal midline
Brn3c
Parv
PKC

Figure 20: The noto tectal neuropil is poorly laminated

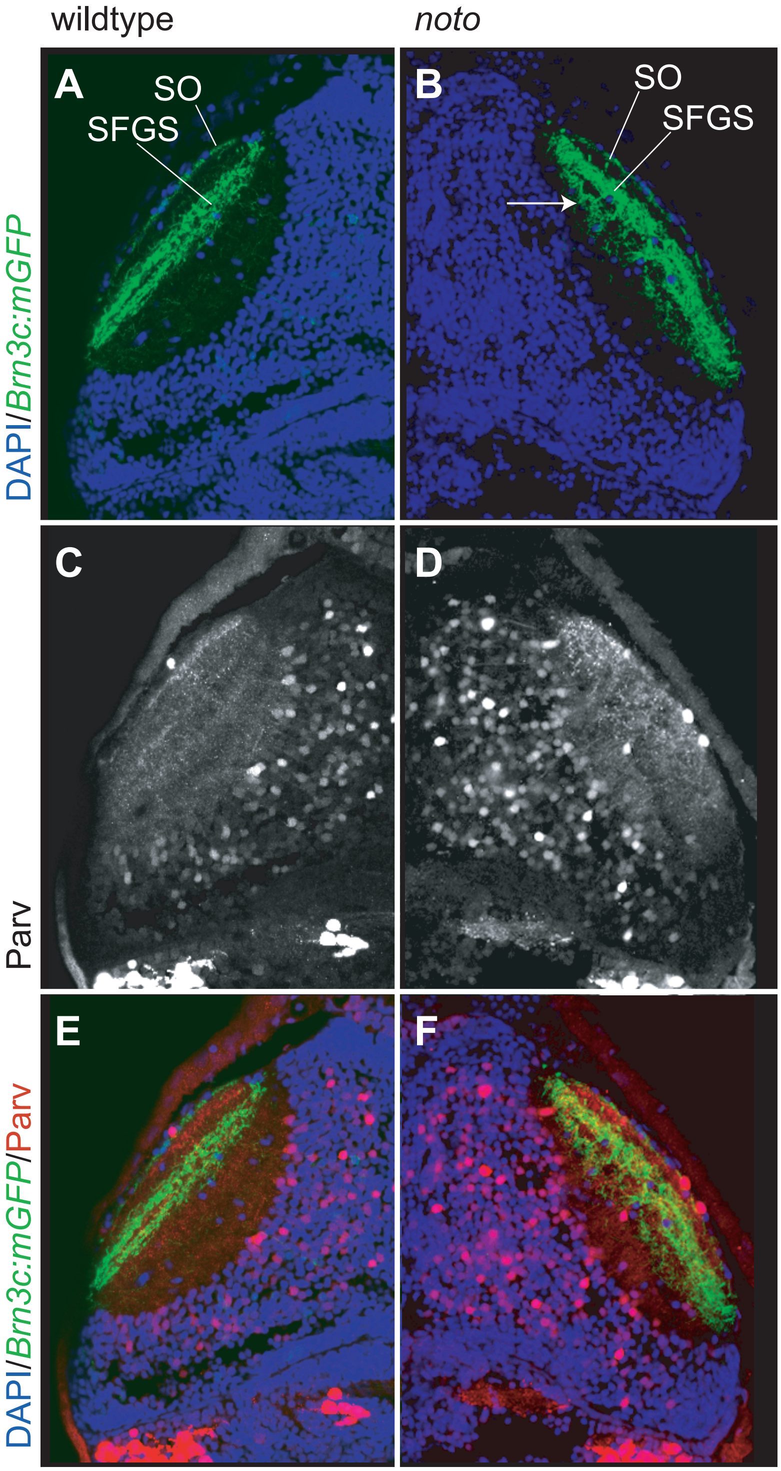
wildtype
noto
A
SO
SFGS
B
SO
SFGS
C
D
E
F
DAPI/*Brn3c:mGFP*
Parv
DAPI/*Brn3c:mGFP*/Parv

Figure 21: Individual noto axons can arborize in more than one tectal lamina

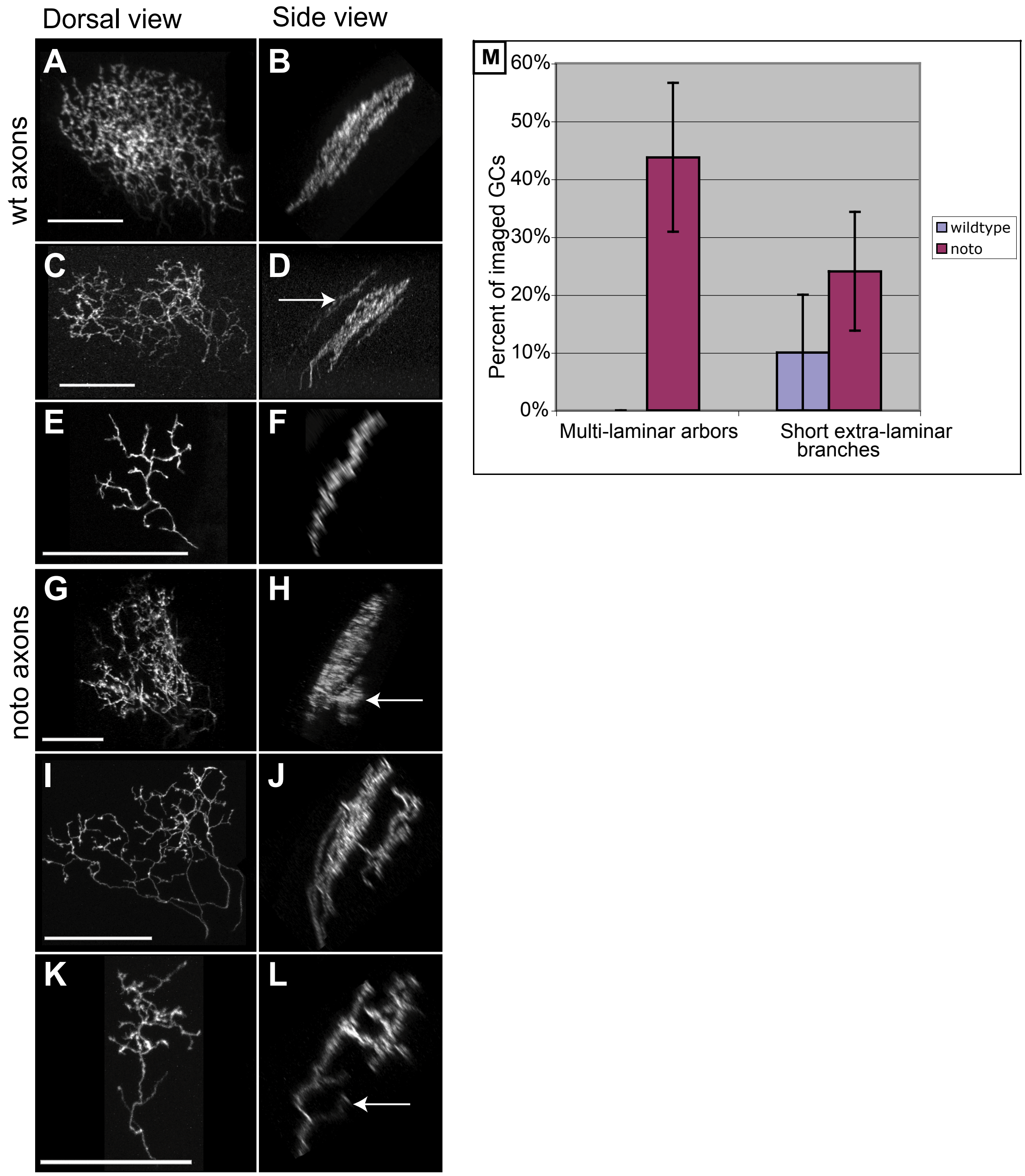
Dorsal view
Side view
wt axons
noto axons
A
B
C
D
E
F
G
H
I
J
K
L
M
60%
50%
40%
30%
20%
10%
0%
Percent of imaged GCs
Multi-laminar arbors
Short extra-laminar branches
wildtype
noto

Chapter 4:

Characterization of tectal cell morphologies in wildtype and *lakritz* mutant larvae

Linda Nevin and Herwig Baier

Abstract

Neurite-neurite interactions during development are believed to influence the mature morphology of neurons, via cell-surface signaling, formation of synaptic contacts, and/or transfer of neurotrophic factors. In the optic tectum, both innervating ganglion cell (GC) axons and tectal neuron dendrites undergo a period of branch addition and subtraction, in which neurite-neurite interactions may be important for morphogenesis. We investigated the role of GC axons in modeling tectal dendrites by analyses of tectal neurons in the absence of ganglion cells. For the study we used antibody staining and single cell labeling in the *lakritz (lak)* mutant, which lacks GCs due to a mutation in transcription factor *atonal homolog 5 (ath5).* One population of tectal neurons, those which express parvalbumin, showed slight changes in neuropil lamination in the absence of GCs. However, analysis of single tectal cells from wildtype and *lak* did not uncover any differences in dendrite morphology. Overall, it appears that the role of GC axons in tectal dendrite morphogenesis is subtle and cell-type specific, or easily replaced by other inputs to the tectum.

Introduction

Interactions between pre- and post- synaptic neurites are central to the development of arbor morphology. This tenet has been well established in the visual cortex of mammals with binocular vision, where afferents from the lateral geniculate nucleus segregate into ocular dominance columns in a process that depends on transient synapse formation with multiple target dendrites (Hahm et al. 1999; Muir-Robinson et al. 2002). More recently, single cell labeling and *in vivo* imaging have shown neurites forming temporary contacts as connections are refined (Jontes et al. 2000; Keller-Peck et al. 2001). The optic tectum has been used extensively for the study of neurite development, both of the axons from retinal ganglion cells (GCs) and of the dendrites of tectal neurons. *in vivo* time lapse imaging has shown that both GC axons and tectal cell dendrites arborize by extension and retraction of branches (Wu et al. 1999; Wu and Cline 2003; Cohen-Cory and Lom 2004). At least three lines of evidence from *Xenopus* and chick suggest that, as GC axons and tectal dendrites grow and probe the environment, contact and synaptic transmission between the two is important in determining their final morphologies. First, synaptic transmission appears to be required for the appropriate refinement of axons to their region of the topographic map. Blockade of retinal activity (Schmidt 1991; Schmidt and Buzzard 1993), and reduction of the available pool of loaded glutamatergic vesicles (Smear et al. 2007) results in overgrown GC axonal arbors. Reciprocally, blockade of NMDA-type glutamate receptors limits the rate of change and growth in complexity of tectal dendrites, while enhanced visual stimulation causes an increase in arbor dynamics (Cline 2001). Second, time course imaging of axons and dendrites suggests that new branches form in proximity to successfully established synapses (Alsina et al. 2001; Niell et al. 2004). Third, manipulating the expression of signal transduction molecules such as Calcium-calmodulin dependent kinase II (CamKII) in tectal dendrites can alter the arborization of GC axons (Zou and Cline 1999; Cantallops et al. 2000). All of these strongly support a role for neurite-neurite interaction, including development of transient synapses, in the arbor development of both types of neurite.

Circumstantial evidence suggests that a neurotrophin released from GC axons may be involved in the development of tectal dendrites. Classically, neurotrophic factors are released by post-synaptic cells, taken up by axon terminals, and transported retrogradely to the cell body. Consistent with this common mechanism, tectal- derived brain-derived neurotrophic factor (BDNF) is known to enhance the size and complexity of GC axonal arbors (Cohen-Cory and Lom 2004). However, neurotrophins can also be transported anterogradely and released by axons onto target dendrites, and dendrites, too, can respond to neurotrophins with increased branching (von Bartheld et al. 2001; Wirth et al. 2003). In the retinotectal system, neurotrophin-3 (NT-3) and BDNF are transported anterogradely along GC axons, and retina-derived NT-3 increases the number of synapses in the retinorecipient layers of the tectum (Wang et al. 2003). This research has provided a number of hints that GCs might have a developmental role in modeling tectal dendrites, but an experimental system to test this hypothesis directly has been lacking.

We have begun to explore the role of GCs in the development of tectal neuron dendrites using the zebrafish *lakritz (lak)* mutant. Because wildtype GCs are known to innervate their target laminae directly at the rostral pole of the tectum, prior to any contact with tectal neuron dendrites, we reasoned that these axons might have an instructive role in recruiting synaptic partners to tectal laminae. The shared disorganization of *Brn3c:mGFP+* GC axons and parvalbumin+ tectal dendrites in *notorious* mutants is also suggestive of a developmental relationship between the two cell classes (see Chapter 3). To test this hypothesis, we assessed the morphologies and neuropil lamination of tectal dendrites in *lak.* The *lak* mutant, discussed in Chapter 2, fails to generate any GCs, and is a clean experimental tool because *ath5* is expressed only in the retina (Masai et al. 2000). We found that tectal neurons in *lak* mutants are surprisingly normal in morphology, and that GC innervation is not required to recruit tectal neurites to retinorecipient laminae. At this time, the paucity of knowledge about tectal cell types restricts the interpretations we can make about our findings.

Results and Discussion

Lamination of dendrites in the tectum is largely independent of innervation by retinal axons

We found that *lak* mutants have strikingly normal optic tecta in the absence of a major input. TUNEL staining revealed no increase in cell death, and the tectum is of normal size (data not shown). This is not surprising, as the tectum is the target of many inputs in addition to the retinotectal projection (Nieuwenhuys et al. 1998); the *lak* mutants do not have a completely deafferented tectum. As expected, there is a decrease in the thickness of the neuropil in most sections, which likely reflects the absence of the retinal axons (data not shown). Parvalbumin+ neurites are changed—the immunoreactivity in the SO and SFGS remains, but the medial two bands appear merged into one (Fig 22A,B). In wildtype, these two bands are separated by the SGC arm of the retinotectal projection (see Chapter 3). GC axons appear not to be required for the attraction of co-localizing parvalbumin+ neurites, but rather for the exclusion of parvalbumin neurites from one specific lamina. This finding suggests that repulsive interactions may be important for the lamination of tectal dendrites. Perhaps the GC axons at the *SGC/SAC* boundary exclude parvalbumin+ dendrites via contact-mediated repulsion. Reciprocally, perhaps the neurites that do co-localize with GC axons—the parvalbumin+ dendrites of the SO and SFGS—are shepherded into place via repulsion from non-retinal inputs to the tectum.

To investigate the *lak* phenotype further, we examined single cell morphology of tectal neurons in wildtype and *lak* using focal electroporation of GFP-expressing constructs. Cells were classified by morphology into four basic types. The most common type, which we called the palm tree cell, likely corresponds the type XIV neuron of the goldfish tectum (Meek and Schellart 1978). In palm tree cells a long main dendrite is capped by a densely branched arborization (Fig 22C-J). Our giant kelp cells have an elongated cell body, and a brightly labeled main projection through the neuropil, terminating in an endfoot close to the skin. Multiple short processes extend from the main process, giving it a leafy appearance (Fig 22O,P). These are most likely the GFAP+ radial glia that have been characterized previously in the tectum (Xiao and Baier 2007). Sprout cells are similar to palm cells, but more sparsely branched. Vine cells have cell bodies in the tectum but extend processes ventrally and widely into deeper brain structures. As shown by the examples in Fig 22, each type is represented in the wildtype and *lak* tectum, and the cells are morphologically indistinguishable. We counted 65 wildtype and 32 *lak* cells; no significant differences in the frequency of any cell type were observed (graph Fig 22Q). Measurements of arbor size and branchtip number using morphometric tools in ObjectImage (Ruthazer et al. 2003) did not reveal any trends (data not shown). In addition, palm cells in both wildtype and *lak* show laminar preferences, which can be seen when the volume projection of a z-stack is rotated such that we see the longest axis of each neuron (see figure legend for details). In total, our single cell observations revealed no requirement for GCs and the morphogenesis of tectal dendrites.

Conclusions

We have identified a population of parvalbumin+ tectal dendrites which show slightly altered laminar preferences in the absence of GC input to the tectum. However, overall the dendrites of tectal neurons in the *lak* mutant were surprisingly unaffected by the absence of a major input. This finding is consistent with a study published while these experiments were in progress, in which early enucleation of the eye, prior to innervation of the tectum, did not alter the gross morphology of tectal neurons in the chick (Luksch and Poll 2002).

Given the importance of glutamatergic signaling in the development of tectal dendrites, it seems likely that inputs to the tectum truly are relevant to dendrite morphogenesis. Our finding suggests that the morphogenesis of tectal neurons is largely GC-independent, but alternate explanations are quite possible. As mentioned, the tectum is the target of a number of sensory systems; perhaps in *lak,* other inputs can compensate for the absence of GCs. This might be the case if other axons innervate the retinorecipient laminae in the absence of GCs, and if these alternate inputs are competent to recruit partner dendrites. At this time we have not established what changes in tectal innervation result from the *lak* mutation besides the loss of GCs. An alternative, and likely the most plausible, explanation for our finding is that we were not examining a retinorecipient population of tectal neurons, as the method used selects tectal cells at random. There is currently no method available to specifically label retinorecipient tectal neurons in zebrafish. Currently, a surge of enhancer trap screens to label functionally distinct populations of neurons in the zebrafish nervous system is underway in numerous laboratories (Scott et al. 2007). Hopefully, transgenic lines specifically labeling retinorecipient tectal cells will be identified, and this question can be revisited.

Methods

Fish husbandry, sectioning, immunohistochemistry, and imaging of sections and live fish were performed as in Chapters 2 and 3.

Single cell electroporation

Small numbers of neurons were labeled in live fish using a method adapted from Kurt Haas (Haas et al. 2001). Cells were transfected in this way with either *α-tubulin:GFP, eF1α;GFP*, or mixed *α-tubulin:gal4;UAS:GFP* plasmids. We saw the best labeling using the *α-tubulin* promoter, either with or without the *Gal4;UAS* addition. In our hands, the optimal DNA concentration for electroporation is 1.5μg/μl. When the two constructs were mixed, transfection was only successful when both constructs were concentrated in SpeedVac (Savant Instruments, Inc, Holbrook, NY) to 3μg/μl and then mixed 1:1, such that each maintained the 1.5μg/μl concentration in the pipette tip. Larvae were electroporated at 4 or 5 dpf and imaged at 6 or 7 dpf.

References

Alsina B, Vu T, Cohen-Cory S (2001) Visualizing synapse formation in arborizing optic axons in vivo: dynamics and modulation by BDNF. Nat Neurosci 4(11): 1093-1101.

Cantallops I, Haas K, Cline HT (2000) Postsynaptic CPG15 promotes synaptic maturation and presynaptic axon arbor elaboration in vivo. Nat Neurosci 3(10): 1004-1011.

Cline HT (2001) Dendritic arbor development and synaptogenesis. Curr Opin Neurobiol 11(1): 118-126.

Cohen-Cory S, Lom B (2004) Neurotrophic regulation of retinal ganglion cell synaptic connectivity: from axons and dendrites to synapses. Int J Dev Biol 48(8-9): 947-956.

Haas K, Sin WC, Javaherian A, Li Z, Cline HT (2001) Single-cell electroporation for gene transfer in vivo. Neuron 29(3): 583-591.

Hahm JO, Cramer KS, Sur M (1999) Pattern formation by retinal afferents in the ferret lateral geniculate nucleus: developmental segregation and the role of N-methyl-D-aspartate receptors. J Comp Neurol 411(2): 327-345.

Jontes JD, Buchanan J, Smith SJ (2000) Growth cone and dendrite dynamics in zebrafish embryos: early events in synaptogenesis imaged in vivo. Nat Neurosci 3(3): 231-237.

Keller-Peck CR, Walsh MK, Gan WB, Feng G, Sanes JR et al. (2001) Asynchronous synapse elimination in neonatal motor units: studies using GFP transgenic mice. Neuron 31(3): 381-394.

Luksch H, Poll A (2002) Early enucleation does not alter the gross morphology of identified projection neurons in the chicken optic tectum. Neurosci Lett 331(1): 41-44.

Masai I, Stemple DL, Okamoto H, Wilson SW (2000) Midline signals regulate retinal neurogenesis in zebrafish. Neuron 27(2): 251-263.

Meek J, Schellart NA (1978) A Golgi study of goldfish optic tectum. J Comp Neurol 182(1): 89-122.

Muir-Robinson G, Hwang BJ, Feller MB (2002) Retinogeniculate axons undergo eye-specific segregation in the absence of eye-specific layers. J Neurosci 22(13): 5259-5264.

Niell CM, Meyer MP, Smith SJ (2004) In vivo imaging of synapse formation on a growing dendritic arbor. Nat Neurosci 7(3): 254-260.

Nieuwenhuys H, Donkelaar C, Nicholson C (1998) The Central Nervous System of Vertebrates. New York: Springer.

Ruthazer ES, Akerman CJ, Cline HT (2003) Control of axon branch dynamics by correlated activity in vivo. Science 301(5629): 66-70.

Schmidt JT (1991) Effects of blocking or synchronizing activity on the morphology of individual regenerating arbors in the goldfish retinotectal projection. Ann N Y Acad Sci 627: 385-389.

Schmidt JT, Buzzard M (1993) Activity-driven sharpening of the retinotectal projection in goldfish: development under stroboscopic illumination prevents sharpening. J Neurobiol 24(3): 384-399.

Scott EK, Mason L, Arrenberg AB, Ziv L, Gosse NJ et al. (2007) Targeting neural circuitry in zebrafish using GAL4 enhancer trapping. Nat Methods 4(4): 323-326.

Smear MC, Tao HW, Staub W, Orger MB, Gosse NJ et al. (2007) Vesicular glutamate transport at a central synapse limits the acuity of visual perception in zebrafish. Neuron 53(1): 65-77.

von Bartheld CS, Wang X, Butowt R (2001) Anterograde axonal transport, transcytosis, and recycling of neurotrophic factors: the concept of trophic currencies in neural networks. Mol Neurobiol 24(1-3): 1-28.

Wang X, Butowt R, von Bartheld CS (2003) Presynaptic neurotrophin-3 increases the number of tectal synapses, vesicle density, and number of docked vesicles in chick embryos. J Comp Neurol 458(1): 62-77.

Wirth MJ, Brun A, Grabert J, Patz S, Wahle P (2003) Accelerated dendritic development of rat cortical pyramidal cells and interneurons after biolistic transfection with BDNF and NT4/5. Development 130(23): 5827-5838.

Wu GY, Cline HT (2003) Time-lapse in vivo imaging of the morphological development of Xenopus optic tectal interneurons. J Comp Neurol 459(4): 392-406.

Wu GY, Zou DJ, Rajan I, Cline H (1999) Dendritic dynamics in vivo change during neuronal maturation. J Neurosci 19(11): 4472-4483.

Xiao T, Baier H (2007) Lamina-specific axonal projections in the zebrafish tectum require the type IV collagen Dragnet. Nat Neurosci 10(12): 1529-1537.

Zou DJ, Cline HT (1999) Postsynaptic calcium/calmodulin-dependent protein kinase II is required to limit elaboration of presynaptic and postsynaptic neuronal arbors. J Neurosci 19(20): 8909-8918.

Figure 22

lak tectal neurons laminate in a nearly wildtype pattern, despite the absence of GC axons

A,B: 40X confocal images of 5 dpf optic tecta. Parvalbumin+ tectal dendrites project to four laminae in wildtype, and to three laminae in *lak*. C,E,G,I: Wildtype “palm tree” cells in dorsal view and side view. Lamina-specific arbors are indicated with arrows in the side views. Tectal neurons do not project to laminae as strictly as GC inputs, so laminae are broader, and many partially overlap. D,F,H,J: *lak* palm cells also show laminar specificity, as shown by the arrow in F. Two overlapping cells are shown in H and J. We isolated a single arborization from one cell by selecting the top slices of the stack, which contained branches from that arbor but not from the arbors ventral to it. In the inset in H, all the branches shown within the circle are part of this single arborization, which is rotated to a side view in the inset in J. This arborization is highly lamina-specific. K,L: “Vine” cells from wildtype and *lak.* M,N: “Sprout” cells from wildtype and *lak.* O,P: “Giant kelp” cells—likely radial glia—from wildtype and *lak.* Cell bodies are marked with arrows, endfeet with arrowheads. In both cases, palm cells are labeled right next to the giant kelp cells, and the palm cell dendrites mingle with the large giant kelp cell process. Palm cell main dendrite shafts are labeled with a ‘p.’ Q: Frequency of each morphological cell type observed in wildtype and *lakritz.* Error bars are SEM; no significant differences were observed.

Figure 22: *lak* tectal neurons laminate in a nearly wildtype pattern, despite the absence of GC axons

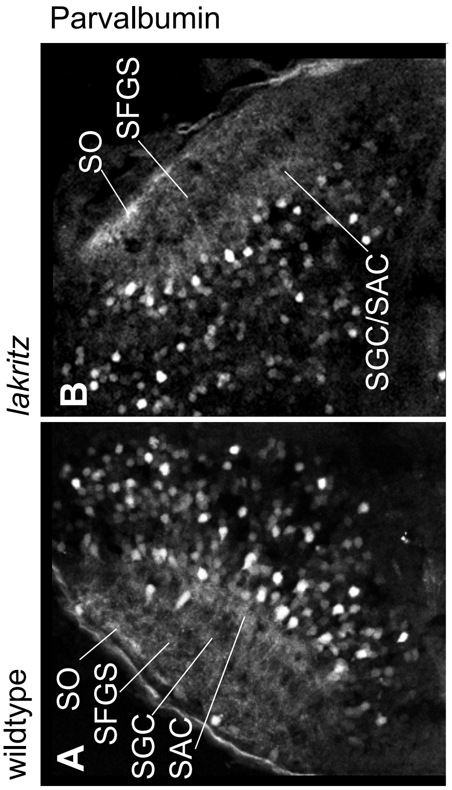
Parvalbumin
lakritz
B
SO
SFGS
SGC/SAC
wildtype
A
SO
SFGS
SGC
SAC

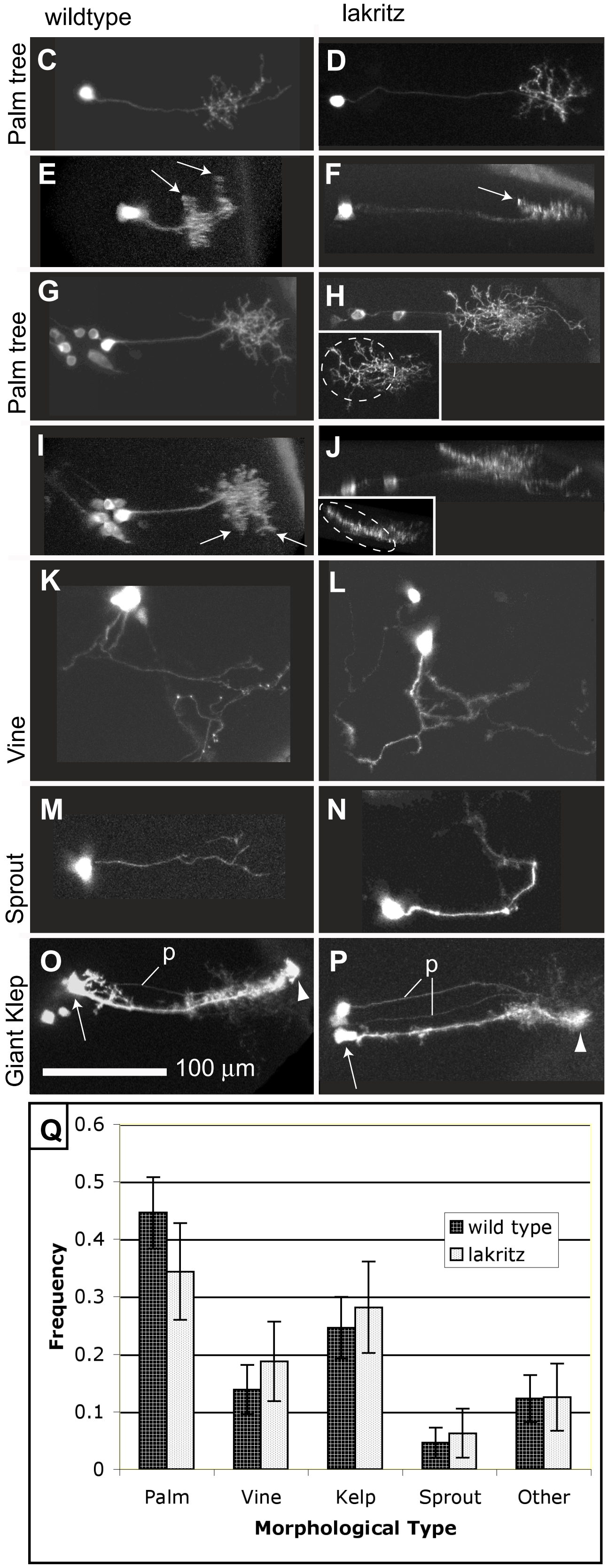
wildtype
lakritz
Palm tree
C
D
E
F
Palm tree
G
H
I
J
Vine
K
L
Sprout
M
N
Giant Klep
O
p
P
p
100 µm
Q
0.6
0.5
0.4
0.3
0.2
0.1
0
Frequency
▦ wild type
☐ lakritz
Palm
Vine
Kelp
Sprout
Other
Morphological Type

Conclusions

The zebrafish IPL and tectal neuropil are organized structures, comprising parallel laminae with distinct innervating neurites. In the IPL, cell type-specific markers of retinal neurons from better studied species label the equivalent cells in zebrafish. In the tectum, we identified two markers—PKC and parvalbumin—that distinguish two types of tectal cells. In both the retina and tectum, each neuronal type projects reproducibly to specific synaptic laminae, where it can form synapses with a consistent (across larvae) subset of potential partners. The zebrafish larva is developmentally distinct from its mammalian counterparts because the process of IPL sublamination, at least until 7dpf, does not depend on visual experience or retinal activity. The single cell studies of AC, BC, and GC development from Rachel Wong's group, cited multiple times in this thesis, were published after I completed these experiments, and corroborated the results. It appears that zebrafish GC dendrites do not follow the two phase mode of development seen in mammals, which consists of exuberant growth followed by refinement. Therefore, activity dependent pruning is not necessary for zebrafish GCs to target sublaminae. Our forward genetic screen lays the groundwork for learning what hard-wired mechanisms control IPL and tectal neuropil lamination. Neurites of different classes tend to share defects in these mutants, suggesting that intercellular interactions play a role in shaping these laminae. GCs, in particular, can alter the projection patterns of other IPL neurites, as seen in *noto*. In this way, relative positioning of neurites can be preserved where absolute organization is perturbed. The only mutant we identified wherein co-localization of partner neurites was lost in the IPL was *mra/ddx19. Ddx19*, by inference from the gene's known function in non-specific mRNA export from the nucleus, likely globally hinders the production of all signaling molecules. That the mutation can act cell non-autonomously in IPL sublamination is further evidence that cell-to-cell instruction is a key player. Hopefully, the identification of the lesions in some of the other mutants, such as *noto*, will lead to specific pathways involved in neurite lamination. In *noto* we have identified targeting errors in both the IPL and tectal neuropil—the gene acts on both axons and dendrites of GCs. Unlike the defects in *mra*, noto IPL sublamination errors are subtle; neurites roughly target the right sublaminae, but the projections are coarse. The *noto* tectal phenotype is more severe. Because the tectum is a more accessible structure for single cell imaging, we were able to show that noto GC axons form arbors in inappropriate laminae. It appears that a restrictive cue that opposes the formation of spurious arbors is lost in the mutants. This cue does not prevent axons from sending short branches between laminae, which we also see in wildtype, but inhibits the formation of arbors.

Though GCs represent a major input to the optic tectum, we did not observe major changes in neurite differentiation and lamination in *lak* mutants. Since the time that these experiments were completed, a number of groups have undertaken enhancer trap screens to specifically label molecularly defined subsets of neurons. Our group in particular has a number of lines expressing fluorophores in subsets of tectal cells. At the time, the best method to look at individual neuron morphology in the tectum was to label at random, in this case by single cell electroporation. However, this method is time consuming and results in sparse data, and there is no guarantee that the neurons labeled were fated to be retinorecipient. The same is true for the PKC+ and parvalbumin+ neurites; we do not know whether these form synapses with GC axons. With the accumulation of trap lines, this experiment may bear repeating if a retinorecipient subset of tectal neurons can be characterized. Perhaps a defined class of retinorecipient neurites will be truncated, or, alternatively, our results will be corroborated as these neurites take up other partners.

Publishing Agreement

It is the policy of the University to encourage the distribution of all theses and dissertations. Copies of all UCSF theses and dissertations will be routed to the library via the Graduate Division. The library will make all theses and dissertations accessible to the public and will preserve these to the best of their abilities, in perpetuity.

Please sign the following statement:

I hereby grant permission to the Graduate Division of the University of California, San Francisco to release copies of my thesis or dissertation to the Campus Library to provide access and preservation, in whole or in part, in perpetuity.

March 27, 2008

Author Signature Date